

IRREVERSIBILITY LINE DETERMINATION  
IN HIGH  $T_c$  SUPERCONDUCTORS

by

MUHAMMAD ASIF

DEPARTMENT OF PHYSICS  
QUAID-I-AZAM UNIVERSITY  
ISLAMABAD, PAKISTAN

1995



252  
PHY  
C-1

*IN THE NAME OF ALLAH  
THE MOST BENEFICENT  
AND THE MOST MERCIFUL*

---

**DEDICATED TO MY FATHER**  
**PROFESSOR RASHID AHMAD**

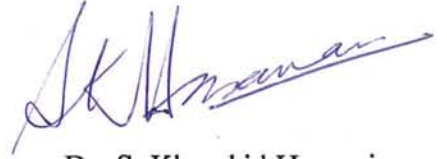
# CONTENTS

List and captions of figures	i	
List of tables	v	
Acknowledgments	vi	
Abstract	vii	
<b><u>Chapter 1</u></b>	<i>Introduction</i>	<i>1</i>
[1.1]	Irreversible effects in superconductors	1
[1.2]	Mixed state	2
[1.3]	Flux pinning	2
[1.4]	Thermally activated flux motion	3
[1.5]	Flux creep	3
[1.6]	Critical state model	4
[1.7]	Role of equilibrium magnetization in the critical state model	7
[1.8]	Anderson-Kim model	9
[1.9]	The irreversibility line	10
[1.9.1]	Effect of thermal activation on the shape of the irreversibility line	12
[1.9.2]	Field and temperature dependence of pinning potential “ $U_0$ ”	14
<b><u>Chapter 2</u></b>	<i>Experimental Techniques</i>	
[2.1]	Vibrating Sample Magnetometer (VSM)	18
[2.2]	Sample holder	20
[2.3]	Temperature measurement/Temperature control system	20

[2.4]	Cryostat	21
[2.4(a)]	Glass dewar	21
[2.4(b)]	Single walled glass tube	21
[2.5]	Susceptometer	21
[2.6.1]	Variable temperature cryostat	23
[2.6.2]	Temperature controller	25
[2.6.3]	Platinum resistance thermometry (Elements PT 100)	25
[2.6.4]	Lock in amplifier	25
[2.7]	Susceptibility measurement technique	26
<b><u>Chapter 3</u></b>	<i>Results and discussion</i>	29
[3.1]	dc magnetization measurements	30
[3.1a]	Obtaining of the exponent 'n'	61
[3.2]	ac susceptibility measurements	72
[3.2a]	Obtaining of the exponent 'n'	79
[3.3]	Role of $H_c(T)$ on the shape of irreversibility line	84
[3.4]	Temperature dependence of the upper critical field	88
[3.5]	Conclusions	90

## CERTIFICATE

This is to certify that the work in this dissertation has been carried out by  
Mr. Muhammad Asif under my supervision.



Dr. S. Khurshid Hasanain

Associate Professor

Department of Physics

Quaid-i-Azam University

Islamabad

Submitted through



Prof. Dr. Kamaluddin Ahmed

Chairman

Department of Physics

Quaid-i-Azam University

Islamabad

---

This work is submitted as a dissertation in  
partial fulfillment of the requirements for  
the degree of MASTER OF PHILOSOPHY  
in PHYSICS, to the Department of Physics  
Quaid-i-Azam University, Islamabad.

## LIST AND CAPTIONS OF FIGURES

- Fig[1.1] Internal flux density profiles for:  
(a) Increasing & (b) Decreasing external magnetic field.
- Fig[1.2] Critical state magnetization behavior for type-II superconductors with:  
(a) Zero reversible magnetization & (b) Non-zero reversible magnetization.
- Fig[1.3] Sketch of the irreversibility line in the H-T plane exhibiting a non-linear behavior with  $H^*$  going to zero at  $T=T_c$ . The dotted lines are depict the  $H^*$  (onset field) value corresponding to the temperature.
- Fig[2.1] Block diagram of Vibrating Sample Magnetometer (VSM), BHV-50 model.
- Fig[2.2] Diagram of different parts of sample holder:  
(a) Steel pipe (b) Teflon holder (c) Glass pipe &  
(b) The whole assembly of the sample holder.
- Fig[2.3] Design and dimensions of the susceptometer.
- Fig[2.4] Block diagram of ac susceptibility measurement system.
- Fig[3.1(i)] Typical magnetization behavior of sample BPS at 77K with the variation of applied magnetic field. The maximum field applied is 5 Koe, whereas the arrow is indicating the onset point of the hysteresis at the field value  $H^* = 1280$  Oe.
- Fig[3.1(ii)] Typical magnetization behavior of sample BPS at  $(92 \pm 0.3)$ K with the variation of applied magnetic field. The maximum field applied is 5 Koe, whereas the arrow is indicating the onset point of the hysteresis(as defined in the text) at the field value  $H^* = 810$  Oe.
- Fig[3.1(iii)] Typical magnetization behavior of sample BPS at  $(95 \pm 0.4)$ K with the variation of applied magnetic field. The maximum field applied is 5 Koe, whereas the arrow is indicating the onset point of the hysteresis (as defined in the text) at the field value  $H^* = 697$  Oe.
- Fig[3.1(iv)] Typical magnetization behavior of sample BPS at  $(97.5 \pm 0.3)$  K with the variation of applied magnetic field. The maximum field applied is 5 Koe, whereas the arrow is indicating the onset point of the hysteresis (as defined in the text) at the field value  $H^* = 589$  Oe.
- Fig[3.1(v)] Typical magnetization behavior of sample BPS at  $(99 \pm 0.3)$  K with the variation of applied magnetic field. The maximum field applied is 5 Koe, whereas the arrow is indicating the onset point of the hysteresis (as defined in the text) at the field value  $H^* = 502$  Oe.



- Fig[3.2(i)] Typical magnetization behavior of sample YBCO at 77 K with the variation of applied magnetic field. The maximum field applied is 15 Koe, whereas the arrow is indicating the onset point of the hysteresis (as defined in the text) at the field value  $H^* = 13552$  Oe.
- Fig[3.2(ii)] Typical magnetization behavior of sample YBCO at  $(84.1 \pm 0.3)$  K with the variation of applied magnetic field. The maximum field applied is 15 Koe, whereas the arrow is indicating the onset point of the hysteresis (as defined in the text) at the field value  $H^* = 8932$  Oe.
- Fig[3.2(iii)] Typical magnetization behavior of sample YBCO at  $(85.7 \pm 0.2)$  K with the variation of applied magnetic field. The maximum field applied is 15 Koe, whereas the arrow is indicating the onset point of the hysteresis (as defined in the text) at the field value  $H^* = 7700$  Oe.
- Fig[3.2(iv)] Typical magnetization behavior of sample YBCO at  $(86.7 \pm 0.2)$  K with the variation of applied magnetic field. The maximum field applied is 15 Koe, whereas the arrow is indicating the onset point of the hysteresis (as defined in the text) at the field value  $H^* = 6468$  Oe.
- Fig[3.2(v)] Typical magnetization behavior of sample YBCO at  $(88.4 \pm 0.4)$  K with the variation of applied magnetic field. The maximum field applied is 15 Koe, whereas the arrow is indicating the onset point of the hysteresis (as defined in the text) at the field value  $H^* = 5236$  Oe.
- Fig[3.2(vi)] Typical magnetization behavior of sample YBCO at  $(89.3 \pm 0.3)$  K with the variation of applied magnetic field. The maximum field applied is 15 Koe, whereas the arrow is indicating the onset point of the hysteresis (as defined in the text) at the field value  $H^* = 4004$  Oe.
- Fig[3.3(i)] Typical magnetization behavior of sample Hg-4 at 77 K with the variation of applied magnetic field. The maximum field applied is 20 Koe, whereas the arrow is indicating the onset point of the hysteresis (as defined in the text) at the field value  $H^* = 13870$  Oe.
- Fig[3.3(ii)] Typical magnetization behavior of sample Hg-4 at  $(93 \pm 0.4)$  K with the variation of applied magnetic field. The maximum field applied is 15 Koe, whereas the arrow is indicating the onset point of the hysteresis (as defined in the text) at the field value  $H^* = 11020$  Oe.
- Fig[3.3(iii)] Typical magnetization behavior of sample Hg-4 at  $(98 \pm 0.3)$  K with the variation of applied magnetic field. The maximum field applied is 15 Koe, whereas the arrow is indicating the onset point of the hysteresis (as defined in the text) at the field value  $H^* = 9940$  Oe.
- Fig[3.3(iv)] Typical magnetization behavior of sample Hg-4 at  $(102.5 \pm 0.5)$  K with the

variation of applied magnetic field. The maximum field applied is 15 Koe, whereas the arrow is indicating the onset point of the hysteresis (as defined in the text) at the field value  $H^* = 9480$  Oe.

- Fig[3.3(v)] Typical magnetization behavior of sample Hg-4 at  $(108 \pm 0.4)$  K with the variation of applied magnetic field. The maximum field applied is 15 Koe, whereas the arrow is indicating the onset point of the hysteresis (as defined in the text) at the field value  $H^* = 8340$  Oe.
- Fig[3.3(vi)] Typical magnetization behavior of sample Hg-4 at  $(111 \pm 0.3)$  K with the variation of applied magnetic field. The maximum field applied is 15 Koe, whereas the arrow is indicating the onset point of the hysteresis (as defined in the text) at the field value  $H^* = 7650$  Oe.
- Fig[3.3(vii)] Typical magnetization behavior of sample Hg-4 at  $(116 \pm 0.5)$  K with the variation of applied magnetic field. The maximum field applied is 15 Koe, whereas the arrow is indicating the onset point of the hysteresis (as defined in the text) at the field value  $H^* = 6500$  Oe.
- Fig[3.3(viii)] Typical magnetization behavior of sample Hg-4 at  $(120.5 \pm 0.7)$  K with the variation of applied magnetic field. The maximum field applied is 15 Koe, whereas the arrow is indicating the onset point of the hysteresis (as defined in the text) at the field value  $H^* = 4660$  Oe.
- Fig[3.3(ix)] Typical magnetization behavior of sample Hg-4 at  $(125 \pm 0.4)$  K with the variation of applied magnetic field. The maximum field applied is 15 Koe, whereas the arrow is indicating the onset point of the hysteresis (as defined in the text) at the field value  $H^* = 3520$  Oe.
- Fig[3.4] Graph of  $H^*$  vs  $T$  plotted on the data obtained from the dc  $M(H)$  measurements of sample BPS. This is the irreversibility line in the  $H$ - $T$  plane which exhibits a non-linear behavior with  $H^*$  going to zero at  $T = 107$ K (line is a guide to the eye).
- Fig[3.5] Graph of  $H^*$  vs  $T$  plotted on the data obtained from the dc  $M(H)$  measurements of sample YBCO. This is the irreversibility line in the  $H$ - $T$  plane which exhibits a non-linear behavior with  $H^*$  going to zero at  $T = 92.5$ K (line is a guide to the eye).
- Fig[3.6] Graph of  $H^*$  vs  $T$  plotted on the data obtained from the dc  $M(H)$  measurements of sample Hg-4. This is the irreversibility line in the  $H$ - $T$  plane which exhibits a non-linear behavior with  $H^*$  going to zero at  $T = 130$ K (line is a guide to the eye).
- Fig[3.7] Plot of  $\ln(1-t)$  vs  $\ln(H^*)$  for sample BPS. From the linearity of the  $\ln(1-t)$  vs  $\ln(H^*)$  a slope of  $0.66 \pm 0.02$  is obtained.
- Fig[3.8] Curve fit on the measurements obtained from the  $M(H)$  loops, recorded at different temperatures on sample BPS. In this fit  $\{1/c(1-T/T_c)\}^{1/n}$  is equated with a

function  $f$ , then  $f$  is fitted to  $H^*$  yielding the value of  $1/n = 0.68$ .

- Fig[3.9] Plot of  $\ln(1-t)$  vs  $\ln(H^*)$  for sample YBCO. From the linearity of the  $\ln(1-t)$  vs  $\ln(H^*)$  a slope of  $0.70 \pm 0.02$  is obtained.
- Fig[3.10] Curve fit on the measurements obtained from the  $M(H)$  loops recorded at different temperatures on sample YBCO. In this fit  $\{1/c(1-T/T_c)^{1/n}\}$  is equated with a function  $f$ , then  $f$  is fitted to  $H^*$  yielding the value of  $1/n = 0.78$ .
- Fig[3.11] Plot of  $\ln(1-t)$  vs  $\ln(H^*)$  for sample Hg-4. From the linearity of the  $\ln(1-t)$  vs  $\ln(H^*)$  a slope of  $0.60 \pm 0.02$  is obtained.
- Fig[3.12] Curve fit on the measurements obtained from the  $M(H)$  loops recorded at different temperatures on sample Hg-4. In this fit  $\{1/c(1-T/T_c)^{1/n}\}$  is equated with a function  $f$ , then  $f$  is fitted to  $H^*$  yielding the value of  $1/n = 0.58$ .
- Fig[3.13(a)] Field Cooled (FC) & Zero Field Cooled (ZFC) curves plotted in the  $\chi$ -T plane: In this plot the hollow circles represent the FC curve and the filled circles represent the ZFC curve. The arrow is indicating merging point of the two curves at  $T^* = 106K$  at applied external dc magnetic field  $H_{dc} = 200$  Oe.
- Fig[3.13(b)] Field Cooled (FC) & Zero Field Cooled (ZFC) curves plotted in the  $\chi$ -T plane: In this plot the hollow circles represent the FC curve and the filled circles represent the ZFC curve. The arrow is indicating merging point of the two curves at  $T^* = 105K$  at applied external dc magnetic field  $H_{dc} = 500$  Oe.
- Fig[3.13(c)] Field Cooled (FC) & Zero Field Cooled (ZFC) curves plotted in the  $\chi$ -T plane: In this plot the hollow circles represent the FC curve and the filled circles represent the ZFC curve. The arrow is indicating merging point of the two curves at  $T^* = 104K$  at applied external dc magnetic field  $H_{dc} = 650$  Oe.
- Fig[3.13(d)] Field Cooled (FC) & Zero Field Cooled (ZFC) curves plotted in the  $\chi$ -T plane: In this plot the hollow circles represent the FC curve and the filled circles represent the ZFC curve. The arrow is indicating merging point of the two curves at  $T^* = 103K$  at applied external dc magnetic field  $H_{dc} = 750$  Oe.
- Fig[3.14] Graph of  $H$  vs  $T^*$  obtained from the  $\chi$ -ac measurements carried out on sample BPS. This graph is showing the irreversibility line in the  $H$ - $T$  plane, exhibiting a non-linear behavior and extrapolating smoothly at  $T \sim 106K$ .
- Fig[3.15] Curve fit on the measurements obtained from the  $\chi$ -ac measurements carried out on sample BPS. In this fit  $\{1/c(T^*/T_c)^{1/n}\}$  is equated with a function  $f$ , then  $f$  is fitted to  $H^*$  yielding the value of  $1/n = 0.79$ .
- Fig [3.16] The values of  $H_{c2}$  obtained from fitting the equilibrium magnetization curves to a standard equation: i.e.  $4\pi M_{cqui} = -T \ln [H_{c2}/H]$ , are fitted to a function of a form:  $H_{c2} = H_{c0} [1 - (T/T_c)]^n$ . From the fit the values of  $n$  and  $H_{c0}$  are obtained, i.e.  $n = 0.51 \pm 0.07$  and  $H_{c0} = 2.81 \times 10^5$ .

## LIST OF TABLES

Table [I]	Data of temperature $T(K)$ , reduced temperature $t$ i.e. $T/T_c$ and $H^*(Oe)$ i.e. the onset field obtained from the $M(H)$ loops of sample BPS.
Table[II]	Data of temperature $T(K)$ , reduced temperature $t$ i.e. $T/T_c$ and $H^*(Oe)$ i.e. the onset field obtained from the $M(H)$ loops of sample YBCO.
Table[III]	Data of temperature $T(K)$ , reduced temperature $t$ i.e. $T/T_c$ and $H^*(Oe)$ i.e. the onset field obtained from the $M(H)$ loops of sample Hg-4.
Table[IV]	Data of $\ln(1-t)$ and $\ln(H^*)$ obtained from the $M(H)$ loops of sample BPS.
Table[V]	Data of $\ln(1-t)$ and $\ln(H^*)$ obtained from the $M(H)$ loops of sample YBCO.
Table[VI]	Data of $\ln(1-t)$ and $\ln(H^*)$ obtained from the $M(H)$ loops of sample Hg-4.
Table [VII]	Data of temperature $T(K)$ , reduced temperature $t$ i.e. $T/T_c$ and $H^*(Oe)$ i.e. the onset field obtained from the $\chi$ ac measurements of sample BPS.
Table[VI]	Data of $\ln(1-t)$ and $\ln(H^*)$ obtained from the $\chi$ ac measurements of sample Hg-4.

## ACKNOWLEDGMENTS

*First of all I am thankful to Almighty Allah who has empowered me to complete my dissertation.*

*I express my profound gratitude to my supervisor Dr. S. Khurshid Hasanain who introduced me to the subject and brought me to the level of research. Working under his able guidance and supervision, I gained a great deal of knowledge as well as experience of research work. I am also grateful to Dr. Kamaluddin Ahmed, the Chairman, Department of Physics, for providing me all the facilities during my research work.*

*My sincere thanks are due to Kiyani, Shaista, Arif and specially to Muneeb for their co-operation and friendly association throughout the period of experimental work.*

*I highly appreciate the moral support from my friends Majeed, Ashar, Zahoor, M.K. Jadoon, A.G. Solangi and Jamal Nasir in the crucial times during my M.Phil.*

*In the end, I acknowledge my parents for their prayers and encouragement during this work.*

Muhammad Asif

## ABSTRACT

The irreversibility line has been determined for three different polycrystalline superconducting samples. These samples are of composition  $(\text{Bi}_{1.6} \text{Pb}_{0.3} \text{Sb}_{0.1})\text{Sr}_2 \text{Ca}_2 \text{Cu}_3 \text{O}_{9.8}$ ,  $\text{Y}_1 \text{Ba}_2 \text{Cu}_3 \text{O}_{7.8}$  and  $\text{Hg}_1 \text{Ba}_2 \text{Ca}_2 \text{Cu}_3 \text{O}_{x+8}$ . The irreversibility line has been obtained from two methods, viz. vanishing of hysteresis in dc magnetization loops and comparing the temperature dependence of Field Cooled (FC) and Zero Field Cooled (ZFC) ac susceptibilities. Both the methods give very close results. The irreversibility field  $H^*$  obeys a relation of the form:

$$H^* = H_{c0} [1-T/T_c]^n$$

The value of  $n$  lies in the range  $0.6 \leq n \leq 0.8$ . The form of this irreversibility line is compared to the literature and possible explanation of  $n \approx 0.66$  is given in terms of the  $H_{c2}(T)$  dependence observed for at least one of the sample.

# CHAPTER 1

## INTRODUCTION

### (1.1) Irreversible effects in superconductors

The phenomenon of superconductivity was discovered over half a century ago by Kammerlingh Onnes. He observed that the electrical resistance of various metals such as mercury, lead and tin disappeared completely at a certain critical temperature " $T_c$ "[1-3]. Until quite recently it was strictly a low temperature phenomenon. The discovery of the new oxide superconductors, with transition temperatures up to 125K or higher, has opened a new temperature realm for superconducting devices [4] and presented new challenges for both theory and experiment.

Historically, the term "Hysterisis" or "irreversible effect" was first used in the 1930s when it was found that in a certain class of superconductors the Meissner effect[5] occurs over a very limited field region. In these so called hard superconductors, flux penetrates gradually over a wide range of magnetic fields and in decreasing field most of the flux remains trapped in the specimen [6].

Thus in order to have a clear insight into the irreversible effects it will be quite valuable to review the following important topics.

(1.2) Mixed state

(1.3) Flux pinning

(1.4) Thermally activated flux motion

## (1.5) Flux creep

## (1.2) Mixed state

In the mixed state of the type-II superconductors the magnetic field penetrates into the specimen in quantized form called vortices. In this state magnetic flux lines enter into the body of a superconductor without destroying its superconductivity. These flux lines consist of normal regions surrounded by superconducting domains. Superconducting electrons circulate around these flux lines, giving rise to shielding or screening currents.

The mixed state sets up in the field range ( $H_{c1} < H < H_{c2}$ ). Here  $H_{c1}$  &  $H_{c2}$  are the lower and upper critical fields, respectively. Type-II superconductivity had been theoretically predicted first by Abrikosov [7] from the general phenomenological theory of Ginzburg and Landau [8] of superconducting phase transition. This state is possible because of the existence of negative surface energy, which ensures that it is energetically favorable for the vortices to be formed and enter into the superconducting sample.

## (1.3) Flux Pinning

Flux pinning is closely analogous to the trapping of a mobile charged particle in a potential well. In case of superconductors the value of the critical current  $J_c$  can only be non-zero if there is some mechanism to prevent the movement of the vortices despite the Lorentz like driving forces.

$$\vec{F}_L = \vec{J} \times \vec{B}$$

or  $\vec{J} \times \vec{\Phi}_0$  per vortex

This effect is called pinning of vortices. Any defect (line, planer, point etc.) in the crystal structure of magnetic inhomogeneity on the scale of coherence length can act as a center of



pinning. That is, a vortex prefers to reside in a site of locally disturbed crystalline and superconducting order. Typical values of pinning energies are of the order of electron volts (eV) for low 'T<sub>c</sub>' superconductors and have even smaller magnitude for high 'T<sub>c</sub>' superconductors.

When a vortex is pinned, the net force on it is the sum of the Lorentz-like force "F<sub>L</sub>" and pinning force "F<sub>p</sub>" i.e.  $\vec{F} = \vec{F}_L + \vec{F}_p = 0$  (in equilibrium)

#### (1.4) Thermally activated flux motion

In high field applications of type-II superconductors, ideally one would wish to operate as closely as possible to the critical current at which the Lorentz force and pinning force are in a statistical sense, balanced, to achieve maximum utilization of the current carrying capacity of the superconducting material. Since flux motion is necessarily attended by heat generation, and because the pinning force itself is temperature dependent, thermally activated flux motion plays a crucial role in the stability of this balance.

A vortex pinned at a particular site will need to surmount a potential energy barrier (u) before being able to move under the influence of local Lorentz force. Thermal energy even at cryogenic temperatures is sufficient to free pinned vortices at a constant average rate i.e.

$R \propto e^{-U/KT}$ . Once released the vortices are propelled by the driving force  $J \times B$ , generating noise voltages and heat until trapped again at another pinning center. In fact the vortices move in groups known as flux bundles, each carrying many vortices (perhaps as many as hundred) because of the magnetic interaction between them.

#### (1.5) Flux creep

Flux creep or the slow movement of vortices over pinning barriers aided by the flux density barrier, proceeds under steady state conditions for "J" well below the critical current at an

an orderly pace. This becomes progressively slower with time as flux density gradients are gradually reduced by vortex displacement. In practice flux creep can be determined easily only immediately after a transient change, in externally applied magnetic field or current, has been made. This is because it decays logarithmically with time. Equally, flux creep never disappears completely, but the motion reverts to a randomly directed form, as the  $\vec{J} \times \vec{B}$  driving force decays. Here the current density  $\vec{J}$  may be the result of externally applied transport currents or macroscopic screening currents induced in the bulk of a hard type-II material. In both cases a gradient of flux density is supported by the available pinning force and is related to the current density through Ampere's law.

$$\vec{\nabla} \times \vec{B} = \mu \vec{J}$$

#### (1.6) Critical state model

If it were possible to reduce flux pinning to arbitrarily low levels, reversible magnetization curves would be obtained for bulk type-II materials even for field excursion over the complete range ( $H_{c1} < H < H_{c2}$ ).

Consider a material with no pinning centers and then examine the mixed-state behavior as the pinning strength is increased. Irreversible magnetic behavior is usually discussed in terms of the hysteresis losses observed under cyclic magnetization conditions. In type-II superconductors it is equally important to determine the effect of the irreversibility on the maximum direct current that can be carried without loss in the presence of a high ambient magnetic field, as in a solenoid for instance.

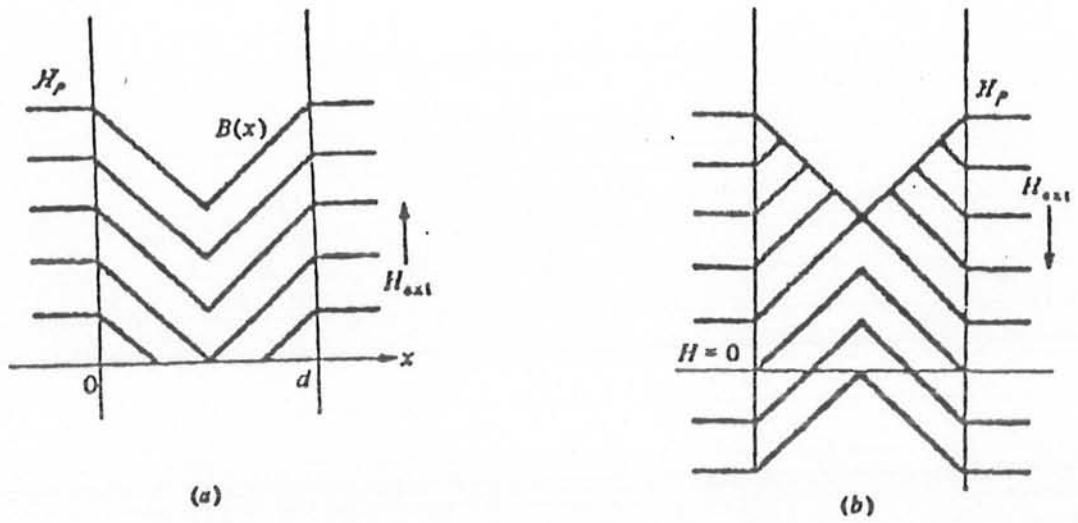
The critical-state model, first proposed by Beans' [9], provided a phenomenological description of the way in which the critical current density is limited by the Lorentz force. We can

illustrate this approach by applying it to the case shown in the figure(1.1). The locally averaged flux density and screening current density are given for a type-II superconducting plate parallel to the plate surfaces. As  $H$  is increased above  $H_{c1}$  flux enters in the interior. In the absence of pinning there is no bulk screening current because the flux density is uniform throughout the plate. In the London penetration regions( the depth to which an applied magnetic field penetrates into the specimen despite its Meissner state) at the plate surfaces, the Meissner screening currents persist until  $H$  approaches  $H_{c2}$  and diamagnetism of the plate disappears. If a moderate amount of pinning is present (e.g. fig. 1.1), the flux density profile in the interior of the plate depends on the pinning strength and the macroscopic screening currents which are induced in the bulk, in addition to the Meissner currents at the surface. In the Bean model for simplicity, the flux-density profile is taken to follow a constant gradient which gives a uniform screening current density  $J_{scr}$ .

Thus,

$$\mu \vec{J}_{scr} = d\vec{B}/dx = \text{constant. (Beans' model)}$$

Increasing the available pinning force per unit volume ' $\alpha$ ' permits larger flux density gradient and, therefore, larger screening current densities. For a stable configuration of flux in the plate, the Lorentz force at any point must not exceed the available local value of pinning strength ' $\alpha_c$ ', so we may write;



Fig[1.1] Internal flux density profiles for:

(a) Increasing & (b) Decreasing external magnetic field.

$$|\vec{J}_{scr} \times \vec{B}| \leq \alpha_c(\vec{B})$$

Where ' $\alpha_c$ ' is a function of local average flux density and temperature. Its value will also depend on the density and type of pinning center present. The relation between the critical current  $J_c$  and the hysteresis is as:

$$\Delta m = kJ_c d$$

Here  $k$  is a geometrical factor, and  $J_c$ , which can be evaluated from the width of the  $M(H)$  loop, approaches zero when hysteresis in the  $M(H)$  loop arises i.e.  $\Delta m = 0$ . The Bean model is more useful at low temperature and high critical current materials. However, it is too simple to completely explain the complex behavior which is generally observed.

### (1.7) Role of equilibrium magnetization in the critical state model

If reversible magnetization i.e. the value obtained for a homogenous type II superconductor on the basis of free energy minimization,  $[(\partial G/\partial B) = 0]$  is zero as assumed in the Bean-Kim's model, then irreversible  $M$  and  $B$  should be symmetric about  $H$ -axis [fig.1.2(a)]. However, this is not observed in the experimental  $M(H)$  or  $B(H)$  curves [fig.1.2(b)].  $M^+(H)$  is the value of magnetization at applied field  $H$  for increasing field and  $M^-(H)$  is the magnetization at field  $H$  for decreasing field. This is because the reversible magnetization is not zero and becomes significant for low field materials. For such magnetization loops, we can find  $M(\text{rev})$  magnetization from total  $M$  which comprises two parts, i.e.

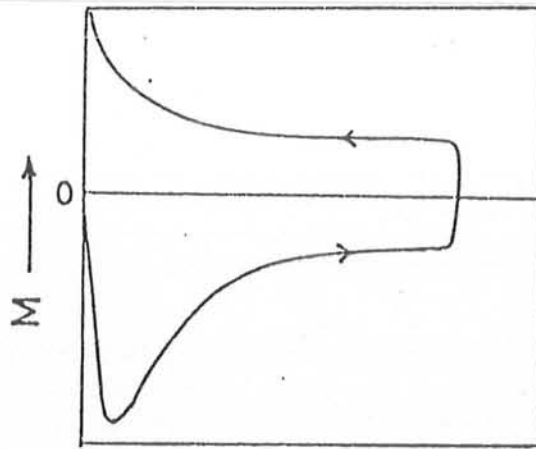
$$M = M_{\text{rev}} + M_{\text{irrev}}$$

From fig.1.2(b) we can find:

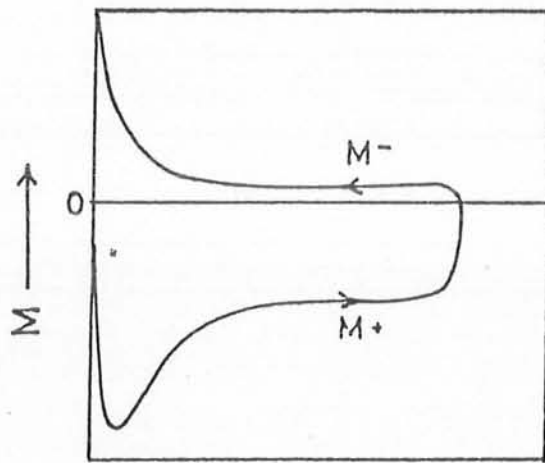
$$M^+(H) = M_{\text{rev}}(H) + M_{\text{irrev}}^+(H) \quad (i)$$

where  $M^+$  is the value for increasing fields.

$$M^-(H) = M_{\text{rev}}(H) + M_{\text{irrev}}^-(H) \quad (ii)$$



(a)  $H \longrightarrow$



(b)  $H \longrightarrow$

Fig[1.2] Critical state magnetization behavior for type-II superconductors with:  
 (a) Zero reversible magnetization & (b) Non-zero reversible magnetization.

where  $M^-$  is the value for decreasing fields.

According to critical state:

$$M_{\text{irrev}}^+(H) = -M_{\text{irrev}}^-(H)$$

or,

$$M_{\text{irrev}}^+(H) + M_{\text{irrev}}^-(H) = 0$$

i.e. the sum of the irreversible magnetization value for increasing fields and decreasing fields become equal to zero when the critical state is reached.

Adding equations (I) & (ii), we can get  $M_{\text{rev}}$  as:

$$M_{\text{rev}}(H) = [M^+(H) + M^-(H)]/2$$

### (1.8) Anderson-Kim model

In most superconductors, particularly in the high  $T_c$  superconductors field dependence of ' $J_c$ ' cannot be ignored, thus, the model put forward by Bean, where ' $\vec{J}_c = \text{constant}$ ', is not very useful. The field dependence of the critical current is incorporated in the Anderson-Kim model [25] by using the following form for  $J_c(B)$ :

$$\vec{J}_c = \alpha / [\vec{B} + \vec{B}_0] \quad (1)$$

i.e. the critical current and the loop width decrease inversely with the magnetic field.

Here ' $\alpha$ ' is the pinning density, ' $\vec{B}_0$ ' is the field parameter which limits  $\vec{J}_c$  as  $\vec{B} \rightarrow 0$ .

As the critical state current obeys the ampere's law i.e.

$$[\vec{\nabla} \times \vec{B}] / \mu_0 = 4\pi \vec{J} / c \quad (2)$$

the possible internal field and current distribution are in principal determined by solving equations (1) & (2).

### (1.9A) Irreversibility onset

It is to be noted that the onset of irreversibility or irreversible magnetization will be a function of temperature & magnetic field, since pinning itself is a function of T & H. Secondly, this onset will manifest itself, in the case of dc magnetization loops, by non vanishing hysteresis i.e.  $M_{\text{irrev}}$  or " $\Delta m = M^+ - M^- = 0$ ".

As the Anderson-Kim model suggests and most experiments clearly show that the hysteresis  $\Delta m$  decreases with magnetic field and temperature. This is because  $\Delta m$  depends on pinning which decreases with magnetic field and temperature. Thus for a particular temperature there is a particular maximum magnetic field upto which irreversibility effects persist

### (1.9B) The irreversibility line

The vanishing of hysteresis in dc magnetization loops can be attributed to several features viz., flux lattice melting, decrease of pinning and thermal activation effects. The melting of the flux lattice occurs due to the increased temperature and magnetic fields. Thus, at high temperature and magnetic field the vortex lattice becomes unstable. The vortices get unpaired and move freely because of the large  $\vec{J} \times \vec{B}$  forces. This results in the decrease of pinning force. Apart from the decrease in pinning force, the thermal activation effects are also incorporated in the vanishing of the irreversibility in dc magnetization loops. The relatively high operating temperatures (e.g. in high- $T_c$  materials) enable vortices to jump out of pinning barriers even when  $(\vec{J} \times \vec{B}) \ll \vec{F}_p$ . This type of behavior is called Thermally Activated Flux Flow (TAAF) [26]. It is of great relevance to



high- $T_c$  materials, and has been used extensively to explain the field and current dependence of dissipation in these materials.

Several experiments on high- $T_c$  superconductors can be explained by using the idea of TAFF and treated quantitatively by noting that the flux motion is a linear diffusion [26]. This diffusion of vortices is occurring along the flux density gradient. These features allow us to define an “irreversibility line” in the (H,T) plane, or more expressively called the “depinning line”,  $T_d(B)$  as suggested by Esquinazi [10], above which pinning effectively vanishes due to thermal, and magnetic effects. In the (H,T) region below the line, the material exhibits irreversible behavior.

In real superconductors there is almost always some pinning present. The predicted “flux lattice melting” effects compete with the change of the average pinning force density  $J_c B$  or critical current density  $J_c$ , which in high- $T_c$  superconductors may drop rapidly with increasing B(magnetic field) or T (temperature) due to thermally activated depinning.

The appearance of an “irreversibility line”  $T^*(H)$  in high- $T_c$  superconductors was reported by Muller et al [11]. According to them the irreversibility line, (which is a line separating the region in the (H,T) plane where the material shows reversible magnetization from that in which the magnetization depends on the previous path or magnetic and thermal history of the samples) appears in the following form:

$$1 - T^*(H)/T_c \propto H^{2/3} \quad 1.9(a)$$

Here  $T^*(H)$  is the irreversibility temperature and  $T_c$  is the bulk critical temperature in zero applied field. As 1.9(a) indicates, with increasing temperature the field region where irreversible behavior may be seen, becomes increasingly reduced, and vice-versa.

Theoretically, de Almeida and Thouless [12] first derived the line separating ergodic(non-hysteric) and non-ergodic(hysteric) regions.

$$H = H_0[1-T_g(H)/T_g(0)]^\gamma \quad 1.9(b)$$

where  $\gamma = 3/2$ .

Such a relation resembles known phenomena in spin glass physics [21] and was interpreted in terms of the “superconducting glass state”. In this picture, the irreversibility line, typical of glassy systems, originates in the randomness of the superconducting state, due to the weak links in the system. This model however has not been widely used. The sketch of the irreversibility line in the (H,T) plane, is shown in the figure (1.3).

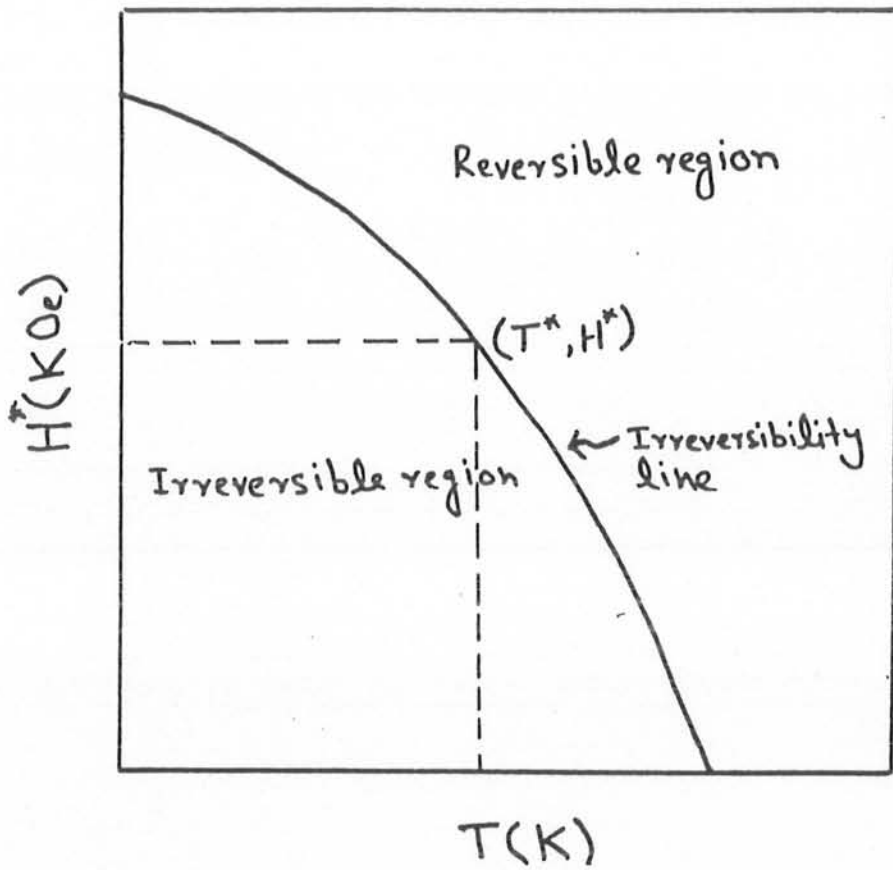
On the other hand Yeshurun and Malezemoff [13] derived a similar variation of  $T^*(H)$  in the classical flux pinning picture, considering the limitation of the critical current density by ‘giant’ or very large thermally activated flux creep. This model will be used in our work

### (1.9.1) Effect of thermal activation on the shape of the irreversibility line

We consider the role of thermal activation in the determination of critical current density using an approximate but well established relation for the variation of critical current density with magnetic field and temperature, viz.

$$\vec{J}_c = \vec{J}_{c0} [1-(KT_c/U_0)\ln(\vec{B}d\Omega/E_c)] \quad 1.9(c)$$

Here  $\vec{J}_{c0}$  is the critical current in the absence of thermal activation, “ $\vec{B}$ ” is the magnetic induction, “d” is the distance between pinning centers, “ $\Omega$ ” is oscillation frequency of a flux line in a pinning well and “ $E_c$ ” is minimum measurable voltage per meter. For typical parameters, the



Fig[1.3]

Sketch of the irreversibility line in the H-T plane exhibiting a non-linear behavior with  $H^*$  going to zero at  $T=T_c$ . The dotted lines depict the  $H^*$  (onset field) value corresponding to the temperature.

logarithmic term is about 30, but since  $KT/U_0$  is of the order of  $10^{-3}$  in conventional low temperature superconductors, the thermal activation term is negligible to 3% correction. But in case high  $T_c$  materials like YBCO, due to weak pinning and high temperature of operation the “ $(KT_c)/U_0$ ” term is nearly equal to “0.04”; and the activation term can be almost close to unity. Thus from equation (3) it is apparent that, critical current measurements and even magnetic measurements of  $H_{c2}(T)$  may be strongly affected by thermally activated flux creep. In particular, the creep term in equation (3) could contribute to the large temperature dependence of the measured critical current. This was described as “giant flux creep” by Yeshurun and Malezemoﬀ [13].

### (1.9.2) Field and temperature dependence of pinning potential “ $U_0$ ”

Next we consider the field and temperature dependence of  $U_0$  following reference [13]. They adopt a general scaling approach to obtain possible behaviors. For example near  $T_c$  and for sufficiently low applied field they use the Anderson-Kim form:

$$U_0 = H_c^2 \xi^3 / 8\pi \quad 1.9(d)$$

with clean limit Ginzburg-Landau formulae [1]

$$H_c = (1.73)H_{c0}(1-t) \quad (H_{c2} = (2)^{1/2}\kappa H_c) \quad (i)$$

$$\xi = (0.74)\xi_0(1-t)^{-1/2} \quad (ii)$$

where  $t = T/T_c$  is the reduced temperature. Putting (i)&(ii) in equation [1.9(d)], gives:

$$U_0 = [(1.73)H_{c0}(1-t)]^2 [(0.74)^3 \xi_0^3 (1-t)^{-3/2}]/8\pi \quad [1.9(e)]$$

simplifying one get,

$$U_0 = [(1.21) H_{c0}^2 \xi_0^3 (1-t)^{1/2}]/8\pi \quad [1.9(f)]$$

$a_0$  is the flux lattice spacing given as is usual by,

$$a_0 = (1.075)(\vec{\Phi}_0/\vec{B})^{1/2} \quad (iii)$$

Also,  $a_0 = f\xi_0$  or  $\xi_0 = a_0/f$ , with  $f$  about 6.  $U_0$  becomes limited in the two dimensions by  $a_0$ .

Along the third dimension the minimum possible characteristic length is  $\xi$ . Thus, one expect  $U_0$  to scale as:

$$U_0 = [H_c^2 \xi^2 \xi]/8\pi$$

$$\text{or } U_0 = [H_c^2 (a_0/f)^2 \xi]/8\pi$$

$$U_0 = [H_c^2 a_0^2 \xi]/8\pi f^2 \quad [1.9(g)]$$

putting the values of  $H_c$ ,  $\xi$  and  $a_0$  from (i), (ii) & (iii) in [1.9(g)] one get:

$$U_0 = [\{1.73H_{c0}(1-t)\}^2 \{1.075(\Phi_0/\vec{B})^{1/2}\}^2 \{(0.74)\xi_0(1-t)^{-1/2}\}] / 8\pi f^2$$

Simplifying we get,

$$U_0 = [(2.56) H_{c0}^2 \vec{\Phi}_0 \xi_0 (1-t)^{3/2}] / 8\pi f^2 \vec{B} \quad [1.9(h)]$$

This simple scaling argument predicts that “ $U_0$ ” decreases with temperature and leads to the conclusion that, thermal activation causes ‘ $\vec{J}_c$ ’ to drop below the measurement threshold above a critical temperature. This, brings about the onset of hysteresis. At this point “ $\vec{J}_c$ ” becomes zero, as the activation term of equation [1.9(c)] approaches to one (unity).

Now putting  $\vec{J}_c = 0$  in equation [1.9(c)] we get:

$$0 = \vec{J}_{c0} [1 - (KT_c/U_0) \ln(\vec{B}d\Omega/E_c)]$$

$$\text{or} \quad 1 = KT_c/U_0 \ln(\vec{B}d\Omega/E_c)$$

$$\text{or} \quad U_0 = KT_c \ln(\vec{B}d\Omega/E_c) \quad [1.9(j)]$$

Comparing equations [1.9(h)&(j)] we get,

$$KT_c \ln(\vec{B}d\Omega/E_c) = [(2.56) H_{c0}^2 \vec{\Phi}_0 \xi_0 (1-t)^{3/2}] / 8\pi f^2 \vec{B}$$

$$\vec{B}KT_c \ln(\vec{B}d\Omega/E_c) = [(2.56) H_{c0}^2 \vec{\Phi}_0 \xi_0 (1-t)^{3/2}] / 8\pi f^2 \quad [1.9(k)]$$

Here the linear term of “B” is dominant over the logarithmic term, so we regard

$\ln(B\Omega/E_c) \cong \text{constant} = D$ . Hence equation takes the form:

$$\vec{B}KT_cD = [(2.56 H_{c0}^2 \vec{\Phi}_0 \xi_0)(1-T/T_c)^{3/2}]/8\pi f^2$$

$$\text{or } (1-T/T_c)^{3/2} = D [8\pi f^2 KT_c / 2.56 H_{c0}^2 \vec{\Phi}_0 \xi_0] \vec{B} \quad [1.9(l)]$$

Here, the field “ $\vec{B}$ ” is approximately equal to “H”. So, we replace “ $\vec{B}$ ” with “H”.

$$\text{or } (1-t)^{3/2} \propto H \quad ; \text{ we put } t = T/T_c$$

$$\text{or } (1-t) \propto H^{2/3} \quad [1.9(m)]$$

Equation [1.9(m)] is the relation of the irreversibility line in the H-T plane. As the temperature is increased the field, at which the irreversibility point or magnetic hysteresis sets in, decreases correspondingly. Equation [1.9(m)] manifests that the irreversibility field  $H^*$  i.e. the field where the irreversible behavior appears first, decreases with the increasing temperature as a power of 2/3. It is to be noted, however, that the exponent of the irreversibility field  $H^*$  depends on the choice of  $H_{c2}$ . The factor of 2/3 appears only if we take the following usual form of  $H_{c2}$ :

$$H_{c2}(T) \propto (1-t)$$

If the  $H_{c2}(T)$  variation is different from the above assumed form, the equation of the irreversibility line will be changed accordingly.

In this dissertation we shall determine the onset of the irreversibility point at various temperatures experimentally, and see whether the relation [1.9(m)] is obeyed or not. Any deviation from this will be attempted to be explained.

## CHAPTER 2

### EXPERIMENTAL TECHNIQUES

#### (2.1) Vibrating Sample Magnetometer (VSM)

The measurement of magnetization with the applied magnetic field has been carried out by a VSM model BHV-50 of Riken Denshi co. Ltd., Japan. This is a Foner type B-H curve tracer in which a magnetized sample is vibrated at a fixed small amplitude and frequency (30 Hz) and the magnetization strength is found directly from the magnitude of the electromotive force induced in a coil placed in proximity with the sample. The block diagram of BHV-50 model is shown in figure (2.1).

The induced voltage can be obtained by placing a sensing coil, with cross-sectional area 'S' and number of turns 'N', at the XY-plane. The sample is allowed to vibrate at frequency 'w' in the z- direction and the field is along the x-direction. The induced voltage is obtained as, [15].

$$3NSawMx/4\pi r^5 \exp(iwt) \quad (2.1)$$

here M is the magnetization of the sample, S is the cross sectional area of the sample, "a" is the amplitude and "x" is the direction of the field.

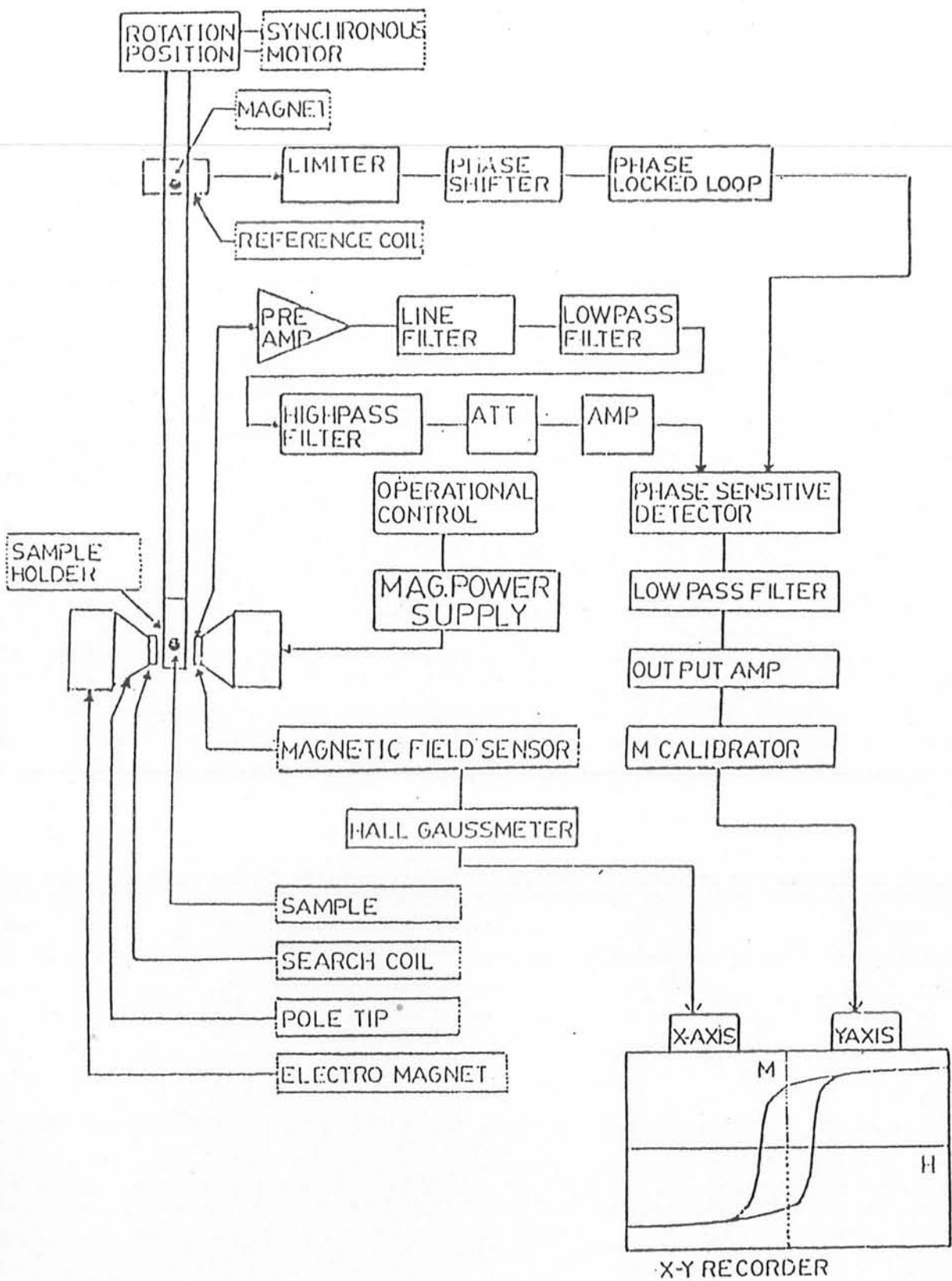
$$V = V_0 \exp(iwt) \quad (2.2)$$

Thereby, V becomes a sinusoidal wave having a frequency of w and an amplitude  $V_0$ , where:

$$V_0 = KafM \quad (2.3)$$

Where  $f = w/2\pi$  and is proportional to the vibrating frequency f and magnetic moment M of the sample. The proportionality constant K is given by [15]:





Fig[2.1] Block diagram of Vibrating Sample Magnetometer (VSM), BHV-50 model.

$$K = 3NSX/2r$$

(2.4)

The position and characteristics of the coil determines this constant  $K$ . If  $M$  is vibrated so that  $a$  and  $f$  remain constant then the electromotive force will be proportional to the magnetic moment  $M$ .

### (2.2) Sample holder

A non-magnetic sample holder made of teflon has been used for measurements. Fig 2.2 displays the dimensions of the holder. Over the entire temperature range ( $77K \leq T \leq 300K$ ), a negligible magnetic signal of the holder has been observed even for the highest fields applied.

### (2.3) Temperature measurement/Temperature control System

Two meters of copper/copper-nickel type T thermocouple wire which was insulated by glass fiber sleeving was used for the temperature measurements. The hot junction tip was welded in an argon atmosphere to eliminate any oxidizing effects of the junction. Type T thermocouple is suitable for measurements in confined spaces.

The thermocouple has been installed in the VSM in such a way that its wires passed through the vibrating rod of VSM and the teflon holder. Its tip was adjusted so that it just touches the surface of the sample (mounted upon the teflon holder). The reference junction was kept at 273K (Zero degree centigrade). The thermocouple voltage was noted by a DVM (Digital Voltmeter). The output voltage is then converted into temperature by consulting the table, prepared by calibrating against room temperature, and the freezing points of ice and ethanol.

## **(2.4) Cryostat**

### **(a) Glass Dewar**

A non-commercial glass dewar has been used for the measurements, since the measurements have been done at cryogenic temperatures (77K and above). This glass dewar can hold liquid nitrogen for longer times i.e. upto 50 minutes without refilling. This is a double walled glass dewar and the space between the two walls is evacuated so as to minimize the heat conduction from the surroundings (constructed at PINSTECH Glow Blowing Workshop).

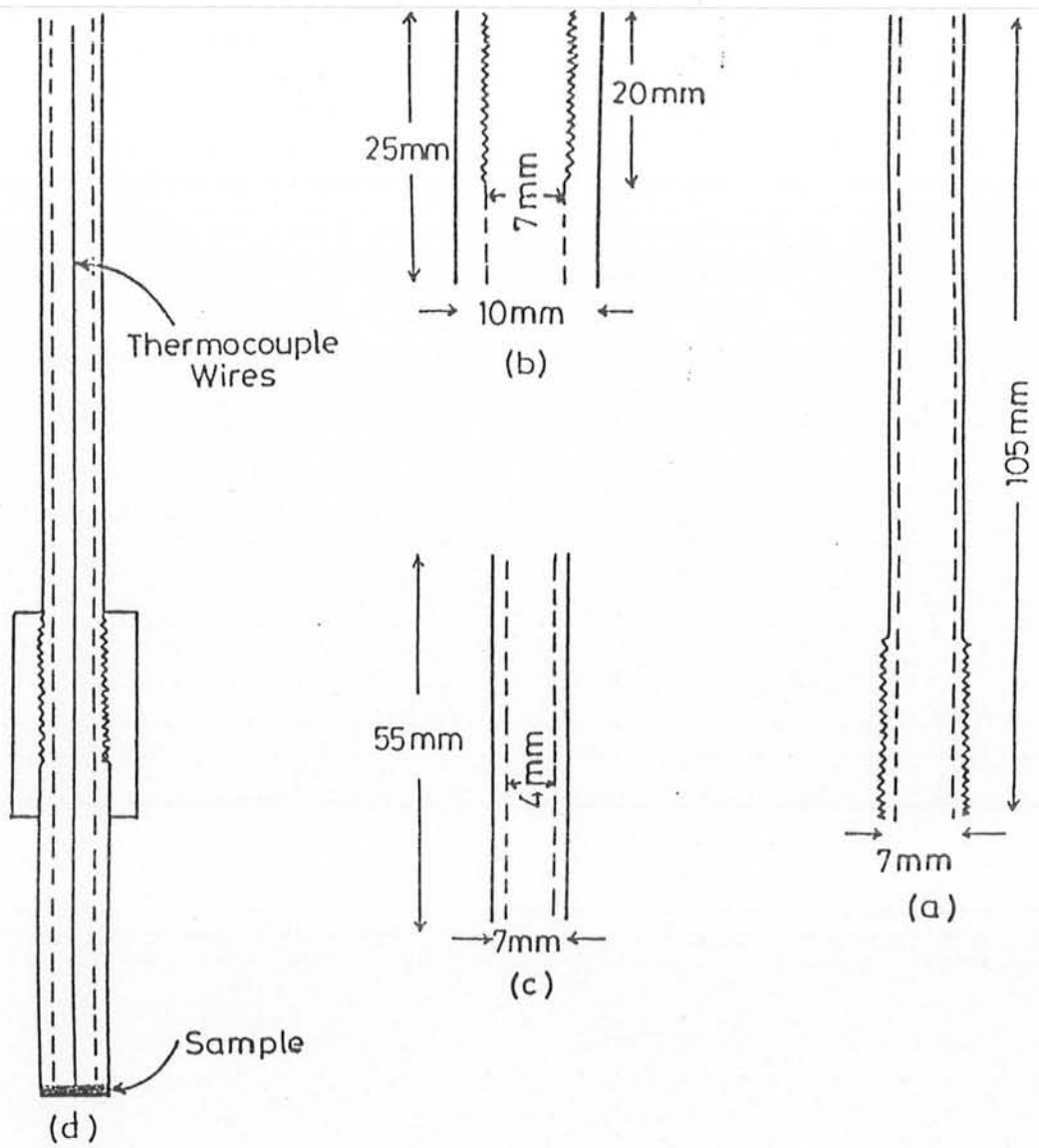
### **(b) Single walled glass tube**

A single walled glass tube was used to provide the sample surroundings with a space which had been evacuated. The temperature of the sample surroundings has been controlled through the volume of the liquid nitrogen in the glass dewar.

## **(2.5) Susceptometer**

We have used a susceptometer for measuring the “ac-susceptibility” of different samples using the principle of electromagnetic induction.

It consists of two coaxial coils, the primary and secondary coils are wound over non-magnetic ebonite core. The two halves of the secondary coil are wound in opposite senses to make the total induced emf equal to zero in the absence of a sample. Design and dimensions of this susceptometer are shown in figure(2.3).



Fig[2.2]

Diagram of different parts of sample holder:

(a) Steel pipe (b) Teflon holder (c) Glass pipe &

(b) The whole assembly of the sample holder.

The coils were tested for the balancing, after winding. Ideally the output of secondary coil should be zero, but in practice it is not so and we obtain a small signal. In order to reduce that signal, the secondary turns have been adjusted so that the output signal becomes negligibly small (approx., 1-2 $\mu$ v) for the temperature ranges  $77\text{K} \leq T \leq 150\text{K}$ .

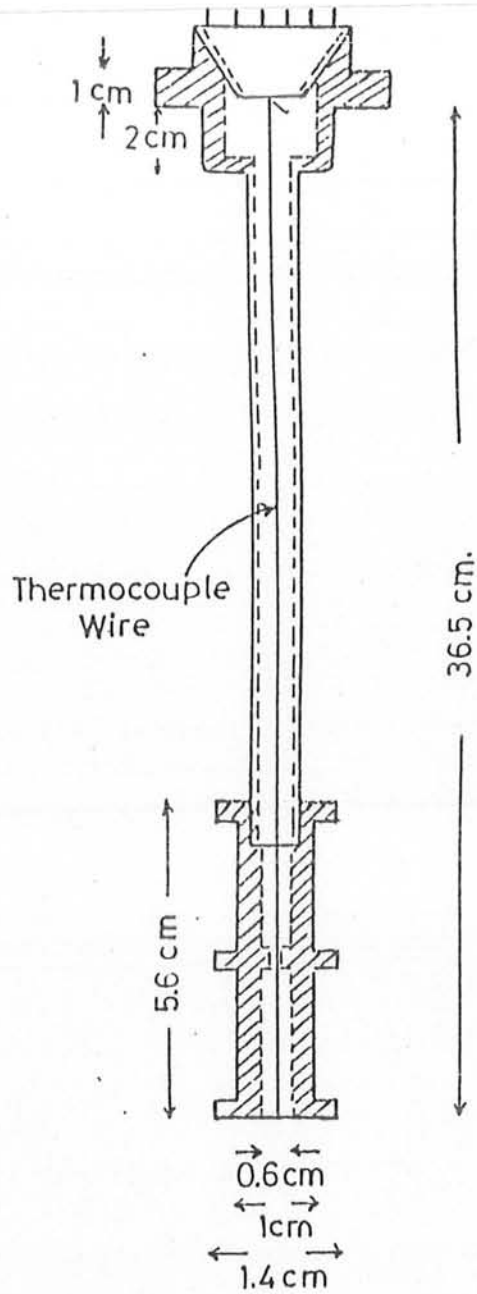
After assuring the minimum balanced signal, a stainless steel pipe has been attached with the coil, where core of the coil has a through hole of diameter 0.6cm. A copper-costantan thermocouple has been used to measure the temperature of the sample. Thermocouple wires were passed through the steel pipe and the coil and its lower end is maintained at the bottom of the coil where we placed our sample.

The other end of the pipe is connected to a multi-pin connector. The contact of the coil wires (primary and secondary) and the thermocouple wires with the equipment outside the cryostat has been made through this multi-pin socket. A coaxial cable with a multi-pin plug has been used for the above purpose.

### **(2.6.1) Variable temperature cryostat**

The susceptometer has been used inside a commercial variable temperature liquid nitrogen cryostat model DN 1710 Oxford Instruments Ltd.

In this cryostat a liquid nitrogen reservoir surrounds the central sample tube and supplies cryogen (liquid nitrogen) via capillary to a heat exchanger. During operation, the flow of liquid nitrogen is controlled by the gas exhaust valve on the cryostat top plate. The heat exchanger is fitted with a 100 ohm Platinum sensor, PT-100, and a heater for variable temperature operation in conjunction with the ITC-4 temperature controller.



Fig[2.3]

Design and dimensions of the Susceptometer.

### **(2.6.2) Temperature controller**

Temperature of the cryostat DN 1710 is being controlled by the temperature controller model ITC-4. Heater of the cryostat is being operated and controlled by ITC-4.

### **(2.6.3) Platinum resistance thermometry (Elements PT 100)**

Platinum film sensors are used for economical precise resistance temperature detection. It consists of a specially formulated platinum ink deposited on an alumina substrate, laser trimmed to form a highly stable metal resistance element. Rated between  $-50^{\circ}\text{C}$  and  $+50^{\circ}\text{C}$  the element characteristic conforms to the temperature resistance relationship defined by the international practical temperature scale 1968, and as such is a derivative of resistance temperature standards. These devices are easily installed by constructing simple bridge circuits, which generates an output voltage characteristic equivalent to the temperature change. This sensor is used to control the temperature in the inner chamber of the cryostat.

### **(2.6.4) Lock-in amplifier**

Lock-In amplifiers are commonly used to get rid of unwanted signal or noise. Ithaco Model 3921, Ithaco, INC Lock-In amplifier has been used. By supplying the reference signal (at the frequency of the primary coil) to the amplifier input, we can take the amplified output with the amplification of upto  $10^6$  for the desired phase, i.e. we can monitor both the in phase and out of phase parts of the secondary voltage. For looking at different phases we can use either the manual or automatic mode. In manual mode the reference phase is fixed by the user, while in auto mode the Lock-in searches for the phase where the largest signal is seen.

## (2.7) Susceptibility measurement technique

We have used a susceptometer for the measurements of susceptibility. The susceptometer, cryostat and temperature controlling system have been described in section (2.4) and the block diagram of the whole system is shown in figure (2.4).

As the primary and secondary coils are designed as a solenoid, so whenever we pass a current "I" through the primary coil there is a uniform magnetic field "H" developed inside the solenoid. The value of "H" is given by the relation [16]:

$$H = 4\pi I' \beta / 10(1+\beta^2)^{1/2} \quad (2.7.1)$$

Where  $I' = NI/2b$ ,  $\beta = b/a$ , I is the current in amperes, "N" is the number of turns of the primary coil, "2b" is the length and "a" is the internal radius of the solenoid. In our case it can be seen that:

$$\beta/(1+\beta^2)^{1/2} \cong 1 \quad (2.7.2)$$

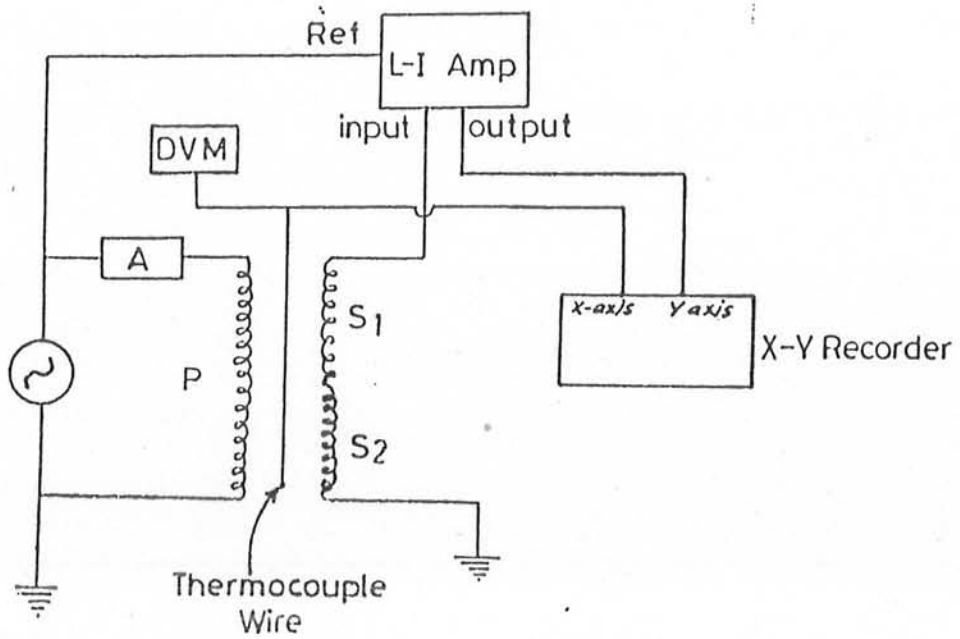
So the equation (2.7.1) reduces to:

$$H = 4\pi I'/10 \quad (2.7.3)$$

This equation will be used in calculating "H" in Oersteds.

When we pass the current through the primary coil, the sample experiences the field due to current inside the coil. Since the sample is placed in the lower half of the secondary coils, that part of the secondary coil would pick up the signal due to the sample and a net voltage is





Fig[2.4] Block diagram of ac susceptibility measurement system.

developed around the secondary coil, i.e. the coils would go off balance. This voltage is taken to the Lock-In amplifier where it is filtered and amplified.

The coil assembly has been placed inside the cryostat in order to be able to change the temperature during the experiment.

## CHAPTER 3

### RESULTS AND DISCUSSION

The determination of the onset point of irreversibility of magnetization and its variation with sample type and temperature has been studied. The variation of the onset point with field and temperature is compared to the theory.

The experimental work can be divided into two major portions.

(3.1) Measurements of dc magnetization loops of a variety of high- $T_c$  superconductors at various temperatures, and determination of the irreversibility line which separates the reversible region from the irreversible region in the H-T phase space. The onset of the irreversibility is determined by locating the field where the hysteresis in the M(H) loop is first observed. The process was carried out for several samples.

(3.2) Measurement and analysis of ac susceptibility  $\chi_{ac}$  of one of the sample  $[\text{Bi}_{1.6} \text{Pb}_{0.3} \text{Sb}_{0.1}] \text{Sr}_2 \text{Ca}_2 \text{Cu}_3 \text{O}_{9-\delta}$  used in (3.1). The variation of  $\chi_{ac}$  with temperature has been studied for both the dc field cooled (FC) and zero field cooled (ZFC) measurements for several values of the dc applied field. A well defined temperature "T\*" marks the FC and ZFC bifurcation, thus separating reversible and irreversible regimes[18]. When T approaches T\*, from above, the value of  $\chi$ , for the zero field cooled and field cooled cases become different. The variation of T\*(H) is compared to the results of (3.1), and to the predictions of chapter No.1.

### (3.1) dc Magnetization Measurements

The observation of  $M(H)$  loops at various temperatures in (3.1) is impelled by the idea that the isothermal field dependence of the magnetization provides us with a method for obtaining the irreversibility line[17]. The temperature  $T^*$  which is defined as the temperature which separates the reversible and irreversible regions is magnetic field dependent and scales with the applied field as  $H^n$ . The exponent 'n' varies considerably in high- $T_c$  systems [11,13,18,19].

The procedure for getting the magnetization curve starts with zero field cooling (ZFC) of the sample to 77K. Then the magnetization is recorded while the field is increased upto a certain maximum value, and then the field is decreased to zero. The irreversibility or hysteresis between the increasing and decreasing branches is recorded. The onset of the hysteresis or irreversibility is thus obtained from the  $M(H)$  loop. This procedure is repeated at various temperatures and hence the field for onset of irreversibility ( $H^*$ ) is obtained as a function of temperature [17].

This procedure has been carried out for the following three samples.

- \*  $(\text{Bi}_{1.6}\text{Pb}_{0.3}\text{Sb}_{0.1})\text{Sr}_2\text{Ca}_2\text{Cu}_3\text{O}_{9.8}$  (Labelled BPS)
- \*  $\text{Y}_1\text{Ba}_2\text{Cu}_3\text{O}_{7.8}$  (Labelled YBCO)
- \*  $\text{Hg}_1\text{Ba}_2\text{Ca}_2\text{Cu}_3\text{O}_{x+8}$  (Labelled Hg-4)

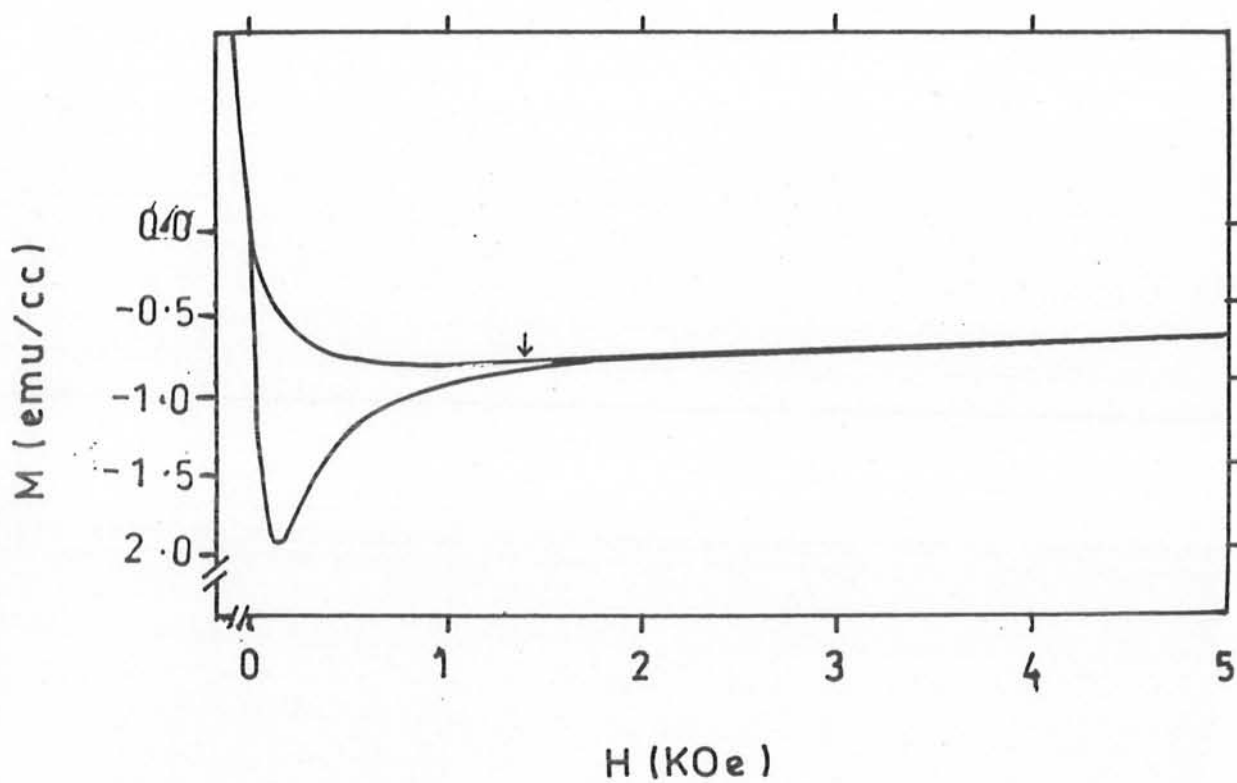
The samples labelled as BPS and YBCO were made in the Superconductivity Laboratory. Whereas, the sample labelled as Hg-4 was acquired from Dr. Jamil A. Khan, of PINSTECH. All the three samples are of granular nature.

Sample BPS has its  $T_c$  at 107K . The maximum magnetization " $\sigma_{max}$ " measured for the BPS sample at the temperature of 77K is 1.8 emu/cc as is shown in figure [3.1(i)]. Whereas, at a higher temperature i.e. 99K the maximum magnetization value " $\sigma_{max}$ " for the BPS sample reduces to 1.1 emu/cc.

The  $T_c$  of sample YBCO is 93K . The maximum magnetization " $\sigma_{max}$ " obtained for sample YBCO is 4.2 emu/cc. This value of magnetization is observed at a temperature of 77K. Like BPS sample, here also at higher temperature i.e. 89.3K the maximum magnetization value " $\sigma_{max}$ " noted for YBCO sample decreases to 2.9 emu/cc. Figures [3.2(i)] & [3.2(vi)] portray these values respectively.

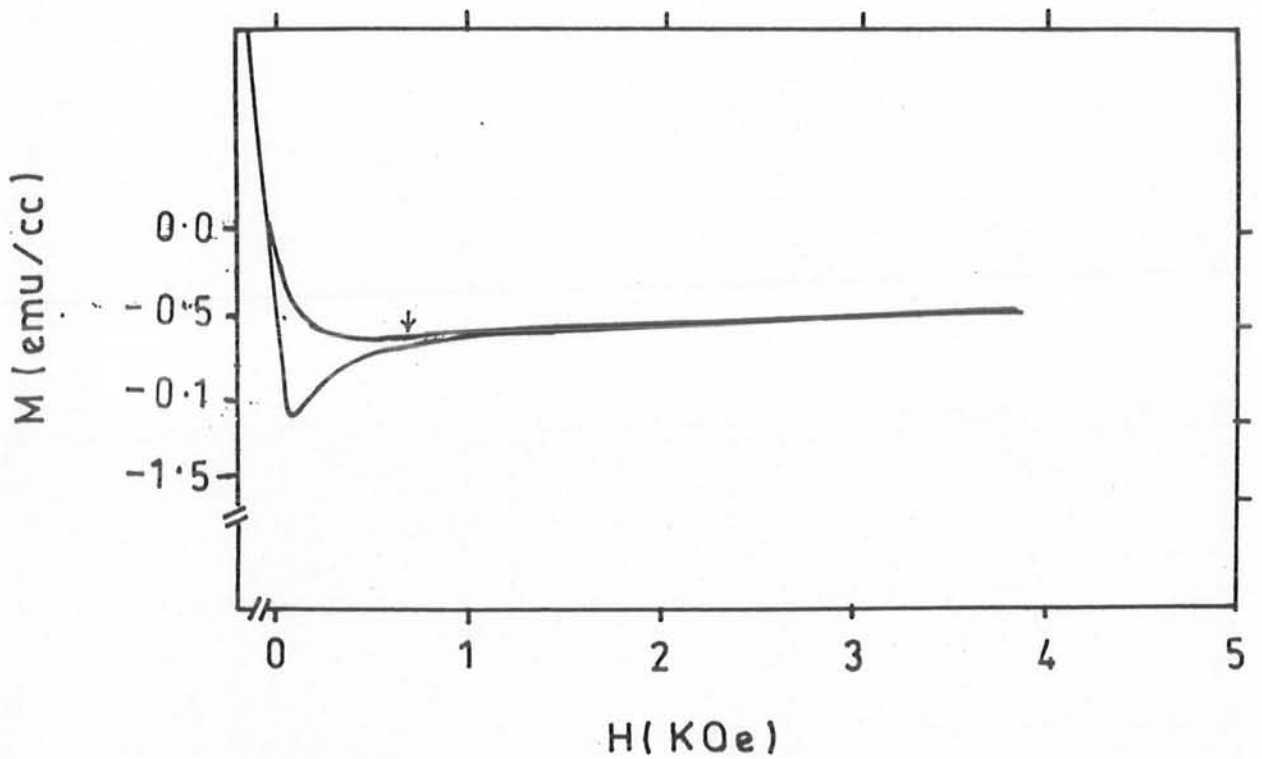
The  $T_c$  of sample Hg-4 is 130K. The maximum magnetization " $\sigma_{max}$ " measured for the sample Hg-4 at the temperature of 77K is 9.3 emu/cc as is shown in figure [3.3(i)]. At a higher temperature i.e.125K the maximum magnetization value " $\sigma_{max}$ " noted for the Hg-4 sample reduces to 4.7 emu/cc as shown in the figure [3.3(v)].

The three samples chosen to be studied differ in some important respects. The  $T_c$ s of the these three samples, are markedly distinct and hence enabling us to analyze the irreversibility line for materials with different  $T_c$ s. Also, the YBCO sample has a relatively stronger pinning as evident from the hysteresis loop widths shown in the figures [3.2 (i)]. The BPS sample is well known to be a weak pinning system, and the loop closes completely around  $H = 1700$  Oe at  $T = 77K$  , whereas, at  $T = 99K$  the  $M(H)$  loop closes at  $H = 1100$  Oe as depicted in the figures [3.1(i) & (v)].

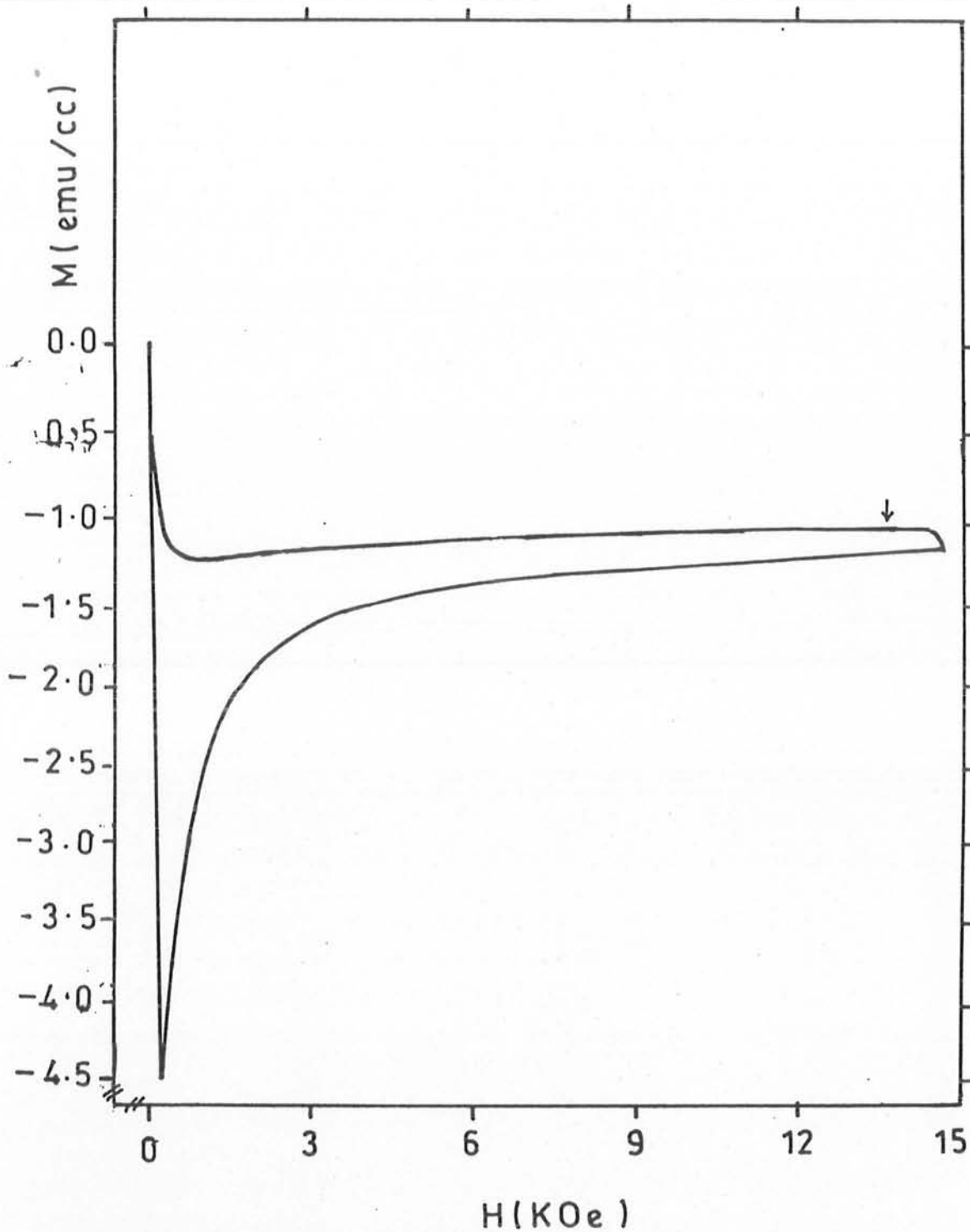


Fig[3.1(i)]

Typical magnetization behavior of sample BPS at 77K with the variation of applied magnetic field. The maximum field applied is 5 Koe, whereas the arrow is indicating the onset point of the hysteresis at the field value  $H^* = 1280$  Oe.

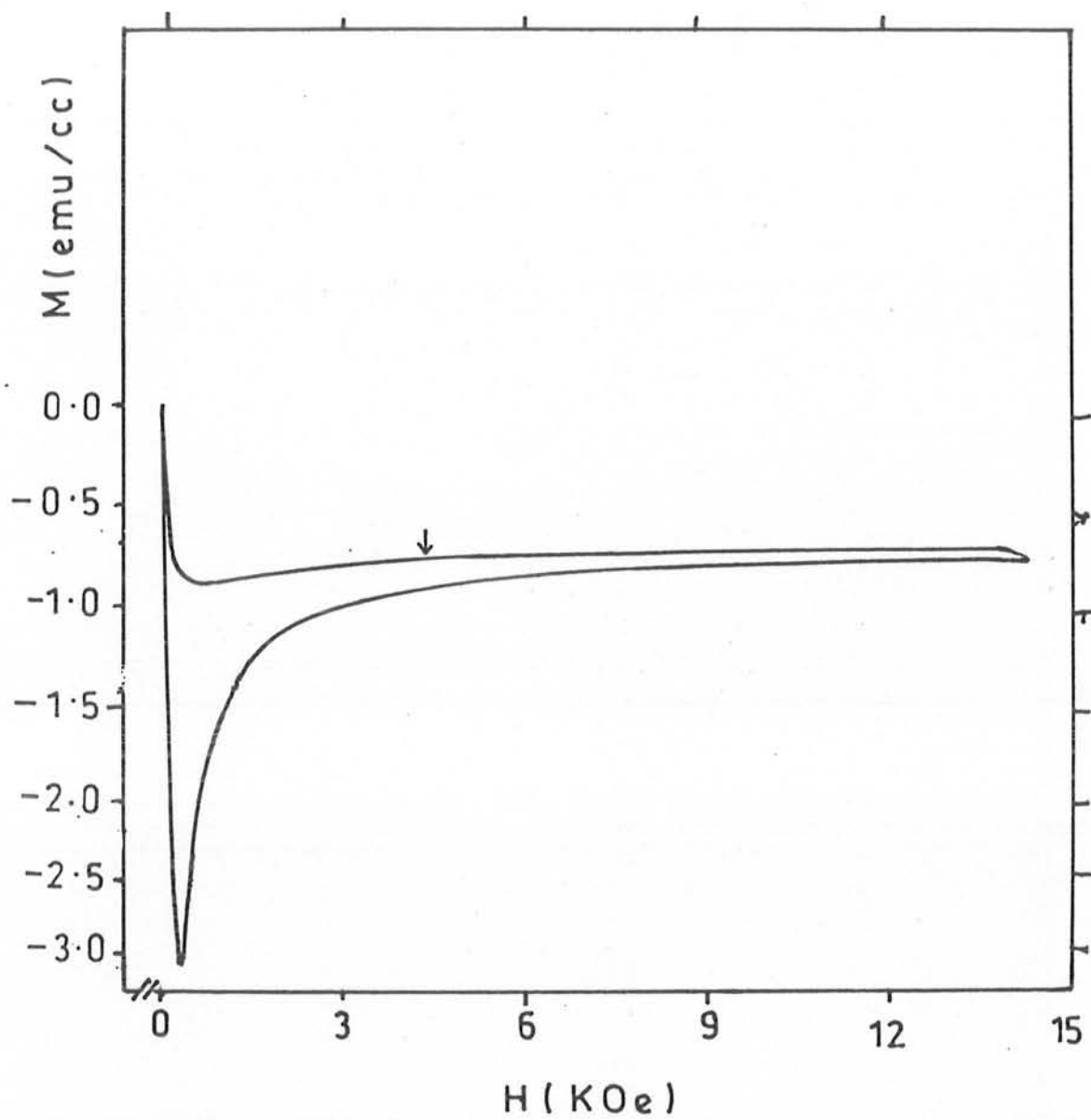


Fig[3.1(v)] Typical magnetization behavior of sample BPS at  $(99 \pm 0.3)$  K with the variation of applied magnetic field. The maximum field applied is 5 Koe, whereas the arrow is indicating the onset point of the hysteresis (as defined in the text) at the field value  $H^* = 502$  Oe.

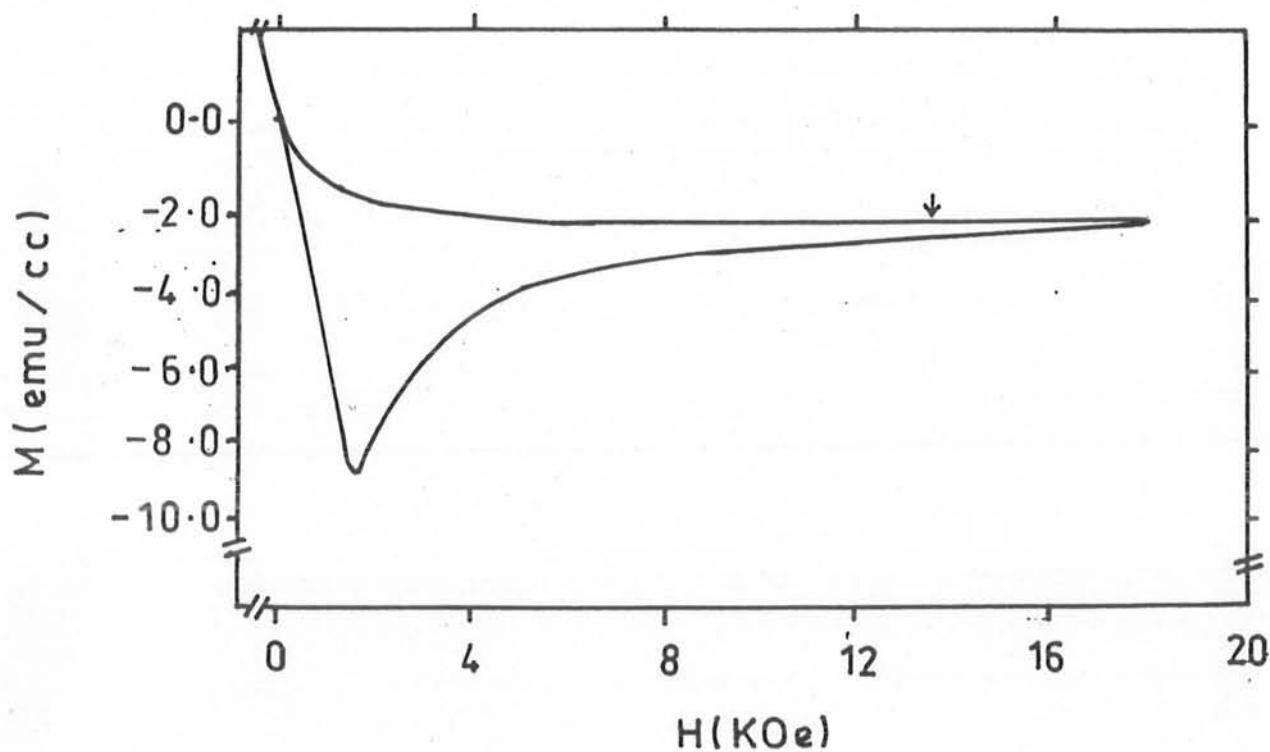


Fig[3.2(i)] Typical magnetization behavior of sample YBCO at 77 K with the variation of applied magnetic field. The maximum field applied is 15 Koe, whereas the arrow is indicating the onset point of the hysteresis (as defined in the text) at the field value  $H^* = 13552$  Oe.

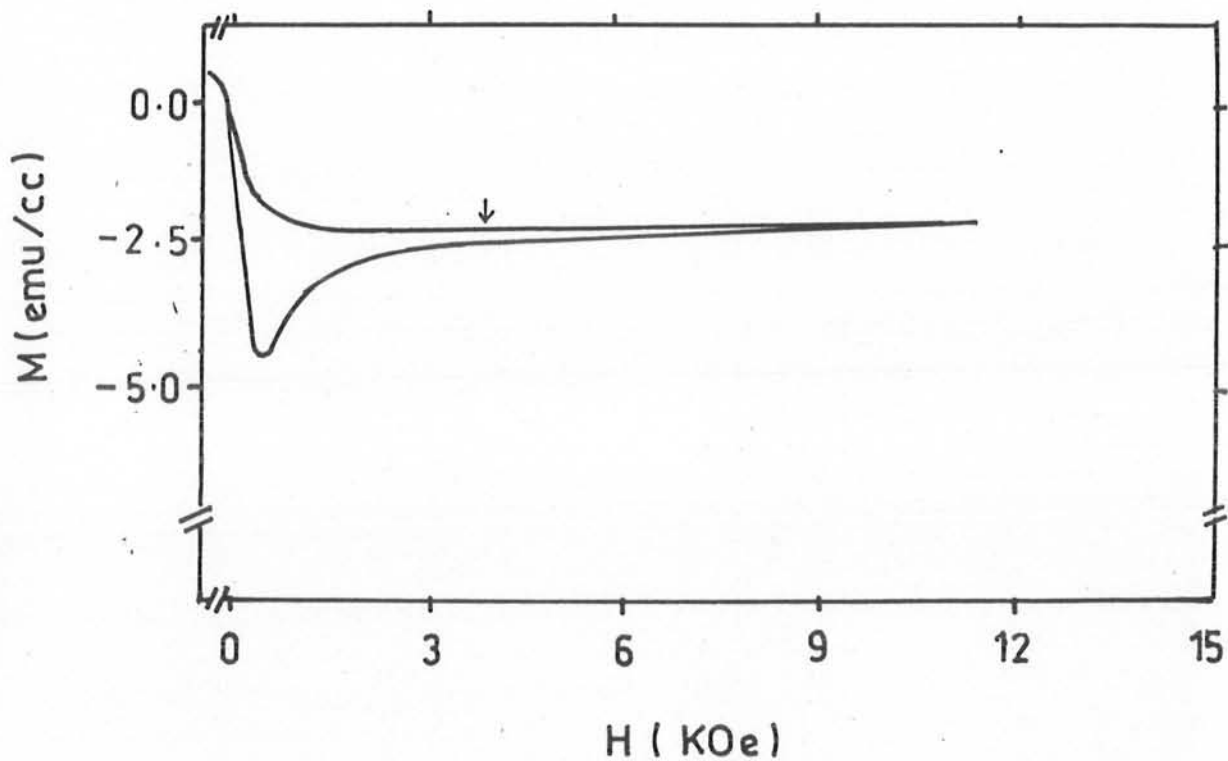




Fig[3.2(vi)] Typical magnetization behavior of sample YBCO at  $(89.3 \pm 0.3) \text{ K}$  with the variation of applied magnetic field. The maximum field applied is 15 Koe, whereas the arrow is indicating the onset point of the hysteresis (as defined in the text) at the field value  $H^* = 4004 \text{ Oe}$ .



Fig[3.3(i)] Typical magnetization behavior of sample Hg-4 at 77 K with the variation of applied magnetic field. The maximum field applied is 20 Koe, whereas the arrow is indicating the onset point of the hysteresis (as defined in the text) at the field value  $H^* = 13870$  Oe.



Fig[3.3(ix)] Typical magnetization behavior of sample Hg-4 at  $(125 \pm 0.4)$  K with the variation of applied magnetic field. The maximum field applied is 15 Koe, whereas the arrow is indicating the onset point of the hysteresis (as defined in the text) at the field value  $H^* = 3520$  Oe.

Typical Magnetization behavior of the samples BPS, YBCO & Hg-4 at 77K with the variation of applied magnetic field is displayed in the figures [3.1(i), 3.2(i), 3.3(I)].

The Hg-4 sample appears intermediate between samples BPS and YBCO regarding their loop widths. The loop width of sample Hg-4 is less than the loop width of sample YBCO but more than the sample BPS at the same temperature. Hence we are studying the effects in samples with a definite trend of decrease of pinning (YBCO  $\rightarrow$  Hg4  $\rightarrow$  BPS),

It is illustrative here to set a criterion, so as to determine the onset point of the irreversible behavior in H-T plane from the M(H) loop. This condition is fulfilled by setting a definite standard for the definition of the hysteresis onset.

Ideally, the point in the M(H) loops where  $\Delta M$ , the width of the loop is nearly equal to zero i.e.  $\Delta M \sim 0$ , should be selected as the onset point of the irreversible regime[17]. However, in practice this choice is not always feasible. For instance in our case the maximum field value available is not sufficient to close the hysteresis loops of the YBCO & Hg-4 samples. Hence a reasonable but consistent criterion has to be set which would be followed for a given sample. Even in the ideal case e.g. for BPS, where the loops do close, it is much more convenient to define a particular loop width as  $\Delta M \cong 0$ ; rather than trying to identify actual  $\Delta M = 0$ .

Hence in our case, we decided that the field at which the resolvable hysteresis in magnetization data on the XY charts is  $\Delta M \sim 1\text{mm}$  or the  $M^+(H)$  and  $M^-(H)$  are 1mm apart is considered to be the onset point of the irreversible regime. The value of  $\Delta M \sim 1\text{mm}$  corresponds roughly to 3.5 % of maximum hysteresis for BPS and to 2.7% for Hg-4 at 77K. The above criterion has been set for Hg-4 & BPS samples. The behavior of the YBCO sample is quite different from these two samples, because of its relatively strong pinning strength. So we decided that the field at which  $\Delta M \sim 4\text{mm}$  would be considered to be the onset point of the irreversible

regime, where the choice of 4mm for YBCO corresponds to  $\Delta M/\Delta M(\max) = 4.3\%$  at 77K.

While these choices of  $\Delta M = 1\text{mm}$  &  $4\text{mm}$ , appear very arbitrary, it should be emphasized that once a criterion has been set for a given sample and obeyed consistently for all temperatures, it can only result in an error in the definition of  $T_c$  obtained from  $T^*$  vs  $H$  curves, but not in the shape of the  $T^*(H)$  function. This is because the data is used in scaled form i.e.  $[t=(T^*/T_c)]$  where the irreversibility line is determined.

Now consider the case of BPS sample, where the field has been increased upto 5Koe and then decreased to zero, at 77K temperature [fig(3.1(i))]. Using the above criterion of loop width  $\Delta M = 1\text{mm}$  as the onset of irreversibility, we find that above  $H = 1280$  Oe applied field, the system enters into the reversible regime, whereas, below this field the system reverts to the irreversible region. Hence this field value of 1280 Oe (at 77K) is the onset point of the irreversible regime. Thus one  $M(H)$  loop at a certain temperature: yields one point in the  $H$ - $T$  plane:  $H^*$  &  $T^*$ , i.e. the irreversible field  $H^*$  corresponding to the temperature  $T^*$ . This is the point obtained at the lowest temperature achievable by us i.e. 77K.

Qualitatively very similar curves to fig [3.1 (i)] have been obtained at various temperatures for sample BPS. As the temperature increases the closure of the loops occur at relatively lower fields, e.g. at  $T = 92\text{K}$ ,  $H^* = 810$  Oe, at  $T = 95\text{K}$ ,  $H^* = 697$  Oe, at  $T = 97.5$  K,  $H^* = 589$  Oe, at  $T = 99\text{K}$ ,  $H^* = 502$  as shown in the figures [3.1(i), (ii), (iii), (iv), (v)] . This data of  $T$ ,  $t$  &  $H^*$  is illustrated in table [I]. The graph of  $H^*$  vs  $T$  is shown in the figure [3.4], exhibiting a non-linear behavior with  $H^*$  going to zero at  $T = 107\text{K}$ . This is the irreversibility line in the  $H$ - $T$  phase space.

The same procedure has been adopted for the rest of the two samples i.e. YBCO and Hg4. The maximum field applied to these samples was 15KOe. For YBCO the onset of hysteresis

is taken as the point where  $\Delta M \sim 4\text{mm}$ , as discussed earlier. In this case the onset of hysteresis varies from  $H^* = 13552 \text{ Oe}$  at  $T = 77\text{K}$  to  $H^* = 4004 \text{ Oe}$  at  $T = 89.3\text{K}$  approx. Figures 3.2 (I), (ii), (iii), (iv), (v), (vi) detail this behavior. This data is displayed in table [II] and the graph of  $H^*$  vs  $T$  is shown in the figure [3.5]. The graph extrapolates smoothly to zero at  $T \sim 92.5\text{K}$ ; again as the critical temperature.

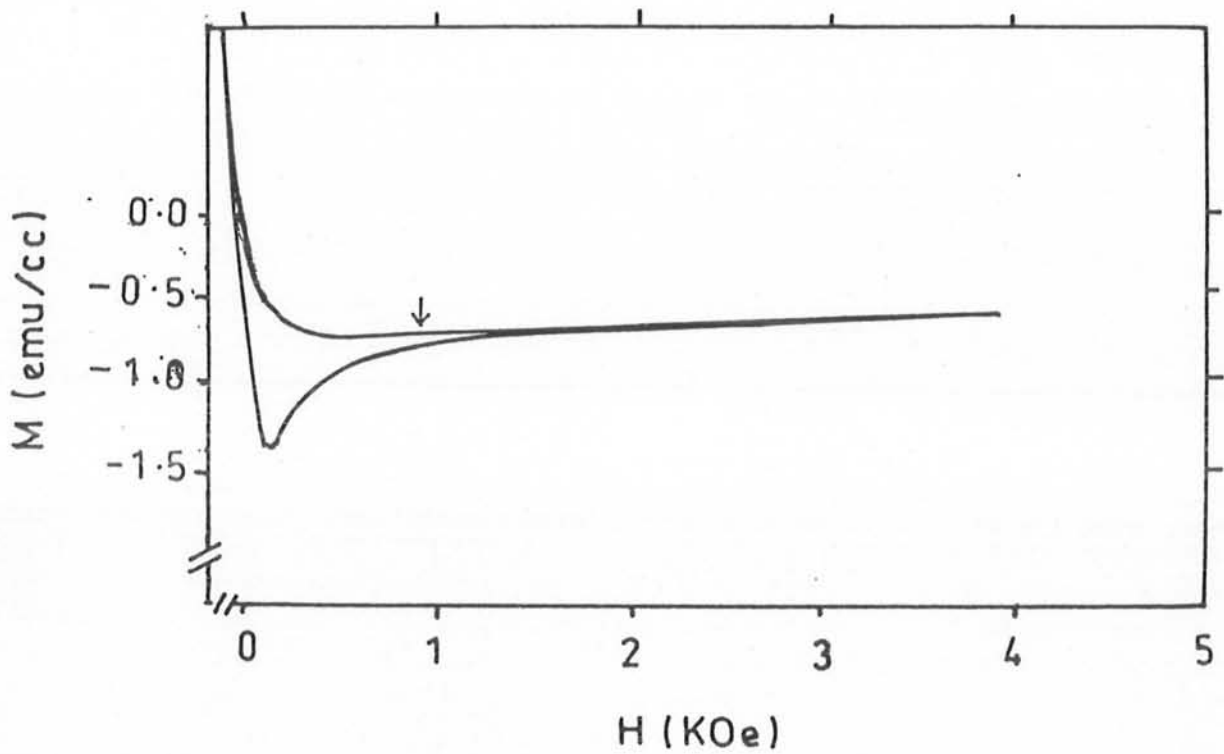
We observed that in case of sample Hg-4 the onset of hysteresis (the onset point has been obtained with the help of the above defined criteria  $\Delta M = 1\text{mm}$ ) varies from  $H^* = 13870 \text{ Oe}$  at  $T = 77\text{K}$  to  $H^* = 3520 \text{ Oe}$  at  $T = 125\text{K}$  approx. Figures, 3.3 (i), (ii), (iii), (iv), (v), (vi), (vii), (viii), (ix) shows the  $M(H)$  loops in this region. The variation of  $H^*(T)$  is depicted in table [III] and the graph of  $H^*$  vs  $T$  is shown in the figure [3.6]. It seems suggested from the graph that the hysteresis vanishes at  $T = 130\text{K}$ , very close to the “ $T_c$ ” measured by the resistivity and susceptibility.

The field dependence of  $T^*$  is shown in the form of a field- temperature phase diagram. The data of all the three samples reveals that the irreversibility point shifts from higher fields to lower fields with the increase of temperature. This is as expected because with the increase of temperature the pinning decreases. It is also clear that  $H^*(T)$  varies non-linearly. Also that  $H^*(T)$  goes to zero at:

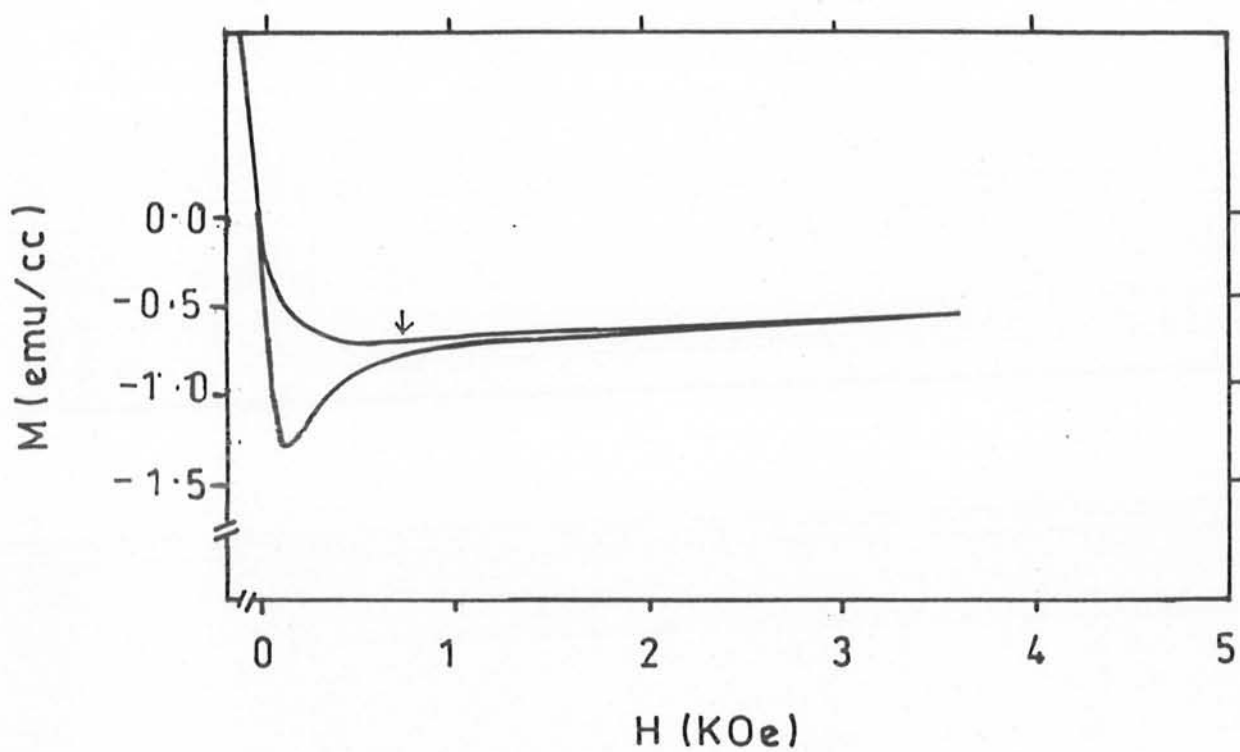
$T = 92.5\text{K}$ , for YBCO sample

$T = 107\text{K}$ , for BPS sample

$T = 130\text{K}$ , for Hg-4 sample

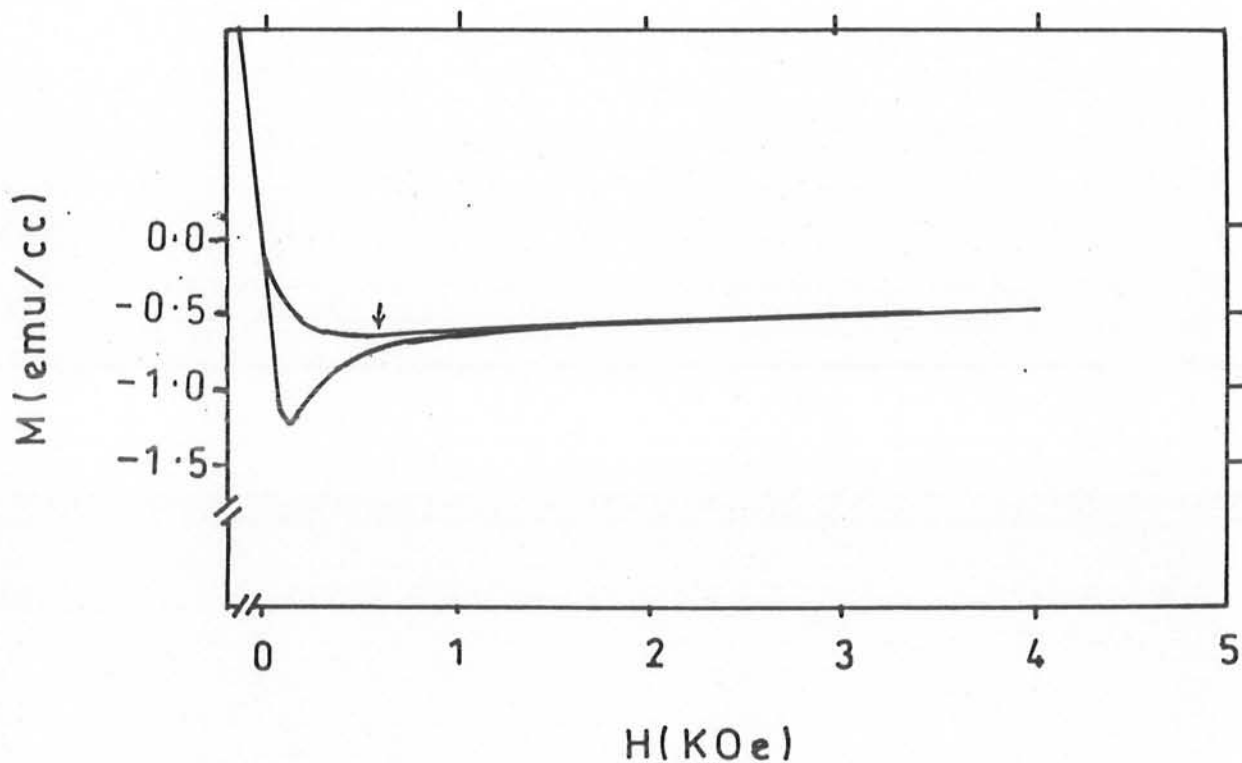


Fig[3.1(ii)] Typical magnetization behavior of sample BPS at  $(92 \pm 0.3)K$  with the variation of applied magnetic field. The maximum field applied is 5 Koe, whereas the arrow is indicating the onset point of the hysteresis(as defined in the text) at the field value  $H^* = 810$  Oe.



Fig[3.1(iii)] Typical magnetization behavior of sample BPS at  $(95 \pm 0.4)\text{K}$  with the variation of applied magnetic field. The maximum field applied is 5 Koe, whereas the arrow is indicating the onset point of the hysteresis (as defined in the text) at the field value  $H^* = 697$  Oe.



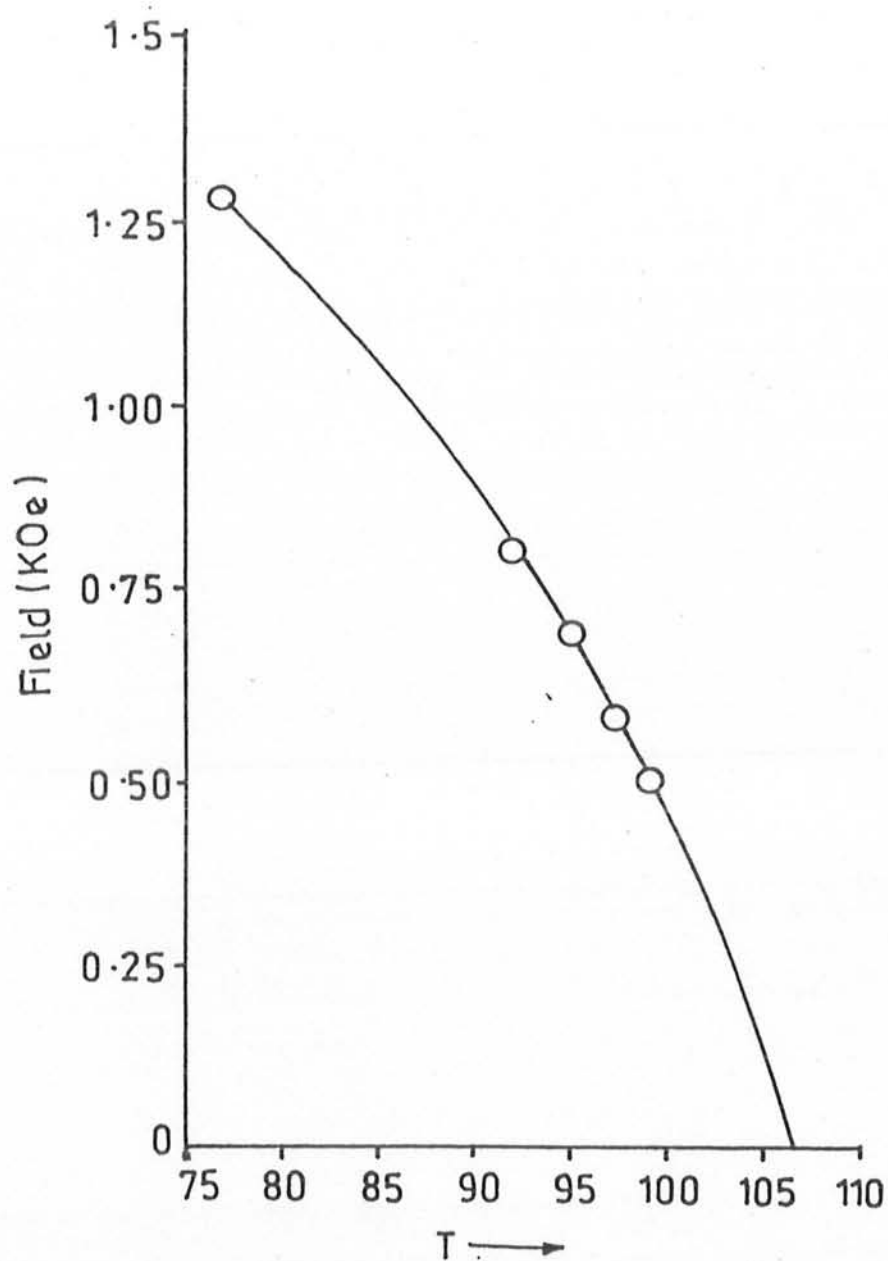


Fig[3.1(iv)] Typical magnetization behavior of sample BPS at  $(97.5 \pm 0.3)$  K with the variation of applied magnetic field. The maximum field applied is 5 Koe, whereas the arrow is indicating the onset point of the hysteresis (as defined in the text) at the field value  $H^* = 589$  Oe.

**Sample BPS ( $T_c = 107K$ )**

<b>T(K)</b>	<b><math>t=T/T_c</math></b>	<b>H*(Oe)</b>
<b>77</b>	<b>0.72</b>	<b>1282</b>
<b><math>92 \pm 0.3</math></b>	<b>0.86</b>	<b>810</b>
<b><math>95 \pm 0.4</math></b>	<b>0.89</b>	<b>697</b>
<b><math>97.5 \pm 0.3</math></b>	<b>0.91</b>	<b>589</b>
<b><math>99 \pm 0.3</math></b>	<b>0.93</b>	<b>502</b>

**Table [I]:** Data of Temperature T(K), reduced temperature  $t$  ( $T/T_c$ ) and the magnetic field  $H^*$  (Oe) at which the hysteresis of the M(H) loop first appears.



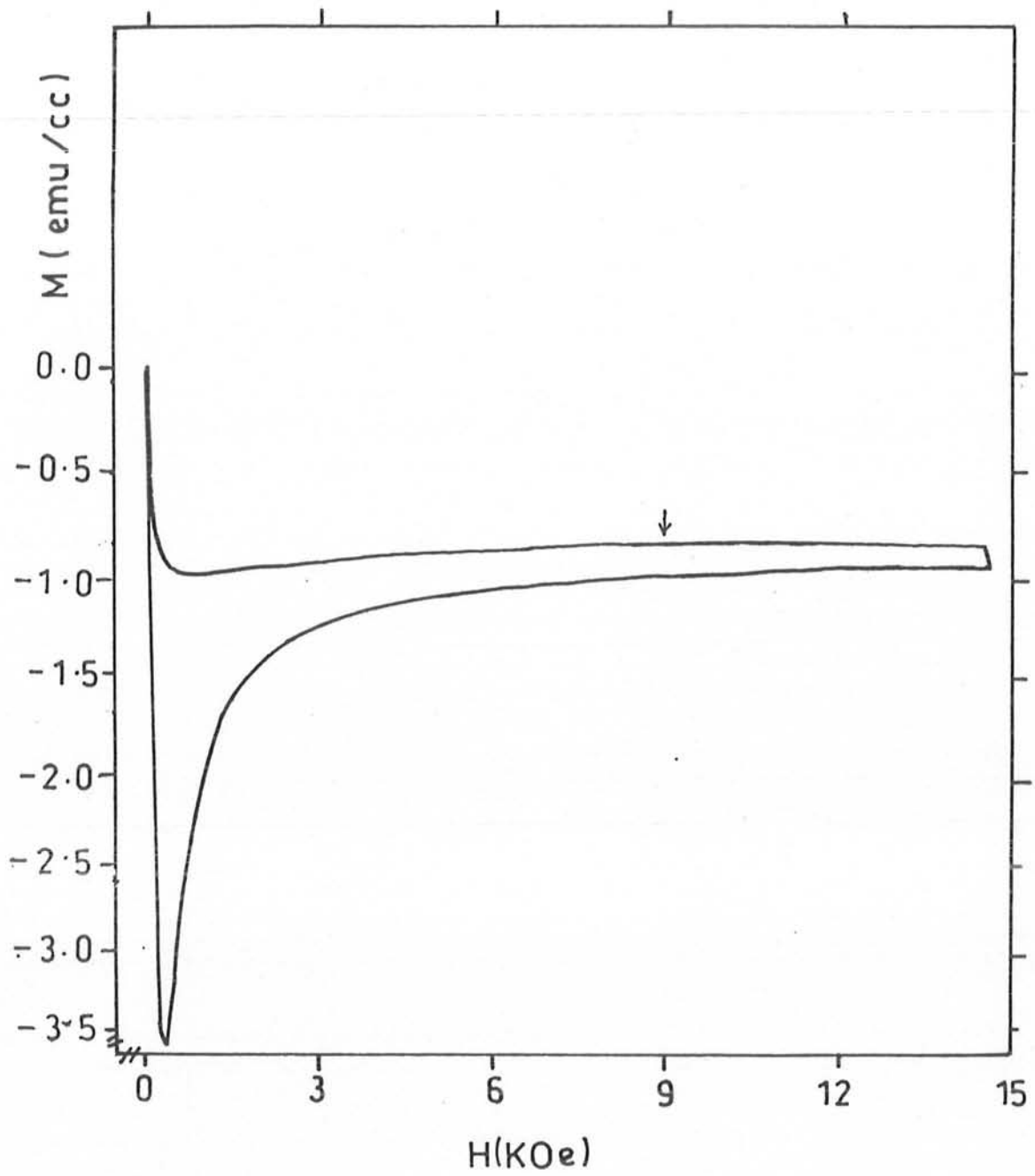
Fig[3.4]

Graph of  $H^*$  vs  $T$  plotted on the data obtained from the dc  $M(H)$  measurements of sample BPS. This is the irreversibility line in the  $H$ - $T$  plane which exhibits a non-linear behavior with  $H^*$  going to zero at  $T = 107\text{K}$  (line is a guide to the eye).

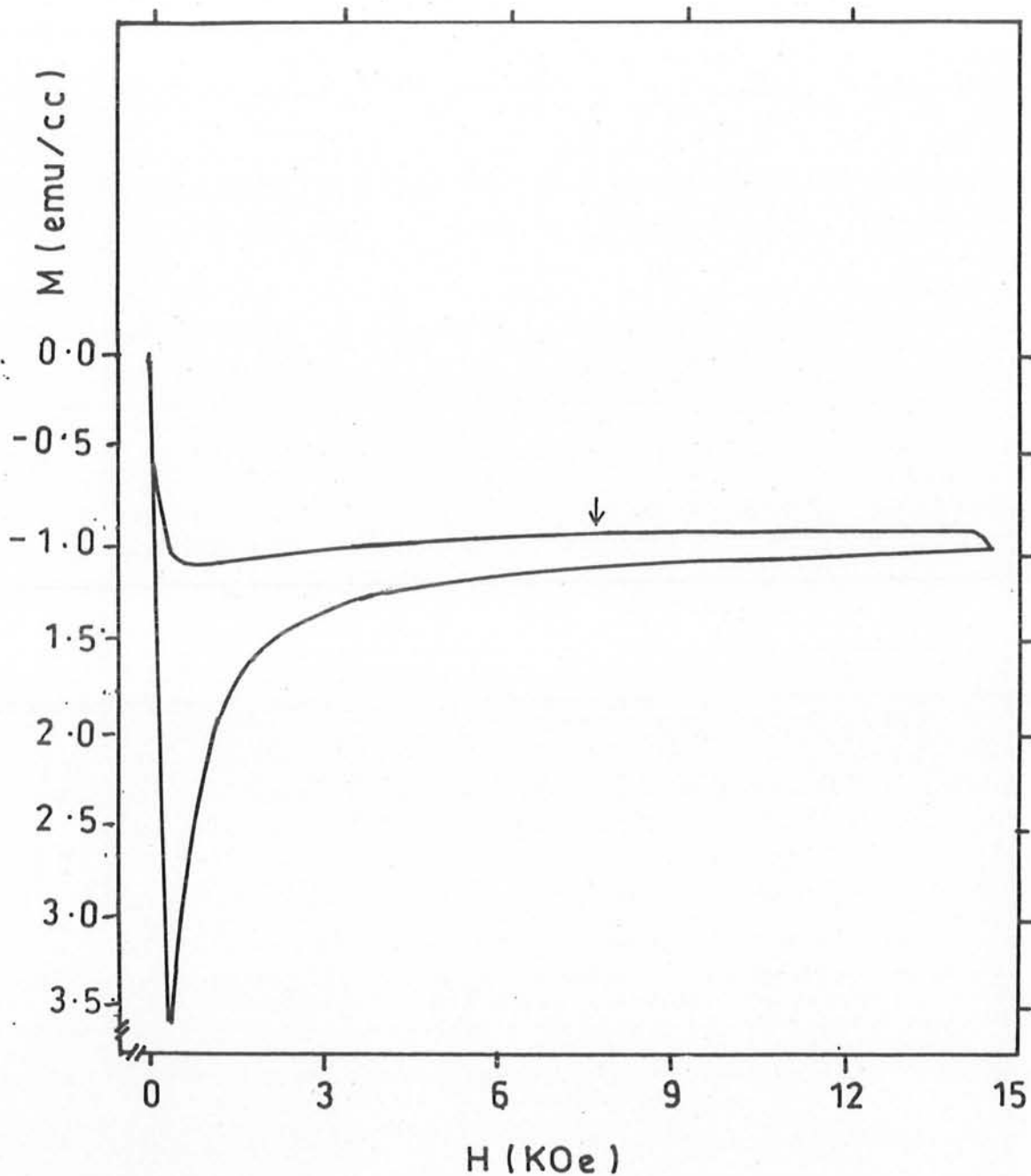
**Sample YBCO ( $T_c = 93\text{K}$ )**

<b>T(K)</b>	<b><math>t=T/T_c</math></b>	<b><math>H^*(\text{Oe})</math></b>
77	0.83	13552
$84.1 \pm 0.3$	0.90	8932
$85.7 \pm 0.2$	0.92	7700
$86.7 \pm 0.2$	0.93	6468
$88.4 \pm 0.4$	0.95	5236
$89.3 \pm 0.3$	0.96	4004

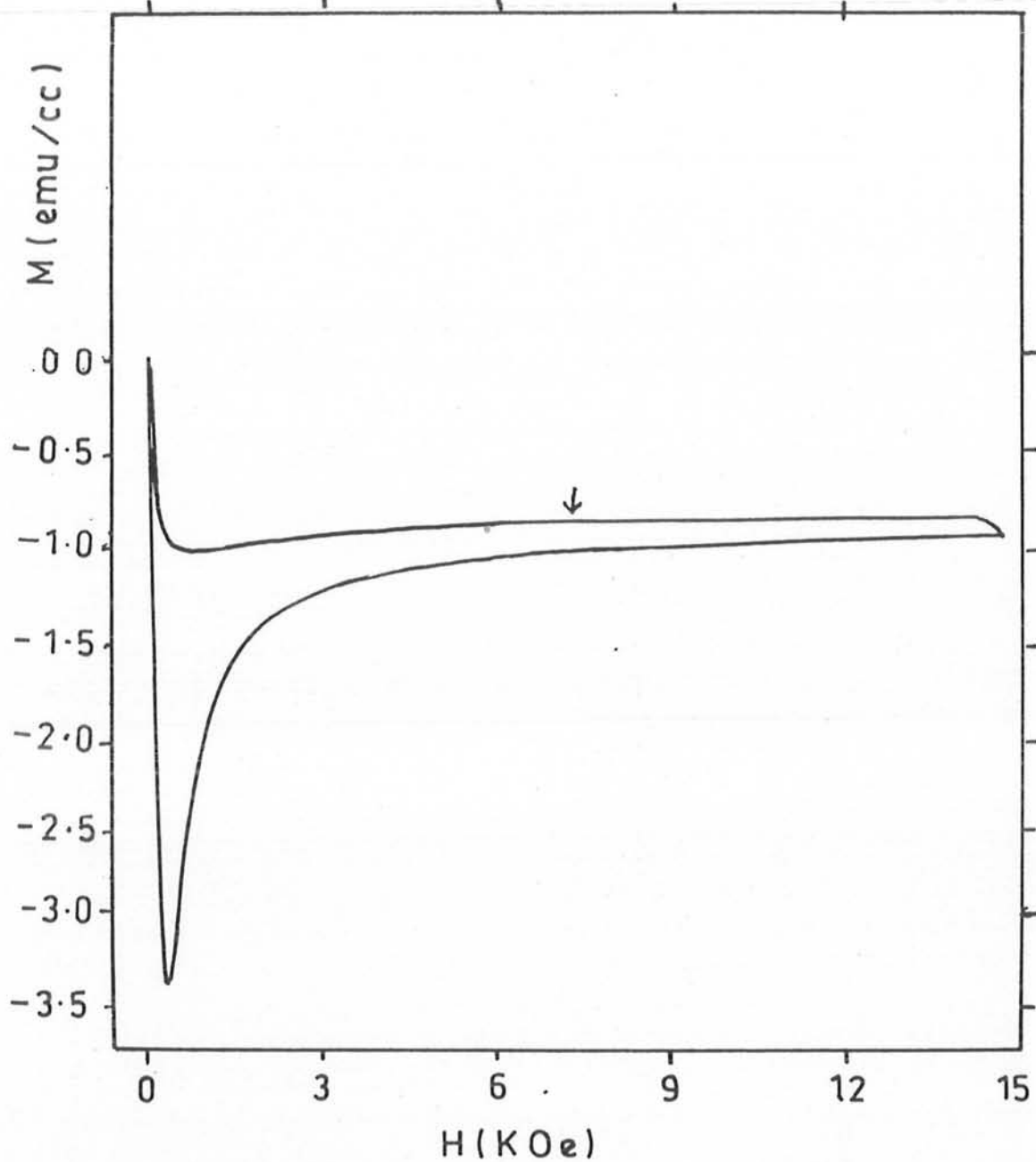
**Table [II]:** Data of Temperature T(K), reduced temperature  $t$  ( $T/T_c$ ) and the magnetic field  $H^*$  (Oe) at which the hysteresis of the M(H) loop first appears.



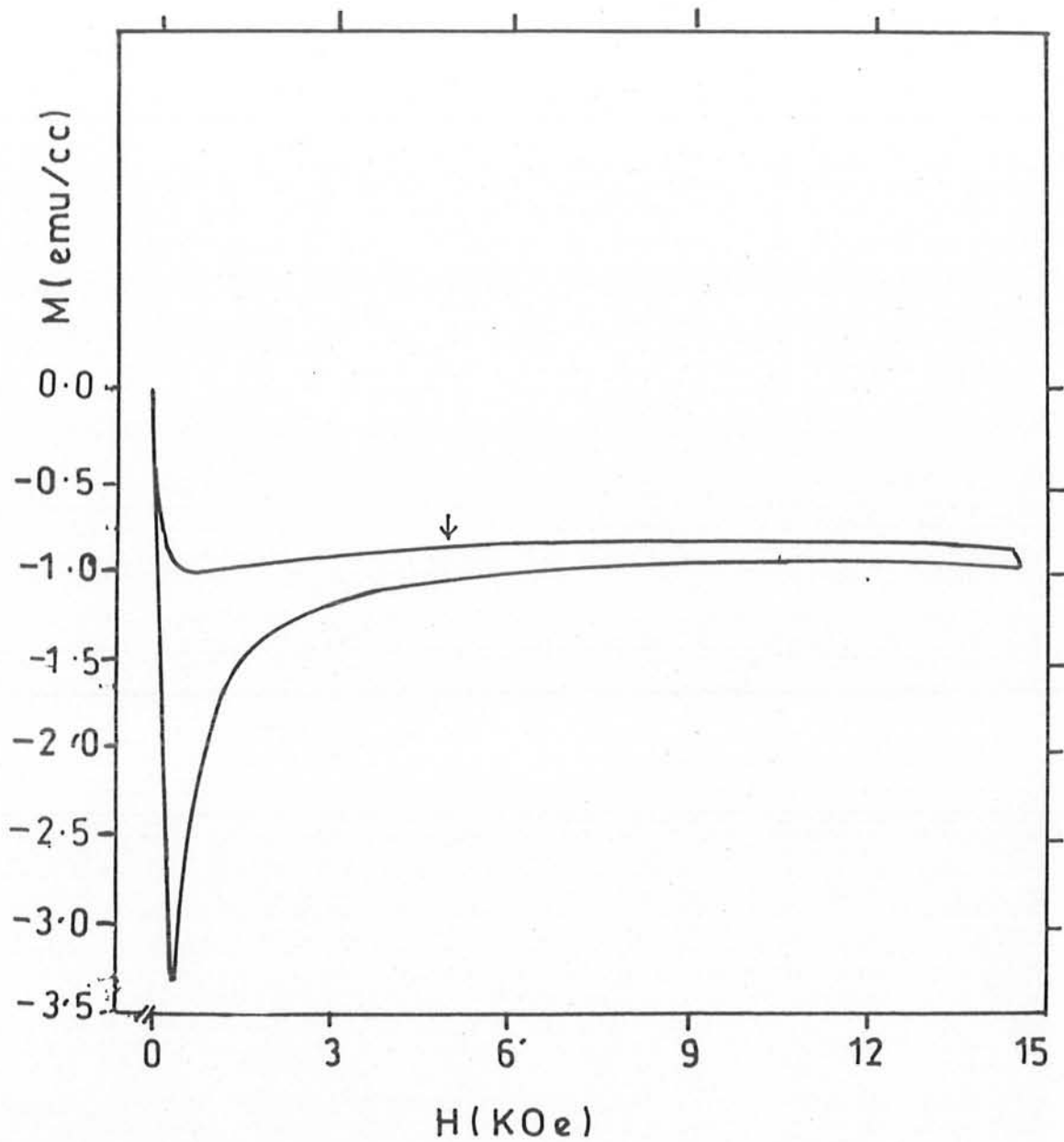
Fig[3.2(ii)] Typical magnetization behavior of sample YBCO at  $(84.1 \pm 0.3)$  K with the variation of applied magnetic field. The maximum field applied is 15 Koe, whereas the arrow is indicating the onset point of the hysteresis at the field value  $H^* = 8932$  Oe.



Fig[3.2(iii)] Typical magnetization behavior of sample YBCO at  $(85.7 \pm 0.2)$  K with the variation of applied magnetic field. The maximum field applied is 15 Koe, whereas the arrow is indicating the onset point of the hysteresis (as defined in the text) at the field value  $H^* = 7700$  Oe.

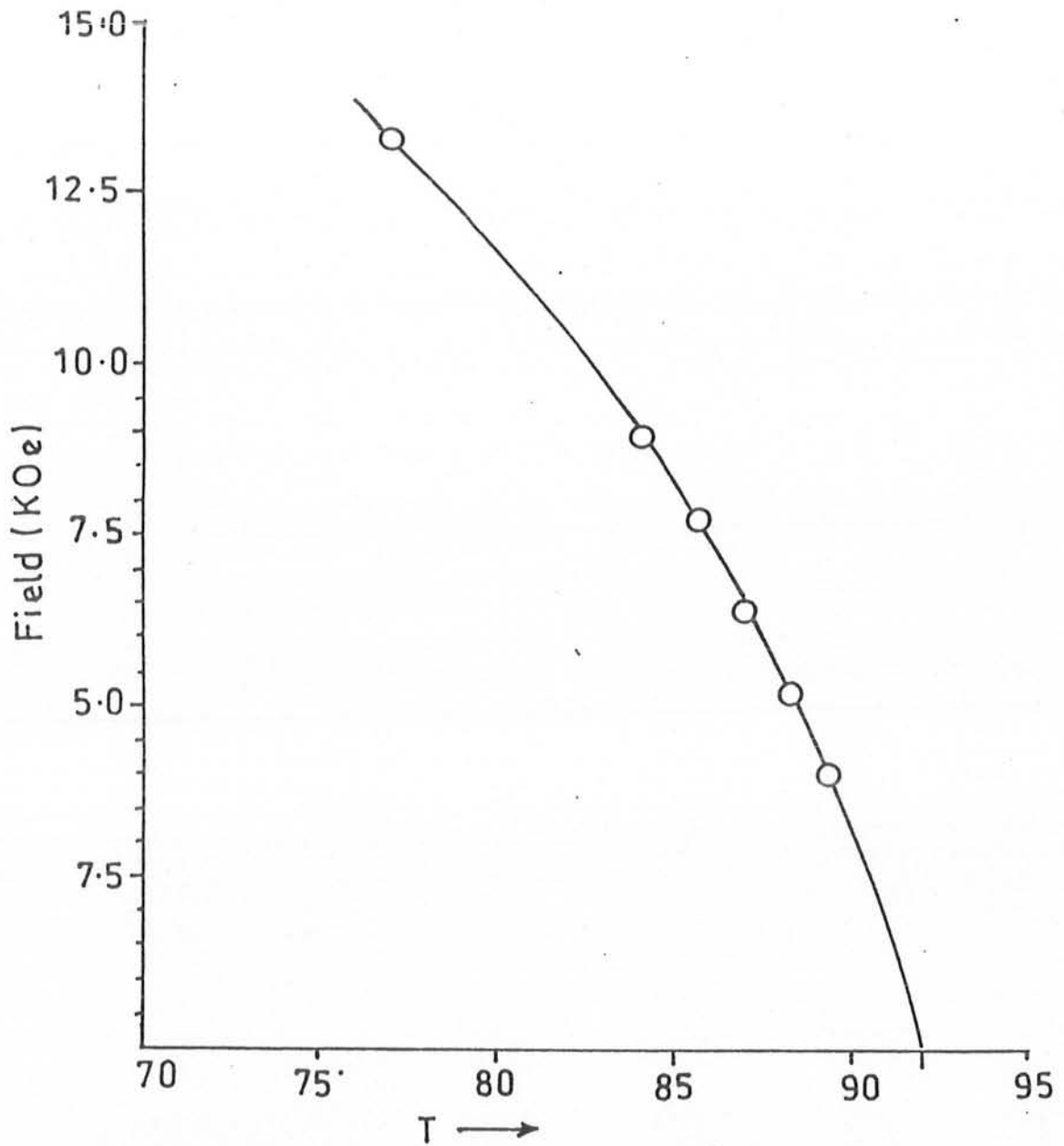


Fig[3.2(iv)] Typical magnetization behavior of sample YBCO at  $(86.7 \pm 0.2)$  K with the variation of applied magnetic field. The maximum field applied is 15 Koe, whereas the arrow is indicating the onset point of the hysteresis (as defined in the text) at the field value  $H^* = 6468$  Oe.



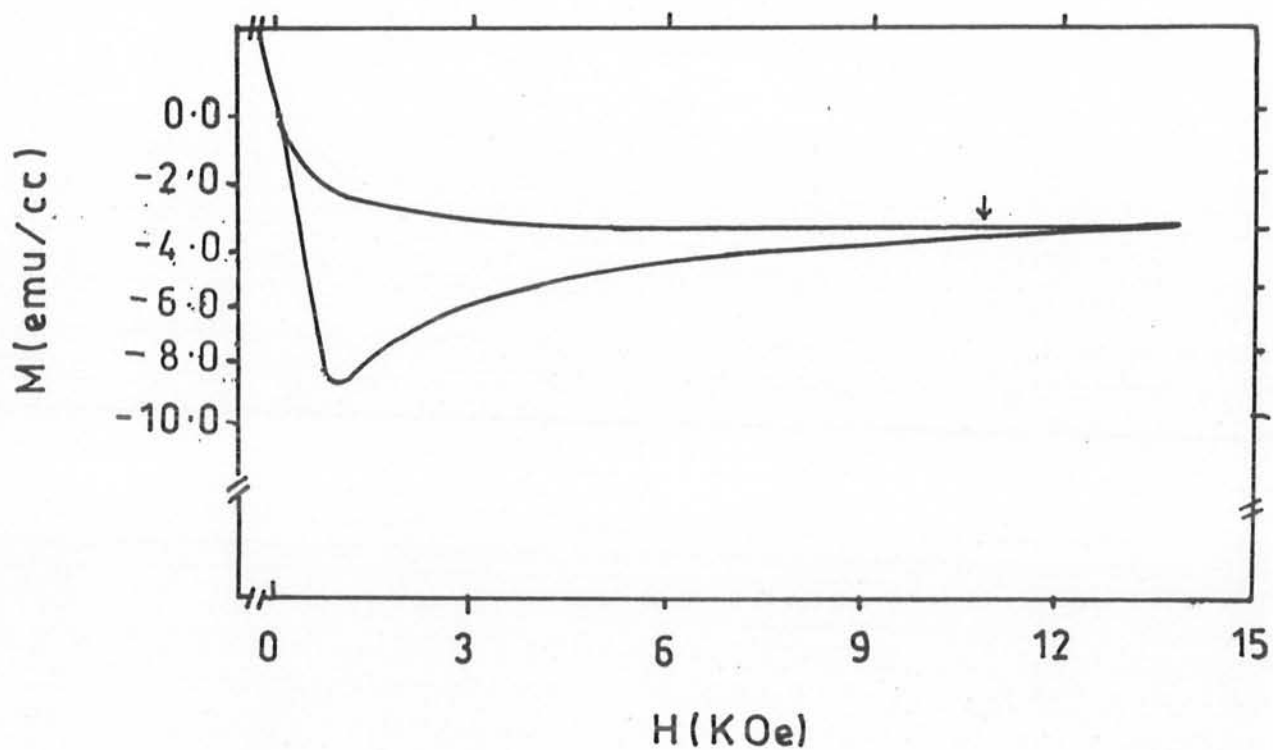
Fig[3.2(v)] Typical magnetization behavior of sample YBCO at  $(88.4 \pm 0.4)$  K with the variation of applied magnetic field. The maximum field applied is 15 Koe, whereas the arrow is indicating the onset point of the hysteresis (as defined in the text) at the field value  $H^* = 5236$  Oe.



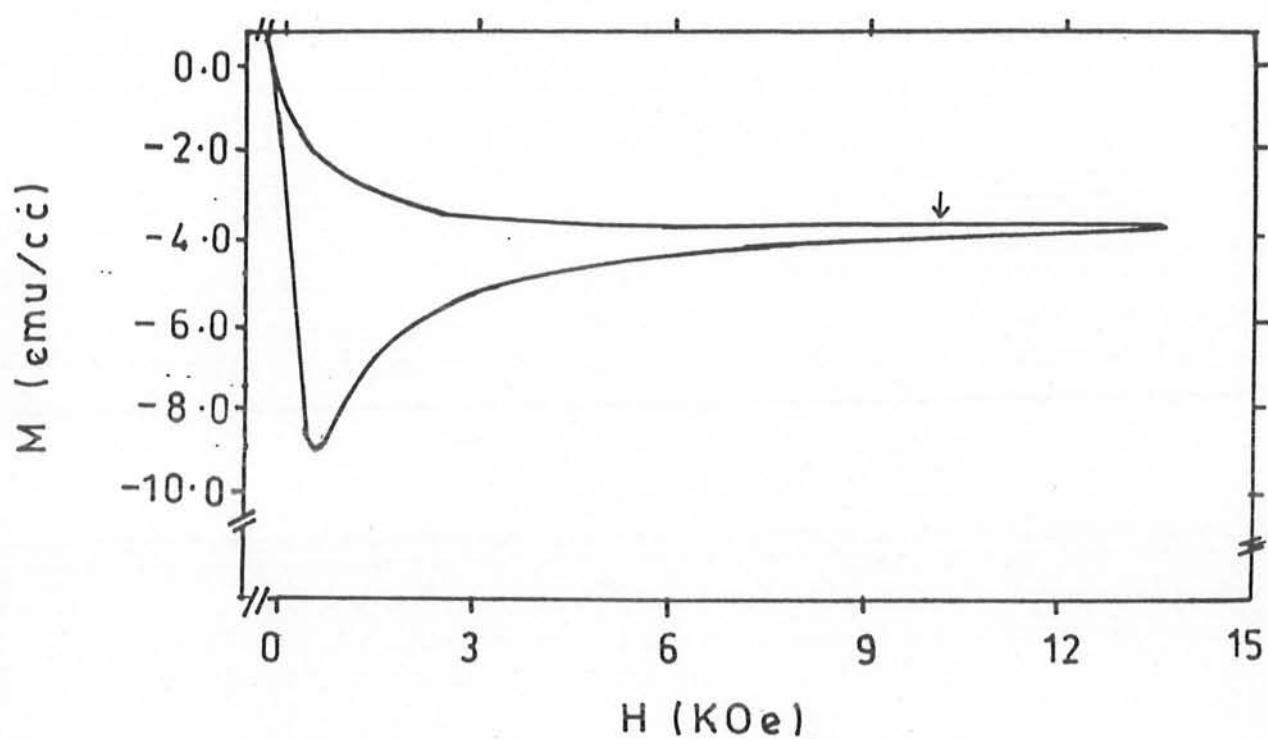


Fig[3.5]

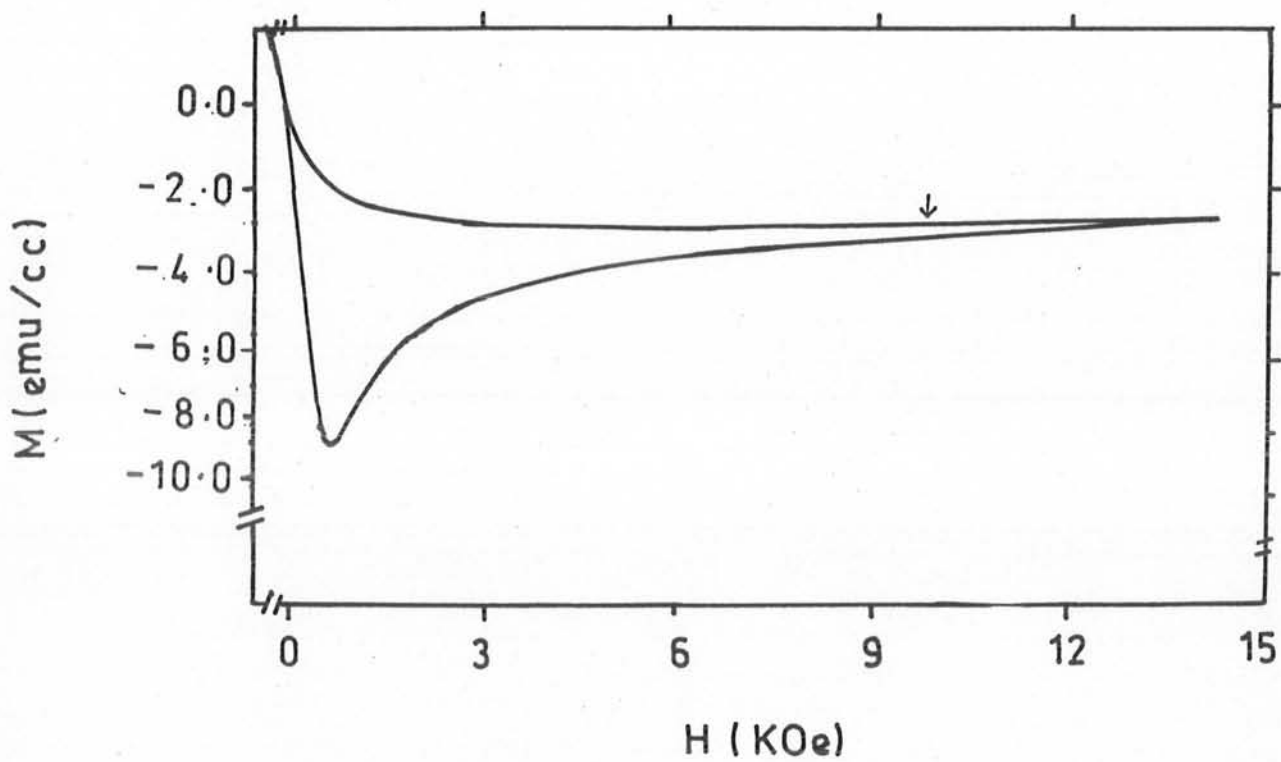
Graph of  $H^*$  vs  $T$  plotted on the data obtained from the dc  $M(H)$  measurements of sample YBCO. This is the irreversibility line in the  $H$ - $T$  plane which exhibits a non-linear behavior with  $H^*$  going to zero at  $T = 92.5\text{K}$ (line is a guide to the eye).



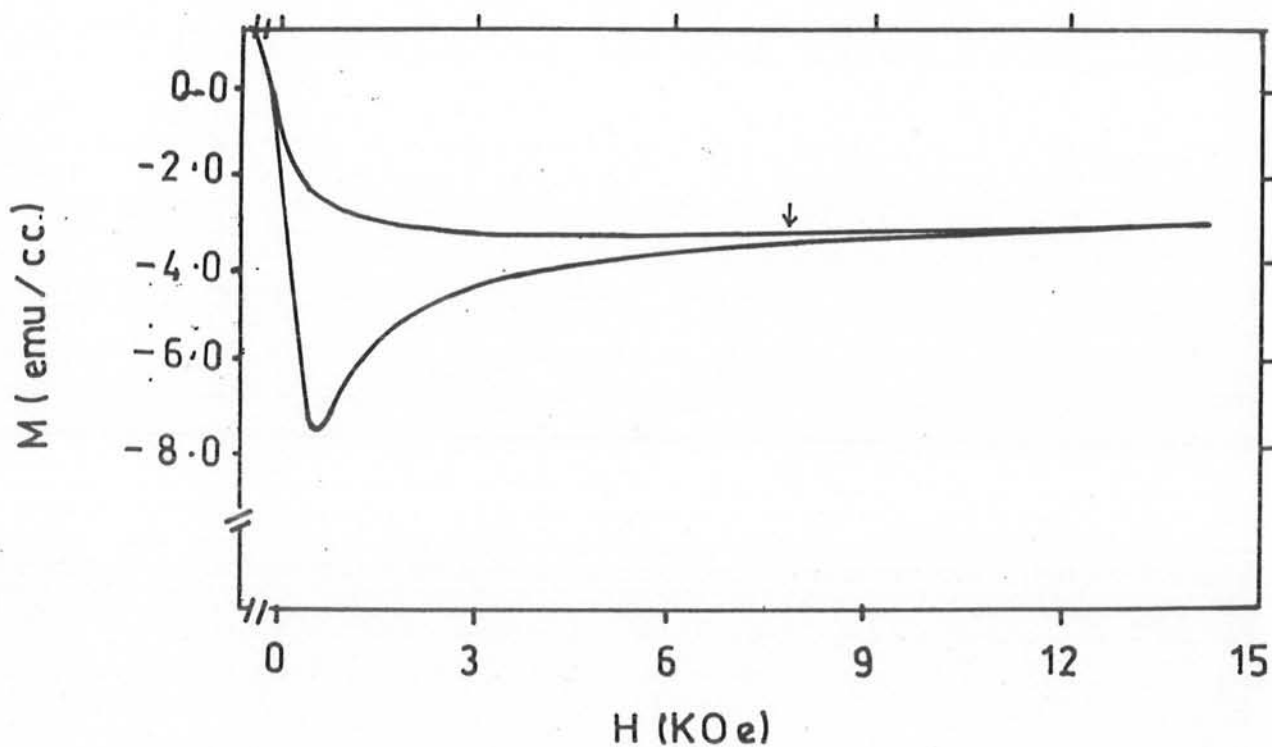
Fig[3.3(ii)] Typical magnetization behavior of sample Hg-4 at  $(93 \pm 0.4)$  K with the variation of applied magnetic field. The maximum field applied is 15 Koe, whereas the arrow is indicating the onset point of the hysteresis (as defined in the text) at the field value  $H^* = 11020$  Oe.



Fig[3.3(iii)] Typical magnetization behavior of sample Hg-4 at  $(98 \pm 0.3)$  K with the variation of applied magnetic field. The maximum field applied is 15 Koe, whereas the arrow is indicating the onset point of the hysteresis (as defined in the text) at the field value  $H^* = 9940$  Oe.

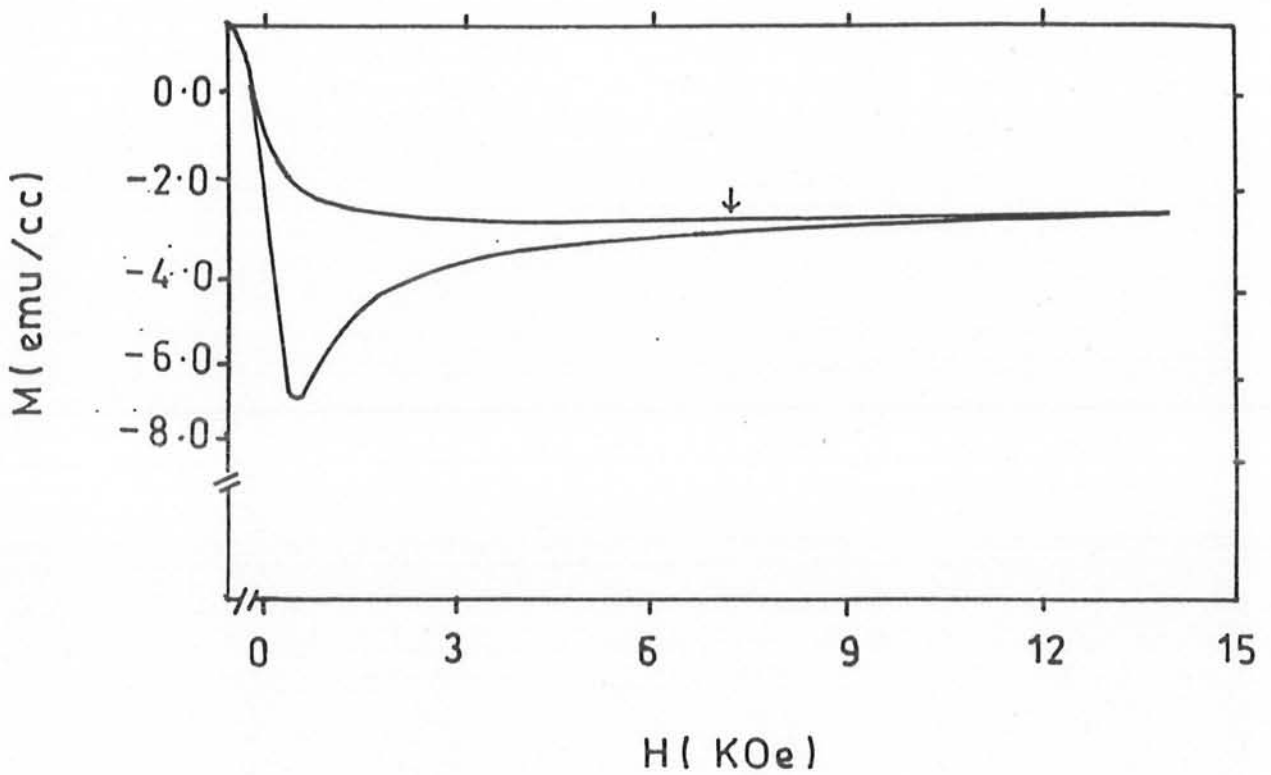


Fig[3.3(iv)] Typical magnetization behavior of sample Hg-4 at  $(102.5 \pm 0.5)$  K with the variation of applied magnetic field. The maximum field applied is 15 Koe, whereas the arrow is indicating the onset point of the hysteresis (as defined in the text) at the field value  $H^* = 9480$  Oe.

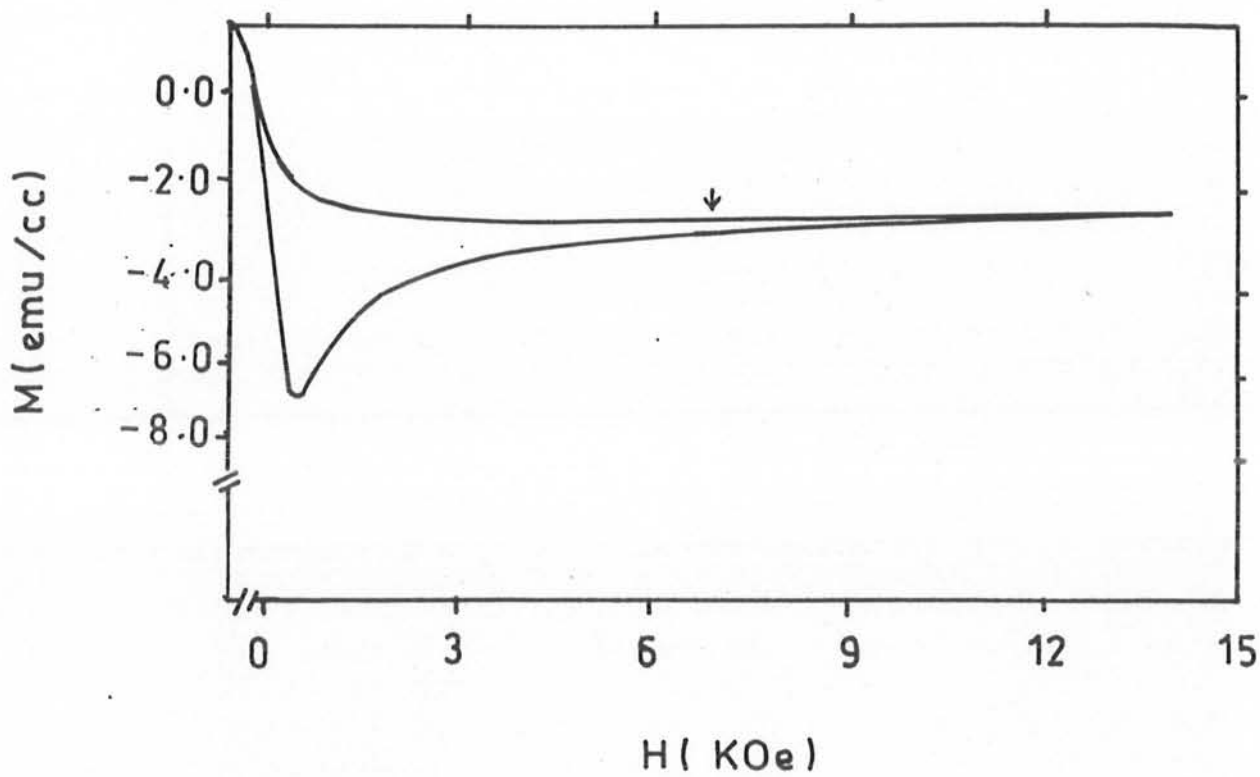


Fig[3.3(v)]

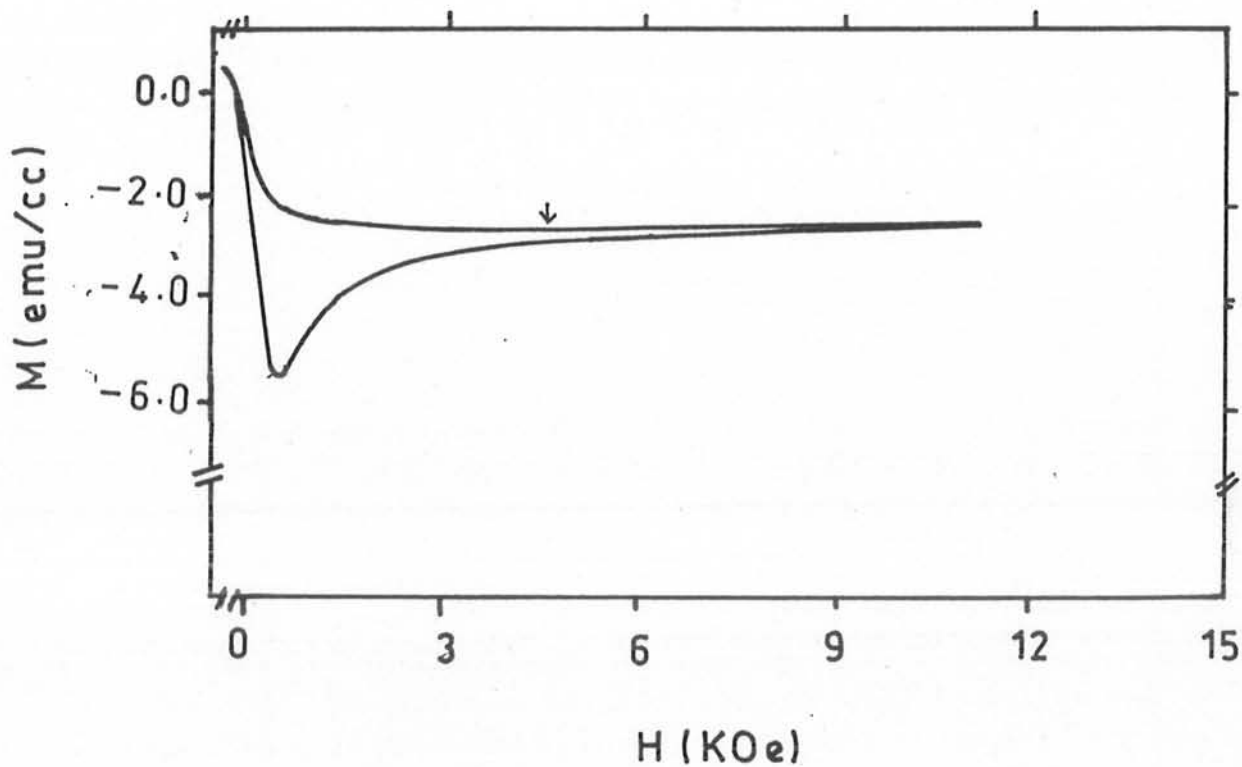
Typical magnetization behavior of sample Hg-4 at  $(108 \pm 0.4)$  K with the variation of applied magnetic field. The maximum field applied is 15 Koe, whereas the arrow is indicating the onset point of the hysteresis (as defined in the text) at the field value  $H^* = 8340$  Oe.



Fig[3.3(vi)] Typical magnetization behavior of sample Hg-4 at  $(111 \pm 0.3)$  K with the variation of applied magnetic field. The maximum field applied is 15 Koe, whereas the arrow is indicating the onset point of the hysteresis (as defined in the text) at the field value  $H^* = 7650$  Oe.



Fig[3.3(vii)] Typical magnetization behavior of sample Hg-4 at  $(116 \pm 0.5)$  K with the variation of applied magnetic field. The maximum field applied is 15 Koe, whereas the arrow is indicating the onset point of the hysteresis (as defined in the text) at the field value  $H^* = 6500$  Oe.



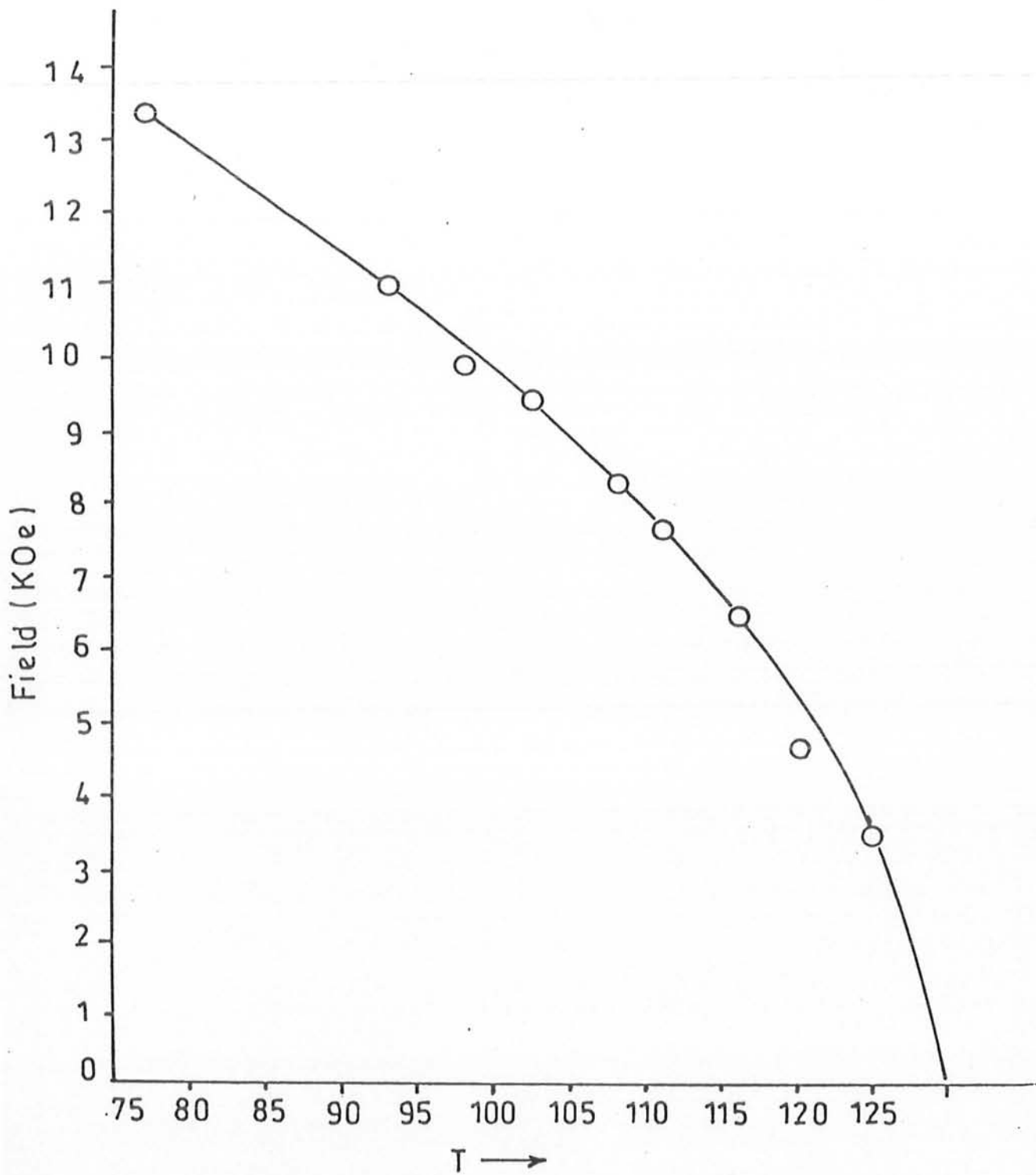
Fig[3.3(viii)] Typical magnetization behavior of sample Hg-4 at  $(120.5 \pm 0.7)$  K with the variation of applied magnetic field. The maximum field applied is 15 Koe, whereas the arrow is indicating the onset point of the hysteresis (as defined in the text) at the field value  $H^* = 4660$  Oe.



**Sample Hg-4 ( $T_c = 130\text{K}$ )**

<b>T(K)</b>	<b><math>t = T/T_c</math></b>	<b><math>H^*(\text{Oe})</math></b>
77	0.59	13870
$93 \pm 0.4$	0.71	11020
$98 \pm 0.3$	0.75	9940
$102.5 \pm 0.5$	0.79	9480
$108 \pm 0.4$	0.83	8340
$111 \pm 0.3$	0.85	7650
$116 \pm 0.5$	0.89	6500
$120.5 \pm 0.7$	$0.93 \pm 0.1$	4660
$125 \pm 0.4$	0.96	3520

**Table [III]:** Data of Temperature T(K), reduced temperature  $t$  ( $T/T_c$ ) and the magnetic field  $H^*$  (Oe) at which the hysteresis of the M(H) loop first appears.



Fig[3.6]

Graph of  $H^*$  vs  $T$  plotted on the data obtained from the dc  $M(H)$  measurements of sample Hg-4. This is the irreversibility line in the  $H$ - $T$  plane which exhibits a non-linear behavior with  $H^*$  going to zero at  $T = 130K$ (line is a guide to the eye).

These temperatures are used as critical temperatures “ $T_c$ ” in the analysis of the irreversibility line, i.e. the reduced temperature  $t = T^*/T_c$ . Here  $T^*$  corresponds to the temperature of a measured hysteresis loop. The figure ( $H^*$  vs  $T$ ) shows the separation of the reversible & irreversible regions of the samples.

### (3.1a) Obtaining the exponent $n$

Finally the irreversible field versus the reduced temperature data is plotted on a log-log scale to obtain the exponent “ $n$ ” in the equation:

$$(H^*)^n = C (1-t) \quad (3.1)$$

Taking log of both sides we get:

$$n \log H = \log C + \log (1-t) \quad (3.2)$$

$$\log H = (\log C)/n + (1/n) \log (1-t) \quad (3.3)$$

For the BPS sample the  $\ln(H)$  vs  $\ln(1-t)$  fit is shown in fig 3.7, from this we obtain a slope of  $0.66 \pm 0.02$  (the data of  $\ln(1-t)$  &  $\ln(H^*)$  obtained for sample BPS from  $M(H)$  loops is given in table[IV]). Since the slope here corresponds to  $(1/n)$  in equation (3.3), therefore, the exponent of  $H$  viz. ( $n$ ) in equation (3.1) is equal to 1.51. This implies that  $(H^*)^{1.5} \propto (1-t)$  or  $H^* \propto (1-t)^{0.66}$ . We further ascertain this result by checking it through curve fitting. Thus, we use the following equation for fitting a curve to the data of  $H^*$  and  $T$ :

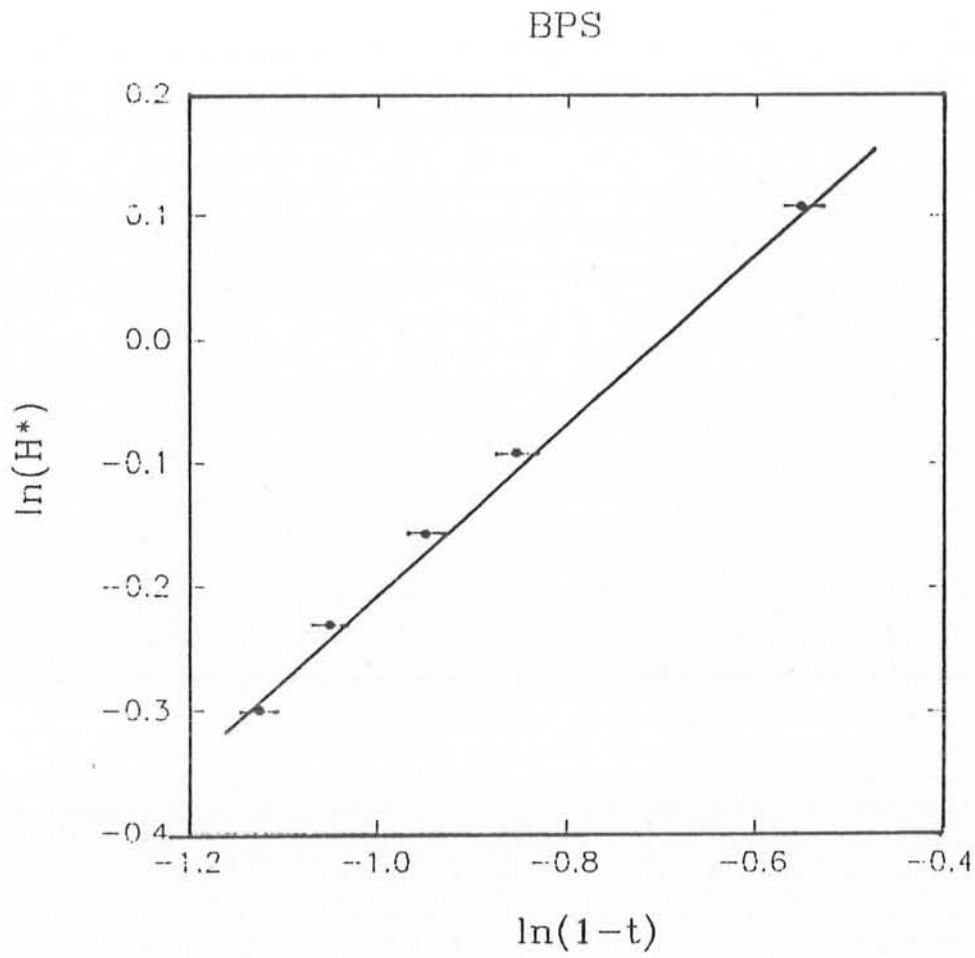
$$f = (1/c) [1-T/T_c]^{1/n} \quad (3.4)$$

In the above equation the slope corresponds to  $1/n$ . After fitting  $f$  to  $H^*$ , we obtain  $n = 1.48$  and hence  $1/n = 0.68$ , as shown in the figure (3.8). The value of slope obtained from the curve fitting method is almost equal the value of the slope obtained from the linearity of  $\log(1-t)$  vs  $\log(H^*)$ . Hence it is verified that the value of  $1/n$  is equal to 0.68 and also that  $H^* \propto (1-t)^{0.68}$ . However, we observe that this is not in agreement with the predictions of Chapter 1.

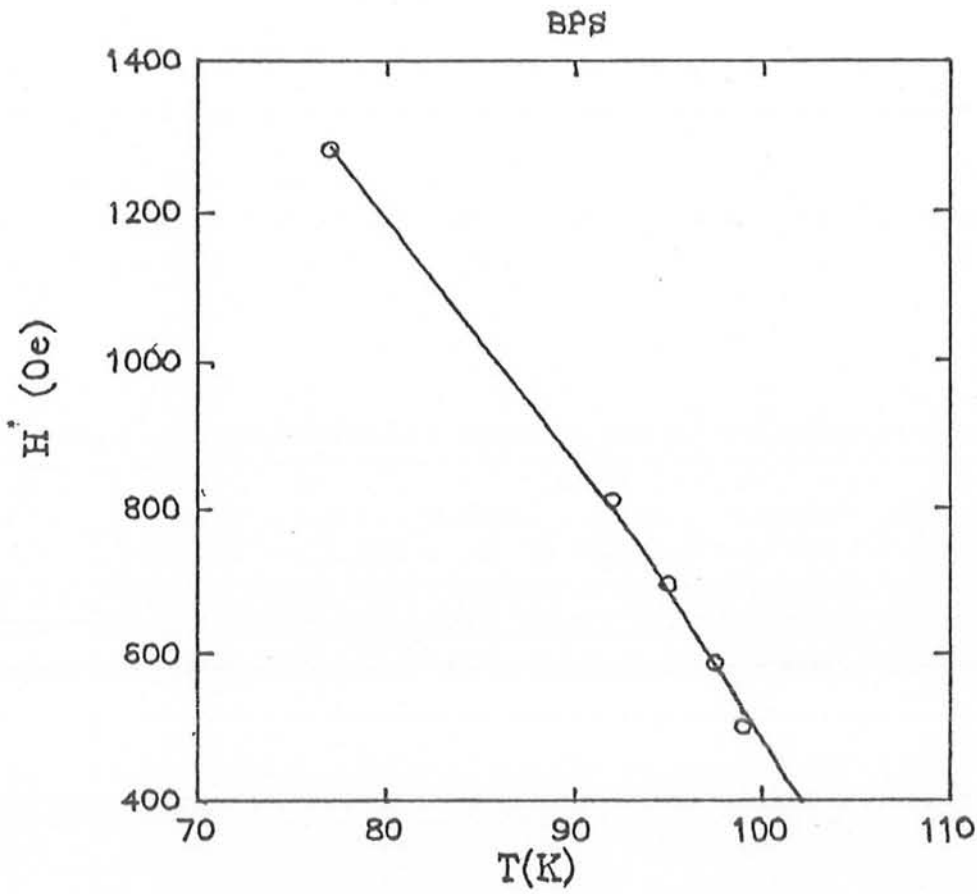
Sample BPS ( $T_c = 107K$ )

$\ln(1-t)$	$\ln(H^*)$
- 0.5522	0.1078
- 0.8532	- 0.0915
- 0.9503	- 0.1567
- 1.0515	- 0.2298
- 1.1260	- 0.2992

Table [IV]: Data of  $\ln(1-t)$  vs  $\ln(H^*)$ .



Fig[3.7] Plot of  $\ln(1-t)$  vs  $\ln(H^*)$  for sample BPS. From the linearity of the  $\ln(1-t)$  vs  $\ln(H^*)$  a slope of  $0.66 \pm 0.02$  is obtained.



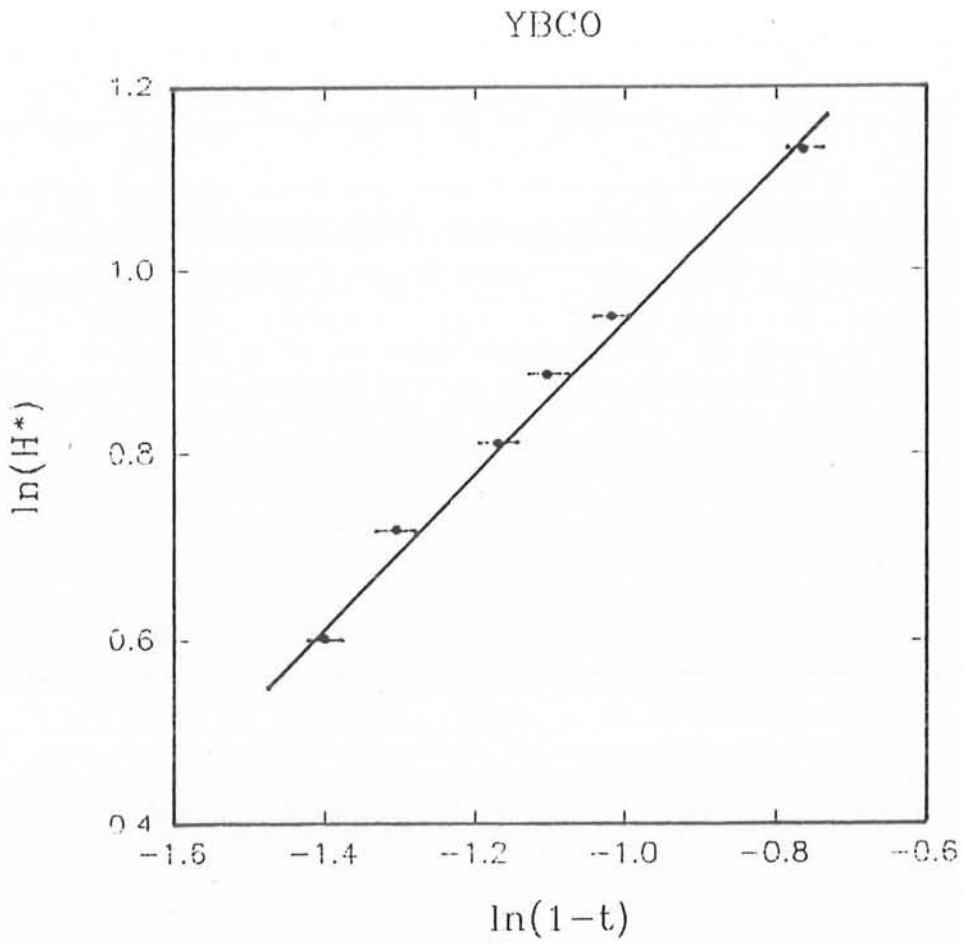
Fig[3.8] Curve fit on the measurements obtained from the  $M(H)$  loops, recorded at different temperatures on sample BPS. In this fit  $\{1/c(1-T/T_c)\}^{1/n}$  is equated with a function  $f$ , then  $f$  is fitted to  $H^*$  yielding the value of  $1/n = 0.68$ .

Sample YBCO ( $T_c = 93K$ )

$\ln(1-t)$	$\ln(H^*)$
- 0.7644	1.1320
- 1.0191	0.9509
- 1.1051	0.8860
- 1.1694	0.8107
- 1.3053	0.7189
- 1.400	0.6024

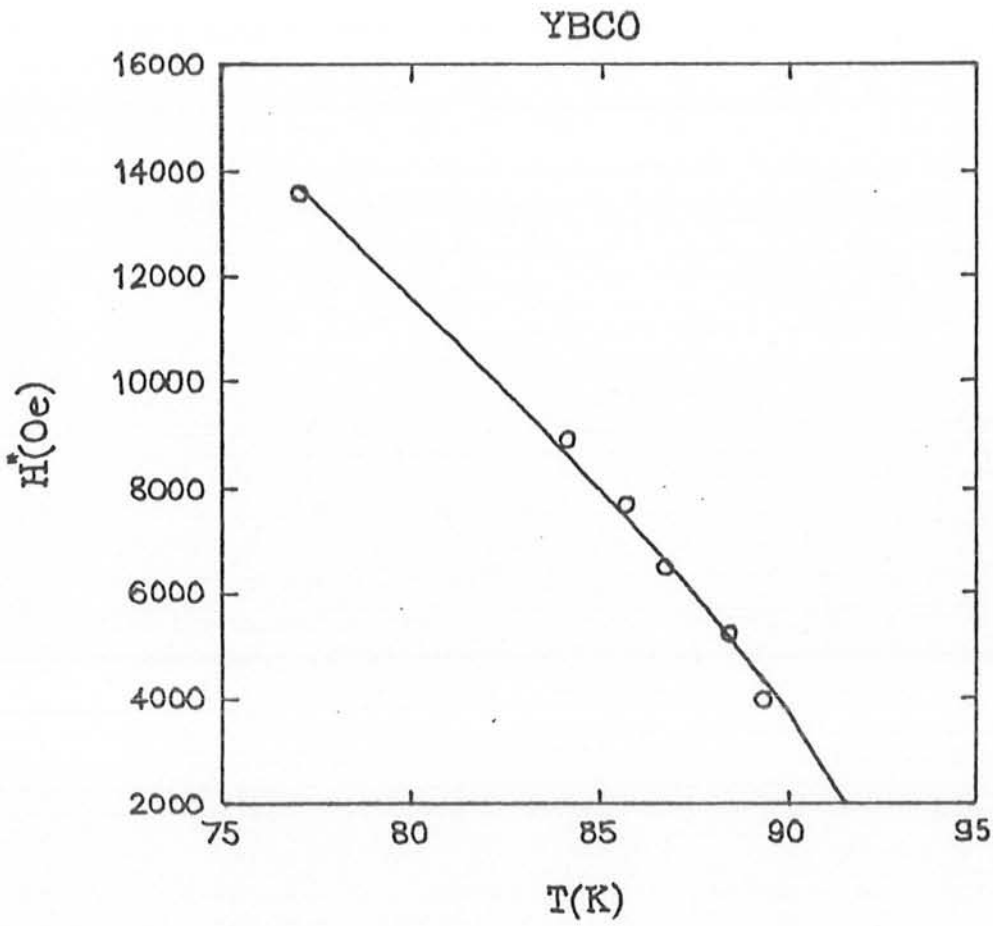
Table [V]: Data of  $\ln(1-t)$  vs  $\ln(H^*)$ .



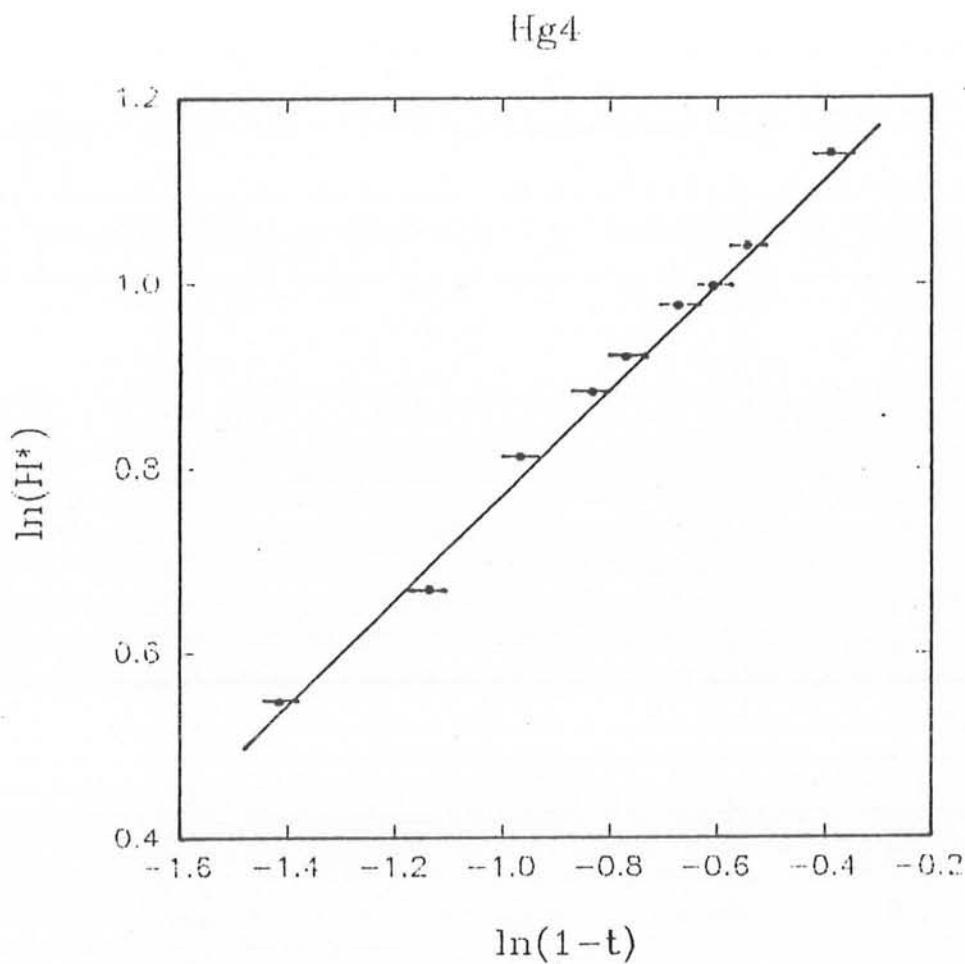


Fig[3.9]

Plot of  $\ln(1-t)$  vs  $\ln(H^*)$  for sample YBCO. From the linearity of the  $\ln(1-t)$  vs  $\ln(H^*)$  a slope of  $0.70 \pm 0.02$  is obtained.



Fig[3.10] Curve fit on the measurements obtained from the  $M(H)$  loops recorded at different temperatures on sample YBCO. In this fit  $\{1/c(1-T/T_c)\}^{1/n}$  is equated with a function  $f$ , then  $f$  is fitted to  $H^*$  yielding the value of  $1/n = 0.78$ .

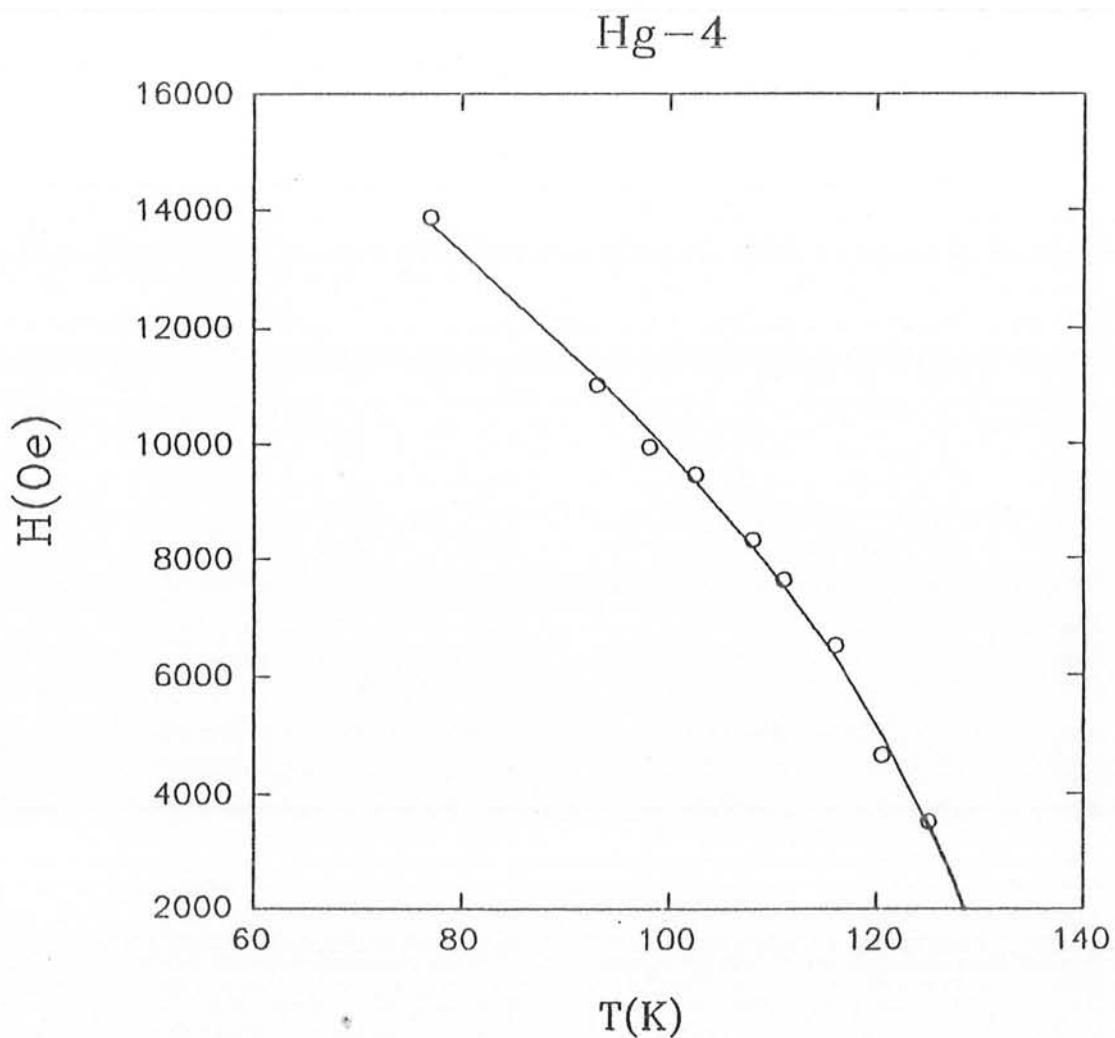


Fig[3.11] Plot of  $\ln(1-t)$  vs  $\ln(H^*)$  for sample Hg-4. From the linearity of the  $\ln(1-t)$  vs  $\ln(H^*)$  a slope of  $0.60 \pm 0.02$  is obtained.

**Sample Hg-4 ( $T_c = 130K$ )**

<b><math>\ln(1-t)</math></b>	<b><math>\ln(H^*)</math></b>
- 0.3896	1.1420
- 0.5457	1.0421
- 0.6087	0.9973
- 0.6746	0.9768
- 0.7715	0.9212
- 0.8350	0.8836
- 0.9678	0.8129
- 1.1361	0.6683
- 1.4145	0.5465

**Table [VI]: Data of  $\ln(1-t)$  vs  $\ln(H^*)$ .**



Fig[3.12]

Curve fit on the measurements obtained from the  $M(H)$  loops recorded at different temperatures on sample Hg-4. In this fit  $\{1/c(1-T/T_c)\}^{1/n}$  is equated with a function  $f$ , then  $f$  is fitted to  $H^*$  yielding the value of  $1/n = 0.58$ .

In the same manner we obtain a slope of  $0.70 \pm 0.02$  for YBCO sample respectively as illustrated in the figure(3.9) The data of  $\ln(1-t)$  &  $\ln(H^*)$  obtained for sample YBCO from M(H) loops is given in table[V]. The slope here is also obtained from the linearity of  $\ln(1-t)$  vs  $\ln(H^*)$  and correspond to  $(1/n)$  in equation (3.3). To confirm these values we employ curve fitting using equation (3.4) and fitting  $f$  to the  $H^*$ . We obtain the value  $n = 1.28$  and from this we obtain the slope  $1/n = 0.78$ , which implies that  $H^* \propto (1-t)^{0.78}$ , as shown in figure (3.10)

The value  $n$  for sample Hg-4 is the same from both the  $\log(1-t)$  vs  $\log(H^*)$  and curve fitting methods i.e.  $n = 1.79$  and thereby the slope  $1/n = 0.59$ , which implies that  $H^* \propto (1-t)^{0.59}$ . Figure (3.11) & (3.12) are displaying these results. The data of  $\ln(1-t)$  &  $\ln(H^*)$  obtained for sample BPS from M(H) loops is given in table[VI].

However, the above mentioned results do not comply with the prediction of Chapter 1. In view of the this disparity between our results and the predicted behavior, we decided to determine this slope by using a different technique, viz. “ac susceptibility measurements”. This technique was employed in order to check that the results obtained by us from the M(H) loops hysteresis onset technique were correct.

### (3.2) ac Susceptibility Measurements

The irreversibility line of BPS sample has been determined by comparing the zero-field-cooled (ZFC) and field-cooled (FC) ac susceptibility measurements. For an applied field  $H$ , the temperature-dependent ZFC & FC susceptibility curves converge at  $T = T^*(H)$ , yielding a point on  $T^*(H)$  line [22]. The work carried out by Y.Yeshurun [19] on magnetic measurements reports that the ZFC branch is clearly metastable and shows a pronounced time effect, whereas,

the FC branch is stable. The difference between FC & ZFC branches is understood to be due to flux trapping in the FC case. However, the two susceptibility curves approach each other somehow asymptotically, and in the case of dc magnetization the determination of this point introduces appreciable errors. At constant temperature the irreversibility field can also be obtained as the field value where the ZFC magnetic moment of the sample equals its Meissner signal (i.e. the FC magnetic moment). Apart from the above mentioned impediment, the time dependence of the magnetization and the difficulty of maintaining the apparatus zero point for a long time in classical dc magnetization measurements create new problems. These problems are less severe in ac susceptibility measurements.

When the irreversibility line is reached, there are two curves which must be identical.. The proposed procedure is applicable for bulk sintered samples with a pronounced granular character. For such samples the transport critical current is limited by Josephson junctions [21] located at grain boundaries, which are very sensitive to applied magnetic fields [23]. On the other hand the intergranular critical current density is relatively high leading to appreciable differences between the grain magnetization in ZFC conditions and for increasing field (pinning to flux entry) and that appearing in FC conditions (paramagnetically trapped flux at pinning centers). At the same time the local magnetic field at the intergrain contacts is directly related to the grain magnetization [24]. The local field at the intergrain contacts depends strongly on cooling conditions. The above differences vanish when the irreversibility point is reached, and in this way  $T^*(H)$  can be determined, as the temperature at and above which the ZFC & FC curves become identical. The degree of preferential crystalline orientation is not very important in this context.

The ZFC process was achieved by cooling down the Bismuth based sample (labelled BPS) to  $T = 77K$  while keeping the magnetic dc field  $H_{dc} = 0$ . The field  $H_{dc}$  was then turned on

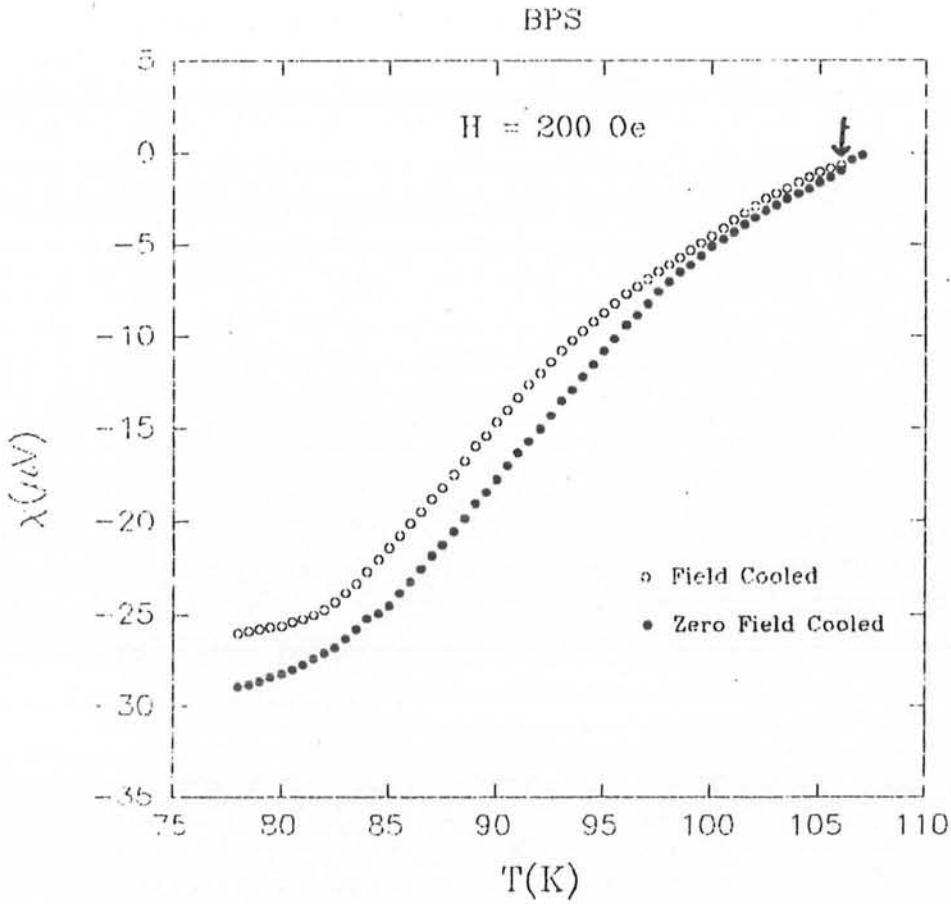
( $H_{dc} > 0$ ) after attaining the minimum possible achievable temperature. Then the sample was heated in steps of 0.5K or less, and the temperature was stabilized within accuracy better than 0.1K within  $\sim 5$  minutes, using an Oxford Instrument Precision Temperature Controller. Hence, with the gradually increasing temperature we measured the ac  $\chi(T)$ . During measurements the we kept the  $H_{ac} = 1.3$  Oe and frequency  $\nu = 135$  Hz.

Unlike the ZFC process, the FC process was accomplished by cooling down the sample under a constantly applied dc magnetic field i.e.  $H_{dc} > 0$ . After reaching the minimum possible attainable temperature, the sample was then heated in the same way as in the case of ZFC and  $\chi(T)$  was measured correspondingly.

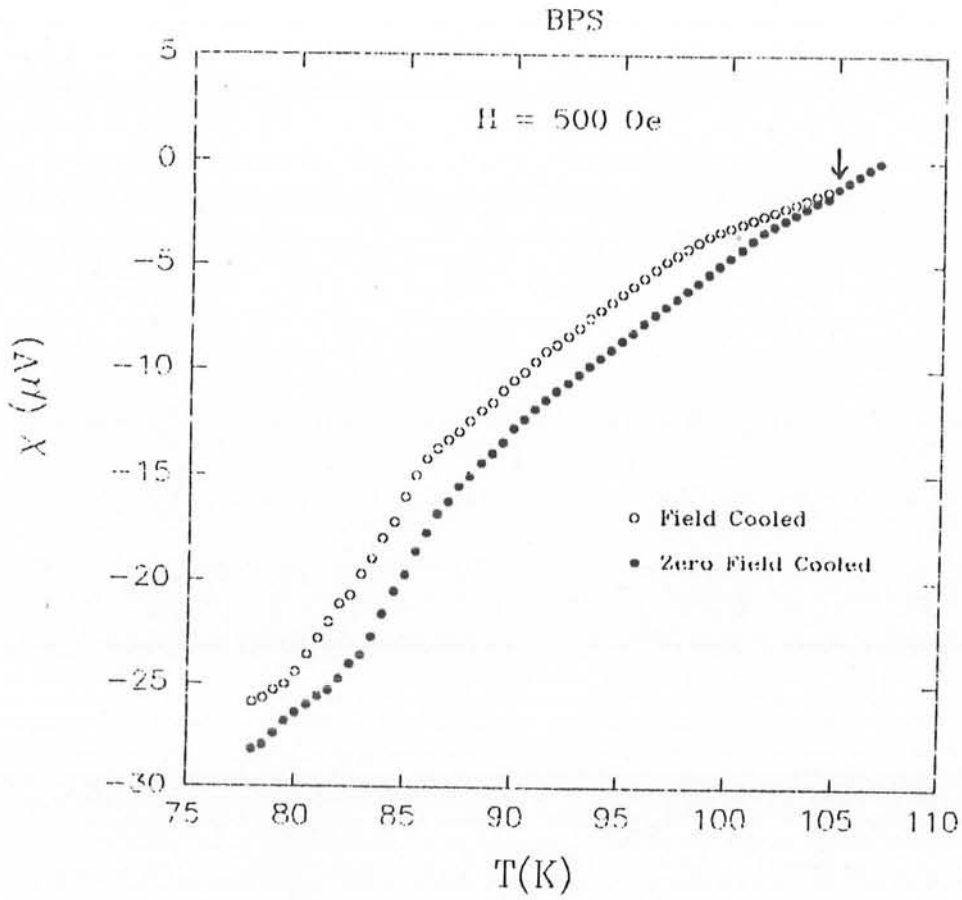
In our experiment the FC & ZFC conditions were first realized at liquid-nitrogen temperature in magnetic field values upto 750 Oe generated by a copper solenoid. The variation of the magnetic field gives us a variety of ZFC-FC curves converging at different temperatures for different applied magnetic fields. This convergence temperature has been noted in the range of 200 Oe to 750 Oe.

At the field value of 200 Oe, we observed that FC and ZFC curves plotted in the  $\chi$ -T plane converged at a temperature value of  $T^* = 106$ K as shown in the figure [3.13 (a)]. At  $H_{dc} = 500$  Oe the FC & ZFC curves meet at point in the  $\chi$ -T plane at a temperature value of  $T^* = 105$ K figure [3.13(b)]. As we further increase the field to  $H_{dc} = 650$  Oe, the convergence point shifts correspondingly to a lower value of temperature i.e.  $T^* = 104$ K figure [3.13(c)]. As we

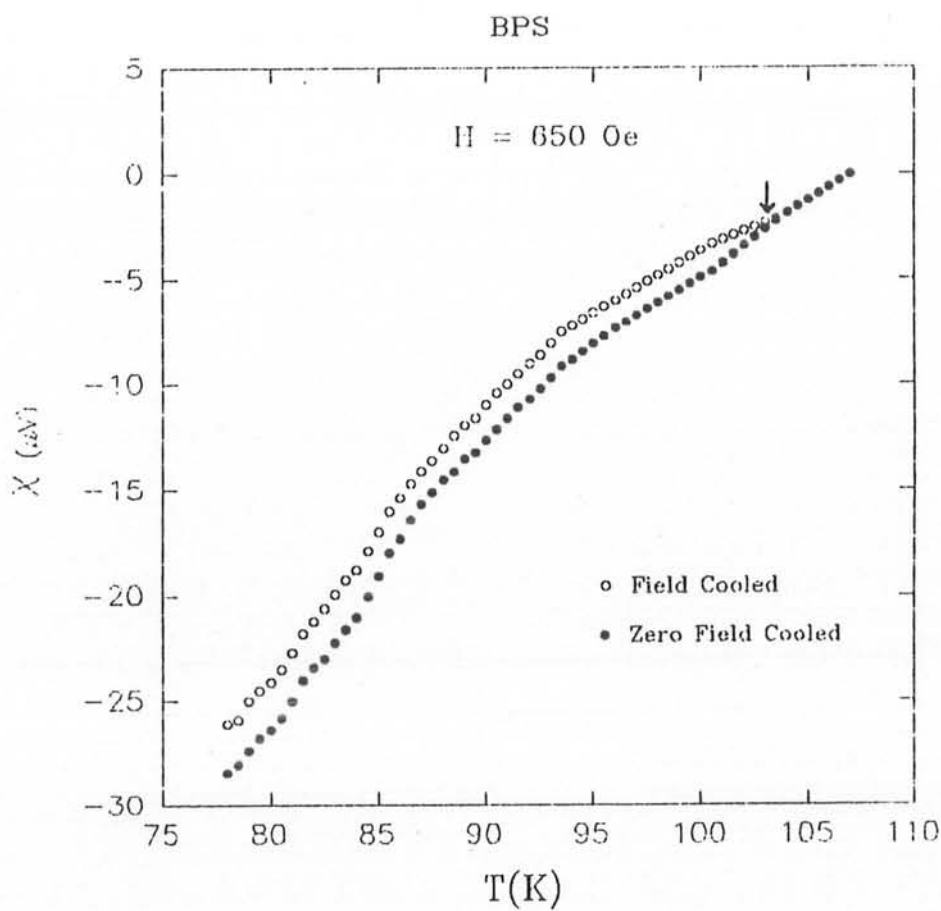




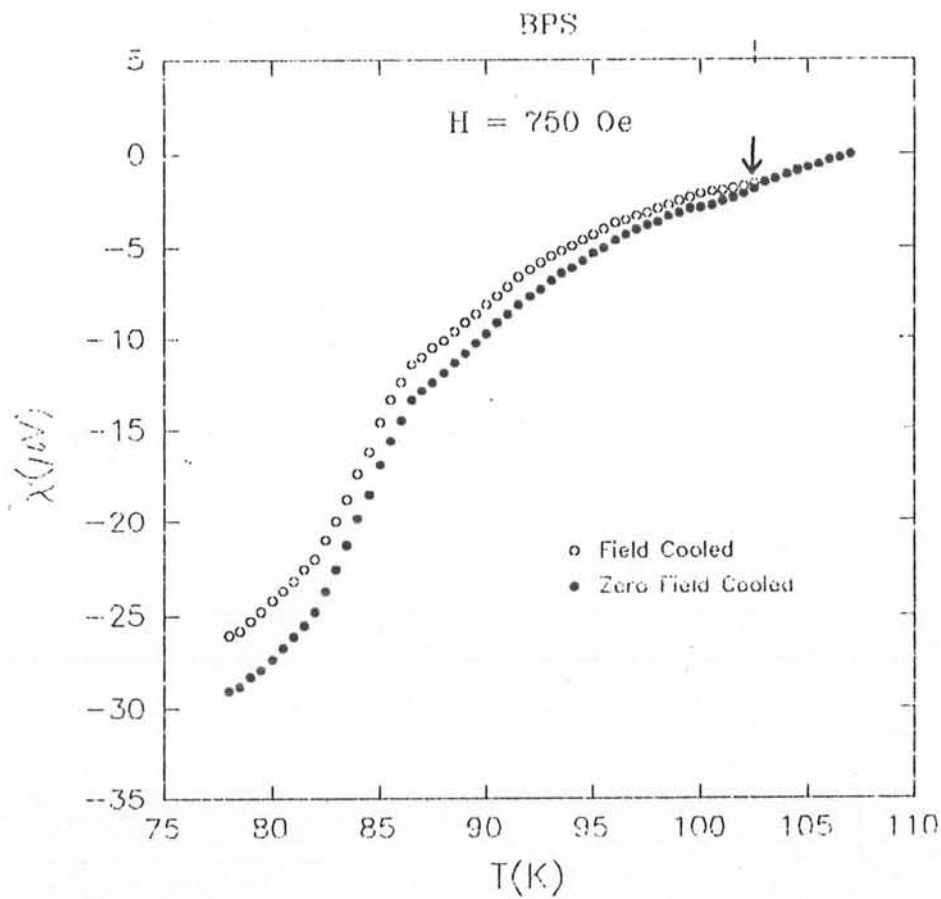
Fig[3.13(a)] Field Cooled (FC) & Zero Field Cooled (ZFC) curves plotted in the  $\chi$ -T plane: In this plot the hollow circles represent the FC curve and the filled circles represent the ZFC curve. The arrow is indicating merging point of the two curves at  $T^* = 106\text{K}$  at applied external dc magnetic field  $H_{dc} = 200 \text{ Oe}$ .



Fig[3.13(b)] Field Cooled (FC) & Zero Field Cooled (ZFC) curves plotted in the  $\chi$ -T plane: In this plot the hollow circles represent the FC curve and the filled circles represent the ZFC curve. The arrow is indicating merging point of the two curves at  $T^* = 105\text{K}$  at applied external dc magnetic field  $H_{dc} = 500 \text{ Oe}$ .



Fig[3.13(c)] Field Cooled (FC) & Zero Field Cooled (ZFC) curves plotted in the  $\chi$ -T plane: In this plot the hollow circles represent the FC curve and the filled circles represent the ZFC curve. The arrow is indicating merging point of the two curves at  $T^* = 104\text{K}$  at applied external dc magnetic field  $H_{dc} = 650 \text{ Oe}$ .



Fig[3.13(d)] Field Cooled (FC) & Zero Field Cooled (ZFC) curves plotted in the  $\chi$ -T plane: In this plot the hollow circles represent the FC curve and the filled circles represent the ZFC curve. The arrow is indicating merging point of the two curves at  $T^* = 103\text{K}$  at applied external dc magnetic field  $H_{dc} = 750 \text{ Oe}$ .

increase the field  $H_{dc}$  to 750 Oe the convergence point drops further to a relatively lower value of temperature i.e.  $T^* = 103K$ , as shown in the figure [3.13(d)]. Plotting  $T^*$  vs  $H$  we obtain a non-linear curve that approaches zero at a temperature value of 106.1K as illustrated in the figure (3.14). This non-linear curve is the irreversibility line in the H-T plane. The area under the curve represents the reversible regime, whereas, the irreversible regime lies above the curve.

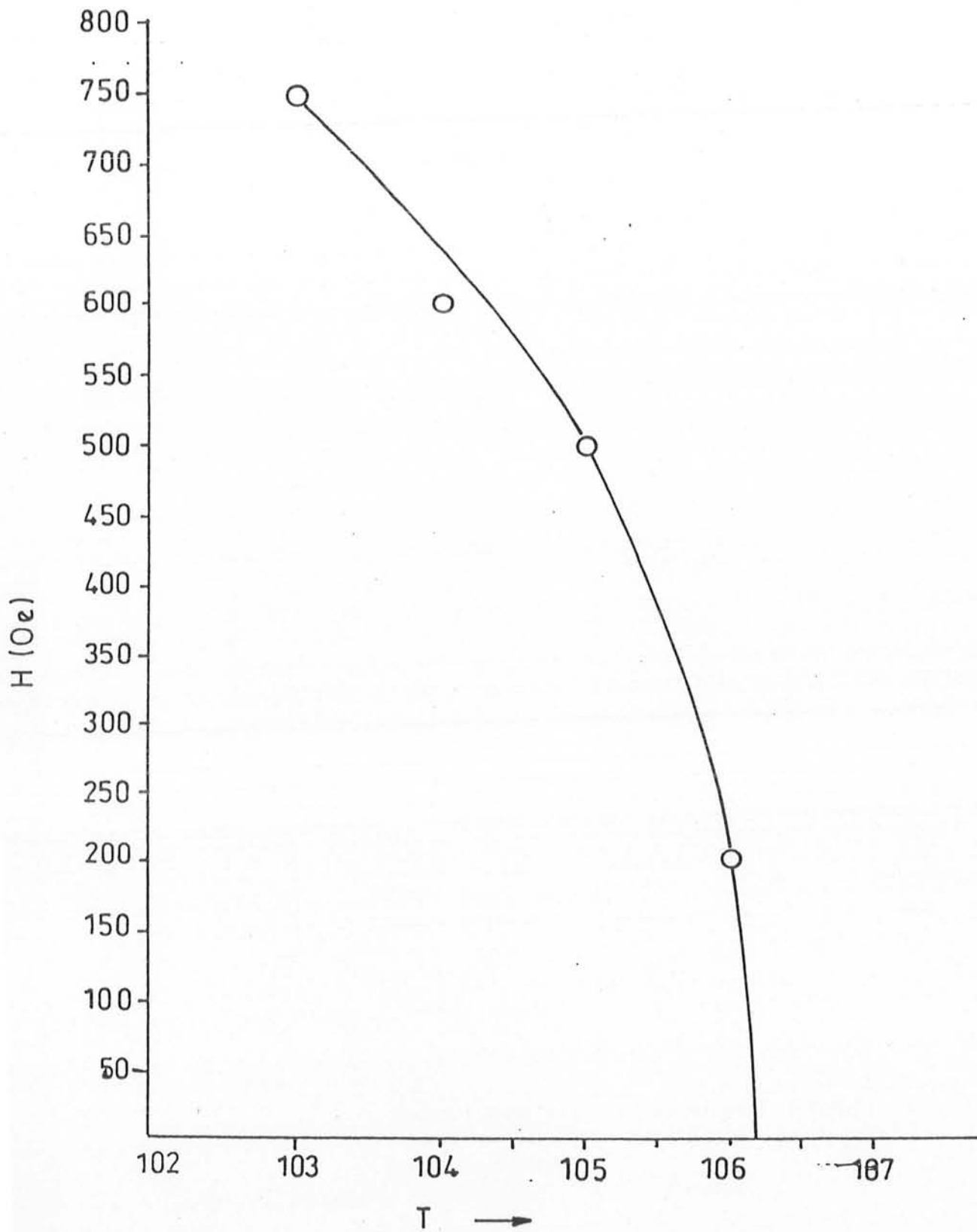
### (3.2a) Obtaining the exponent n

To further ascertain this result we take the reduced form of  $T^*$  i.e.  $T^* = 1 - T^*/T_c$  and apply the curve fitting method for obtaining the exponent n. Thus, we use the following equation for fitting a curve on the data of  $H_{dc}$  and  $T^*$ :

$$f = (1/c) [1 - T^*/T_c]^{1/n} \quad (3.4)$$

In the above equation the slope corresponds to  $1/n$ . After fitting  $f$  to  $H_{dc}$ , we obtained  $n = 0.79 \pm 0.5$  for the BPS sample, as shown in fig. [3.15]. This implies that  $H \propto (1-t)^{0.79 \pm 5}$  and thus it conforms to our previous results obtained by the dc magnetization measurements technique for the same sample i.e. BPS. The data of  $T^*$  and  $H_{dc}$  is given in table(VII), while the data of  $\log(1-t)$  and  $\log(H)$  is illustrated in table(VIII). The slope of  $0.79 \pm 5$  which is nearly equal to 0.66 appeared again though here from an entirely different experimental technique.

Thus, both the ac and dc susceptibility methods described above in sections (3.1) & (3.2) yield the same exponent for the irreversibility line; at least for the case of BPS sample. The YBCO and Hg-4 samples could not be studied by this method because the available field range was not high enough to allow this measurement.



Fig[3.14]

Graph of  $H$  vs  $T^*$  obtained from the  $\chi$ -ac measurements carried out on sample BPS. This graph is showing the irreversibility line in the  $H$ - $T$  plane, exhibiting a non-linear behavior and extrapolating smoothly at  $T \sim 106K$ .

**Sample BPS ( $T_c = 107K$ )**

H(Oe)	T*(K)	$t = T^*/T_c$
200	106	0.99
500	105	0.98
650	104	0.97
750	103	0.96

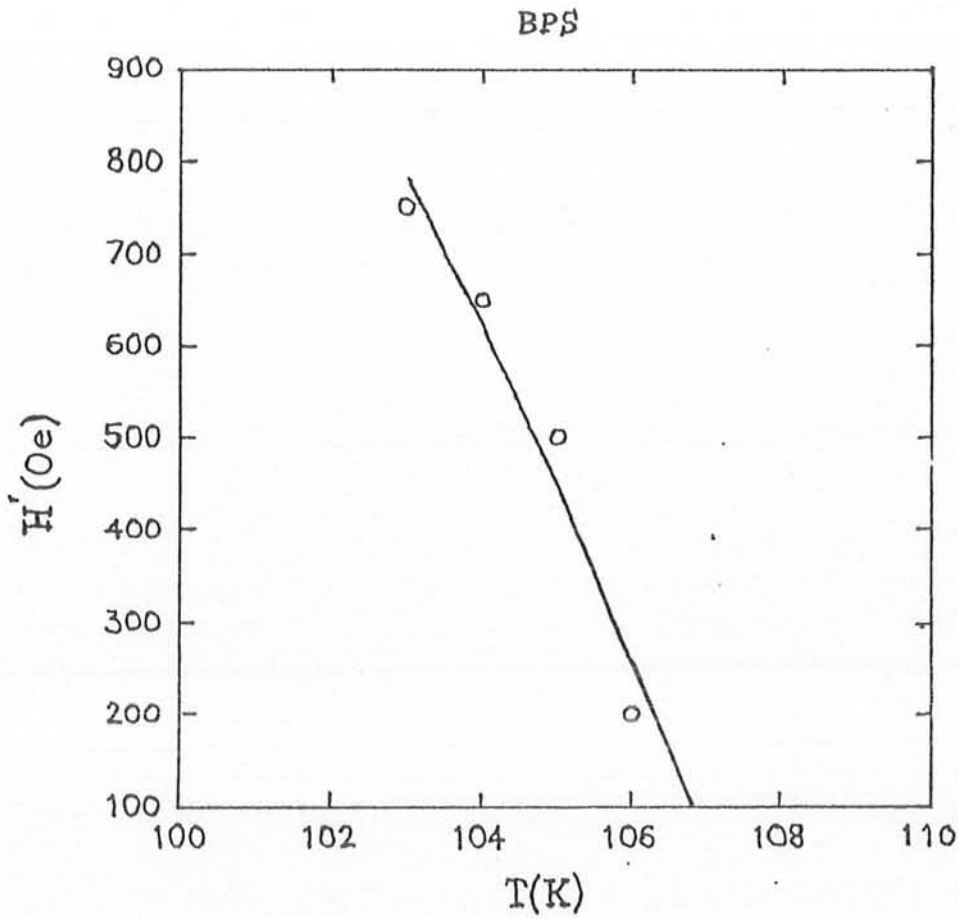
**Table [VII]: Data of dc applied magnetic field H(oe) Temperature T\*(K) and reduced temperature t ( $T = T^*/T_c$ ) form ac susceptibility measurements.**

**Sample BPS ( $T_c = 107K$ )**

<b>ln(H)</b>	<b>ln(1-t)</b>
<b>5.30</b>	<b>- 4.67</b>
<b>6.21</b>	<b>- 3.98</b>
<b>6.48</b>	<b>- 3.57</b>
<b>6.62</b>	<b>- 3.29</b>

**Table [VIII]: Data of ln(H) vs ln(1-t) form ac susceptibility measurements.**





Fig[3.15] Curve fit on the measurements obtained from the  $\chi$ -ac measurements carried out on sample BPS. In this fit  $\{1/c(T^*/T_c)\}^{1/n}$  is equated with a function  $f$ , then  $f$  is fitted to  $H^*$  yielding the value of  $1/n = 0.79$ .

Thus nearly the same value of exponent has been obtained by us for the Bismuth based sample using the curve fitting method. Obtaining the same result through a different experimental technique verifies to the correctness of the results.

Next we address the question why our results do not comply with the theory as proposed by Yeshurun and Malezemoﬀ [13]. As noted in the first Chapter, the form of the irreversibility line depends crucially on the temperature variation of the critical field. Previously we employed the commonly used form i.e.  $H \propto [1-t]^{(1)}$ . *However, Fang et al [14] have found experimentally (in a grain-aligned sample of  $YBa_2Cu_3O_{7.8}$ ) that the upper critical field varies as  $(1-t)^{1/2}$  near  $T_c$  and attributed this dependence to the  $T_c$  enhancement at the twin boundaries..*

The role of  $H_c(T)$  in  $(1-t)$  variation and the mathematical background of the result obtained by Fang et al is detailed as follows:

### (3.3) Role of $H_c(T)$ on the shape of irreversibility line

We next discuss how the observed irreversibility line behavior follows from the  $H_c(T)$  introduced by Fang et al. They showed that the thermodynamic  $H_{c2}$  [ $= (2)^{1/2} \kappa H_c$ ] determined from the onset of reversible magnetization decreases as  $(1-t)^{1/2}$  near “ $T_c$ ” [14] i.e. the decrease of  $H_{c2}$  is slower than expected on the basis of usual mean field theories. As a justification to this argument, Fang et al described the critical temperature enhancement in single crystal materials that arises due to the “Twinning Planes”(TP). The “ $T_c$ ” enhancement (i.e. slower decrease) is attributed to the possibility of phonons along the twinning plane (TP) or to distinct 2-dimensional electronic states. The domain of enhanced electron-electron interaction is, however, localized within a few

interatomic distances of the TP. Whether such an enhancement effect is possible in polycrystalline materials, seems likely, considering that Fang et al observed these effects in grain aligned samples.

Taking into account all these considerations, we use the above mentioned form of  $H_c(T)$

viz.

$$H_c(T) = (1.73) H_{c0}(1-t)^{1/2} \quad [3.5]$$

in equation [1.9(g)].

Equation [1.9(g)] is:

$$U_0 = [H_c^2 a_0^2 \xi] / 8\pi f^2 \quad [3.6]$$

$$U_0 = [(1.73H_{c0})(1-t)^{1/2}]^2 [1.075(\Phi_0/B)^{1/2}]^2 [0.74\xi(1-t)^{-1/2}] / 8\pi f^2$$

Simplifying, we get

$$U_0 = [(2.56)H_{c0}^2 \Phi_0 \xi_0 (1-t)^{1/2}] / 8\pi f^2 B \quad [3.7]$$

Also from equation [1.9(j)], we have:

$$U_0 = KT \ln(Bd\Omega/E_c) \quad [3.8]$$

comparing equations [3.8] & [3.7] and rearranging, we get:

$$BKDT_c = [(2.56)H_{c0}^2 \Phi_0 \xi_0 / 8\pi f^2 B] (1-t)^{1/2} \quad [3.9]$$

Where 'D' is equal to  $\ln(Bd\Omega/E_c)$ , and as before is treated as approximately constant, because  $\ln(B)$  varies much slower compared to B.

Thus,

$$BKDT_c = [(2.56)H_{c0}^2\Phi_0\xi_0/8\pi f^2](1-T/T_c)^{1/2}$$

or

$$(1-T/T_c)^{1/2} = D [8\pi f^2KT_c/(2.56)H_{c0}^2\Phi_0\xi_0]B \quad [3.10]$$

here  $B \sim H = H^*$ , so we can write:

$$H^* \propto (1-t)^{1/2} \quad [3.11]$$

Thus we note that  $H^* \propto (1-t)^{0.5}$  behavior is obtained in this case. This is closer to our observed behavior,  $n \sim 0.7$  than the value of 1.5 obtained on the basis of linear  $H_c(T)$  dependence. The discrepancy between 0.5 & 0.7 is not surprising given that we have used the grain - boundary or twin plane enhancement of  $H_{c2}$  to obtain the irreversibility line. It is of course quite likely that both the usual mean field  $H_c \propto (1-t)$  type and twin plane type enhancements effects combine to give the net effect. This could explain the values of n ranging from 0.59 to 0.8.

Finally, we note that the  $n = 0.5$  exponent in the variation of  $H_c(T)$  has also been explained by some authors, e.g. Tinkham [20] as being due to the fluctuation effects in the order parameter  $\psi$ . However, such an explanation would be feasible for T very close to  $T_c$ . We have been describing our results for a fairly wide range of t (i.e.  $T/T_c$ )  $0.59 \leq t \leq 0.96$ . One may not consider fluctuation effects to be generally important for  $t < 0.9$ . However, one point needs to be remembered. The  $T_c$  being used in our discussion is bulk  $T_c$ ; or the  $T_c$  of grains. It is well known that intergrain  $T_c$ 's are quite significantly lower. It is possible that the effects we have measured

relate to the fluctuation effects in the intergrain region. That would be consistent with the fact that we observe the  $H^* \propto (1-t)^{0.7}$  behavior in 3 - different types of granular samples.

### (3.4) Temperature Dependence of upper critical field

Since the form of irreversibility line depends crucially on the upper critical field i.e.  $H_{c2}(T)$  variation. Thus, in our case we need to know what it is for our sample. The  $H_{c2}$  cannot be measured directly from the  $M(H)$  loops because very high magnetic field is required for obtaining it. The procedure which we adopted for evaluating the  $H_{c2}$  comprises the determination of  $M(H)$  at different temperatures. The fitting of the equilibrium magnetization curves to a standard equation was carried out by M. Asim [27] on the basis of Ginzburg - Landau and London models:

$$4\pi M_{\text{equi}} = -\Gamma \ln [H_{c2}/H]$$

Where  $H$  is the applied magnetic field and  $\Gamma$  is a constant. The value of  $\Gamma$  obtained from the fit is 3.97 Oe.

The values of  $H_{c2}(T)$  obtained from the above mentioned scaling procedure, are then fitted to a function of the following form :

$$H_{c2} = H_{c0} [1 - (T/T_c)]^n$$

where  $H_{c0}$  is the value of magnetic field at absolute zero and was left as fitting parameter along with  $n$ . From the fit we obtain  $n = 0.51 \pm 0.07$  and  $H_{c0} = 2.81 \times 10^5$ , as shown in the figure (3.16). **This shows the validity of our model for the irreversibility line, i.e. YBCO sample does show the kind of temperature dependence of  $H_{c2}$  required to give the irreversibility number we have obtained.**

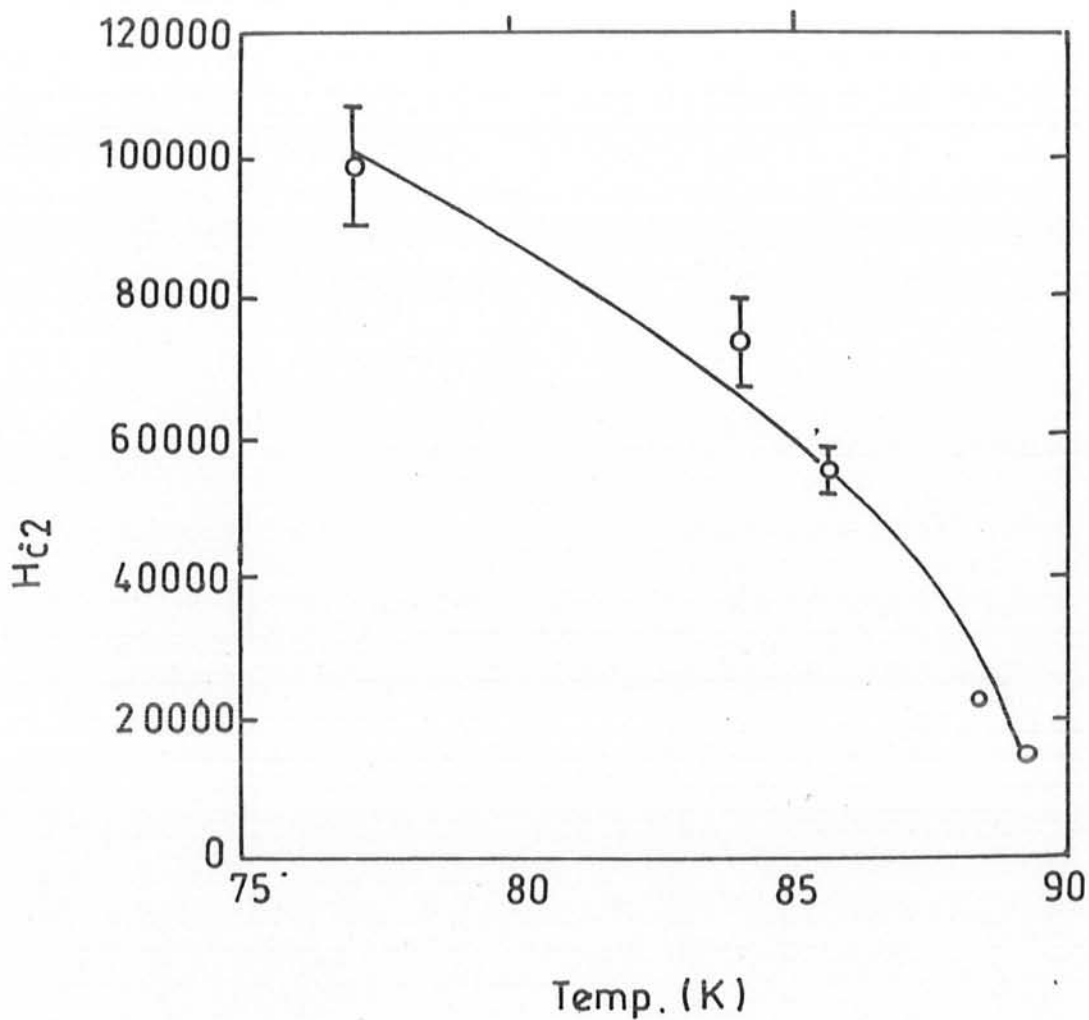


Fig [3.16]

The values of  $H_{c2}$  obtained from fitting the equilibrium magnetization curves to a standard equation: i.e.  $4\pi M_{\text{equi}} = -\Gamma \ln [H_{c2}/H]$ , are fitted to a function of a form:  $H_{c2} = H_{c0} [1 - (T/T_c)]^n$ . From the fit the values of  $n$  and  $H_{c0}$  are obtained, i.e.  $n = 0.51 \pm 0.07$  and  $H_{c0} = 2.81 \times 10^5$ .

### (3.4) Conclusions

We have carried out a study of the temperature dependence of the irreversibility field  $H^*(T)$  in three different polycrystalline samples. The method used has been mainly the vanishing of dc-hysteresis, while for one case (BPS) the convergence of field cooled and zero field cooled ac susceptibilities, has been taken to be the signal for reversibility onset.

The  $H^* \propto (1-t)^n$   $0.6 \leq n \leq 0.8$  behavior observed by us in all these cases is quite different from the behavior observed in most cases. However, there are instances[22] where values for  $n$  different from  $n = 3/2$  have been reported previously. Our observed behavior shows a slower decrease of  $H^*$  with temperature than predicted by the theory based on linear decrease of  $H_{c2}(t)$ . We have shown that if the theory of the irreversibility line as developed by Yeshurun et al. is modified by using  $H_{c2}(t) \sim H_{c0}(1-t)^{0.5}$  then one obtains  $H^* \propto (1-t)^{0.5}$ , closer to our observed behavior.

The half power dependence of  $H_{c2}(T)$  was discussed by Fang et al. to be consequence of critical field enhancement by twin plane boundaries (somewhat similar to critical field enhancement in the superconducting films). It is not yet clear whether this or some other reasons exist for their unusual  $H_{c2}(t)$  behavior in our samples. However, as discussed earlier, at least one of our samples YBCO, does show the  $H_{c2}(t) \sim (1-t)^{1/2}$  dependence (others have not been investigated). This provides support that at least for the case of YBCO labelled sample, the unusual  $H^*(t)$  behavior is correctly explained by the  $H_{c2}(T)$  behavior assumed in the analysis discussed earlier in this thesis.

Thus it seems very reasonable to conclude that the observed behavior of the irreversibility is adequately explained by our analysis as developed in this thesis. Finally we note that the results



for the irreversibility line follow the same pattern in both the dc and ac methods. This testifies to the reliability of the analysis and the results.

## REFERENCES

- [1] M. Tinkham, Introduction to Superconductivity (Mcgraw Hill Kogakusu, Tokyo, 1975).
- [2] C. Kittel, Introduction to Solid State Physics (John Willey & Sons, Inc. New York, 1976).
- [3] T. Van Duzer and C.W. Turner, Principles of Superconductive Devices and Circuits (Elsevier Inc. New York, 1981).
- [4] Jeffry W. Lyhn, High Temperature Superconductivity (Springer - Verlag, New York Inc., 1990).
- [5] W. Meissner, R. Ochenfeld, Natur Wiss, **21** (1933) 787.
- [6] R.D. Parks, Superconductivity (Marcel Dekker Inc., New York, 1969).
- [7] A.A. Abrikosov, J. Phys. Chem. Solids **2** (1957) 199.
- [8] V.L. Ginzburg, L.D. Landau: zh. Eksp. Teor. Fiz. **20** (1950) 1064 (English translation in "Men of Physics": L.D. Landau, Vol. 1, ed. by D. Ter Haar, Pergamon Press, New York, 1965).
- [9] C.P. Beans', Phys. Rev. Lett. **8** (1962) 250.
- [10] Pablo Esquinazi, Solid State Communications, **74** (1990) 75-77.
- [11] K.A. Muller, M. Takashige and J.G. Bednorz, Phy. Rev. Lett. **58** (1987) 1143.
- [12] J.R.L. de Almeida and D.J. Thouless, J. Phys. **A 11** (1978) 983.
- [13] Y. Yeshurun and A.P. Malezemoff, Phy. Rev. Lett. **60** (1988) 2202.
- [14] M.M. Fang, V.G. Kogan, Finnemere, J.R. Clem, L.S. Chumbley and D.E. Farrel, Phy. Rev. B, **37** (1988) 2334.
- [15] Vibrating Sample Magnetometer (V.S.M) Instruction Manual, Rickey Denishi Co. Ltd. Japan.
- [16] B. Schulz, B. Schliepe, W. Wisney, K. Baberschke, Solid State Communication, **80** (1991) 111.
- [17] Y. Wolfus, Y. Yeshurun and I. Felner, Phy. Rev. B, **39** (1989) 690.
- [18] I. Felner, Y. Wolfus, G. Hilscher, and N. Pillmayr, Phy. Rev. B, **39** (1989) 225.

- [19] Y. Yeshurun, I. Felner and H. Sompolinsky *Phy. Rev. B*, **36** (1987) 840.
- [20] M. Tinkham, *Phy. Rev. Lett.* **61** (1988) 1658.
- [21] C. Ebner and A. Stroud, *Phy. Rev. B*, **31** (1985) 165.
- [22] Li Miu, *Phy. Rev. B*, **46** (1992) 1172.
- [23] R.L. Peterson and J.W. Ekin, , *Phy. Rev. B*, **37** (1988) 9848.
- [24] E. Evetts and B.A. Glowacki, *Cryogenics*, **28** (1988) 641.
- [25] P.W. Anderson and Y.B. Kim, *Rev. Mod. Phys.* **36**, (1964) 39.
- [26] P.H. Kes, J. Aarts, J. Van den Berg, C.J. Van der Beak and J.A. Mydosh, *Supercond. Sci. Technol.* **1** (1989) 242.
- [27] M. Asim, Ph.D. Thesis (Quaid-i-Azam University, 1995)